Inclusion Body formation of Familial Amyotrophic Lateral Sclerosis Associated Cu, Zn-Superoxide Dismutase Mutants in *Escherichia coli*

by

Johnathan Almey

A thesis

presented to the University of Waterloo

in fulfilment of the

thesis requirement for the degree of

Master of Science

in

Chemistry

Waterloo, Ontario, Canada, 2015

Authors Declaration

I hereby declare that I am the sole author of this thesis. This is a true copy of the thesis, including any required final revisions, as accepted by my examiners.

I understand that my thesis may be made electronically available to the public.

Abstract

Protein aggregation is a common occurrence when overexpressing protein in bacteria, it is also a hallmark of some neurodegenerative diseases such as amyotrophic lateral sclerosis (ALS). Mutations in the enzyme Cu, Zn- superoxide dismutase (SOD1) have been implicated in causing the familial form of ALS. Here, a number of SOD1 mutants expressed in *E.coli* are analysed for their propensities to aggregate in the form of inclusion bodies. The inclusion bodies are also analysed for their metal content of both Cu and Zn. The latter experiments were conducted both by a spectrophotometric assay using the metallochromic chelator 4-pyridylazo-resorcinol and inductively coupled plasma atomic emission spectroscopy.

The SOD1 variants showed a large amount of variability in their propensities to aggregate and when compared to other physiochemical properties such as the thermal stability, there were clear trends, in particular between the aggregation propensity and the thermal stability of the reduced apo SOD1. In comparing the aggregation propensity to one aspect of the ALS phenotype, disease duration, there was no correlation. The metalation status of the SOD1 mutant inclusion bodies was found to be variable, even within repeated experiments with the same mutant. As metals are required for the enzymes activity, the metals present support the possibility that the inclusion bodies may retain activity. This may prove useful in the future if there is ever a need for an insoluble superoxide catalyst. The results of these experiments also further our understanding of SOD1 aggregation and metalation which may help future investigations in understanding ALS pathology.

Acknowledgments

I would like to thank my supervisor Dr. Meiering for her guidance and encouragement. I would also like to thank the members of the Meiering lab for their help throughout my work here and Ralph Dickhout for his assistance with the ICP-AES experiments. Finally, I would like to thank my family.

Table of Contents

List of Figures

List of Tables

List of Abbreviations

AFM ..... Atomic Force Microscopy
ALS ..... Amyotrophic Lateral Sclerosis
βME 2-mercaptoethanol
CCS ..... Copper Chaperone for SOD1
DSC ..... Differential Scanning Calorimetry
DTPA ..... Diethylene triamine pentaacetic acid
EDTA ..... Ethylenediaminetetraacetic acid
fALS ..... Familial Amyotrophic Lateral Sclerosis
FTIR ..... Fourier Transform Infrared Spectroscopy
GdnHCl ..... Guanidine Hydrochloride
GFP ..... Green Fluorescent Protein
IBs ..... Inclusion Bodies
ICP-AES ..... Inductively Coupled Plasma Atomic Emission Spectroscopy
IPTG ..... isopropyl-β-D-thiogalctopyranoside
LB ..... Luria Broth
NTA ..... Nitrilotriacetic acid
O.D. ..... Optical Density
OmpF ..... Outer Membrane Protein F
pWT ..... Pseudo Wild Type
sALS ..... Sporadic Amyotrophic Lateral Sclerosis
SDS-PAGE ..... Sodium Dodecyl Sulfate Polyacrylamide Gel Electrophoresis
SOD1 ..... Cu, Zn-Superoxide Dismutase
TEN buffer ..... Tris/EDTA/NaCl buffer
WT ..... Wild Type
YFP ..... Yellow Fluorescent Protein

1.0 Introduction

1.1 General protein information

1.1.1 Protein structure

Proteins are some of the most important components of life, they serve a wide array of functions without which, we as humans would not exist. A protein is a large biomolecule formed by a folded chain or multiple chains of amino acids. During the synthesis of the chain, even before it is released from the ribosome where it is being assembled, the protein may begin to fold through a process that is highly dependent on the energetic properties of the chain, the surrounding solvent, and other components such as chaperone proteins. The final structure of a protein defines its function, whether that be for structural support of a cell, molecular transport, or the catalysis of a chemical reaction.

Generally, entropy favours a chain that is disordered, which means that the folds have to form structures that can overcome that energy. A hydrophobic collapse involving the coalescence of hydrophobic groups, expelling water from the core of the protein, is one of the first protein folding events to occur. From this point, the protein does not have to undergo as many large changes in conformation to achieve its native structure, with a series of relatively complex motions leading to a more well-defined structure with the formation of extensive non-covalent interactions[1,2]. There are a small number of common secondary structures that are observed in the folded form, including α-helices, β-sheets, β-turns, and loops[3]. The tertiary folding process may begin to occur at the same time as the secondary structure forming, with the combination of hydrophobic interactions, electrostatic forces, and in some cases the formation of disulfide bonds all involved in the folding to the final native state[2].

Many proteins are not limited to a single polypeptide chain, they may consist of multiple chains which, whether identical or different, may fold and associate with each other to form an oligomer. The proportion of proteins within an organism that are oligomeric is quite high, with approximately three quarters of the proteins in *E.coli* believed to be oligomers[4,5].The protein of interest in the studies proposed here, Cu, Zn – Superoxide dismutase (SOD1) is a dimer of 2 identical subunits[6] and will be described in more detail in section 1.4.

The environment in which a protein exists plays an important role in determining its structure. A cell is a very complex entity with diverse contents, many biomolecules within a cell require narrowly defined conditions to function. Much of the inside of a cell is the cytosol, the liquid filler of a cell, containing the molecules and ions required for the synthesis of biomolecules as well as the cells own architecture and function. Salts and other natural kosmotropic substances assist in keeping a protein folded after it has been synthesized. The cell also contains proteins which function solely to stabilize other proteins such as heat shock proteins, which can bind to another protein in times of stress or simply help a protein fold for the first time[7–10].

The process of folding within a cell entails molecular vibrations and rotations to form the most stable conformation possible for the given environment. It is an amazing feat to have a simple sequence of amino acids consistently form complex cellular machinery. The folding pathways that proteins take may be different from each other and there is still much to be discovered in this field[8,11].

1.1.2 Function

As mentioned above, proteins may have various functions, such as the structural support of a cell, the transport of materials into, out of, and throughout a cell, or a large number of catalytic roles. Many proteins utilize cofactors to assist in their purpose; these "extra" molecules can be organic, metallic, or a combination of both and can allow a protein to fill a very specific structural or functional role. Most enzymes are proteins and these can show great specificity in the reactions they catalyse. By using their complex structures, enzymes can not only catalyse a wide range of specific reactions, but each can catalyze their particular reaction with great effectiveness. In some cases an enzyme can increase the rate of a reaction to approximately 10^{15}-10^{17} fold over its original speed[12]. When a cofactor is involved, the protein when bound to the cofactor is known as a holoenzyme, and without the cofactor is termed an apoenzyme[3]. The protein of interest here, SOD1, contains two metal cofactors, 1 Zn and 1 Cu per subunit; the Zn stabilizes the protein structure while the copper is involved in catalysis and is described in more detail in section 1.4.2[6].

1.2 Protein aggregation

1.2.1 Misfolding and formation of aggregates

The proper folding of a protein is an important factor with regards to its function and stability. Improper folding, when the protein does not conform to its native state, can induce changes in the level of function or even cause the complete loss of function. It can also affect the state of the proteins quaternary structure, possibly compromising a proteins ability to properly oligomerize. All of this may have a serious impact on an organism's health in a variety of ways[13]. Environmental factors that may affect the folding process include some of those

mentioned in the previous section; temperature, pH, and the presence of the proper chaperones necessary for production.

Aggregates may arise when specific hydrophobic regions of improperly folded or incompletely folded proteins interact with each other, or possibly also native like conformations of multiple proteins interact, similar to polymerization[13]. There are multiple forms of aggregates, such as amorphous aggregates, annular oligomers, fibrils, and inclusion bodies (IBs), some of which may have common intermediate structures. A stability diagram can be seen below in Figure 1.1 depicting the energy state of the protein through the folding and misfolding processes.[14]

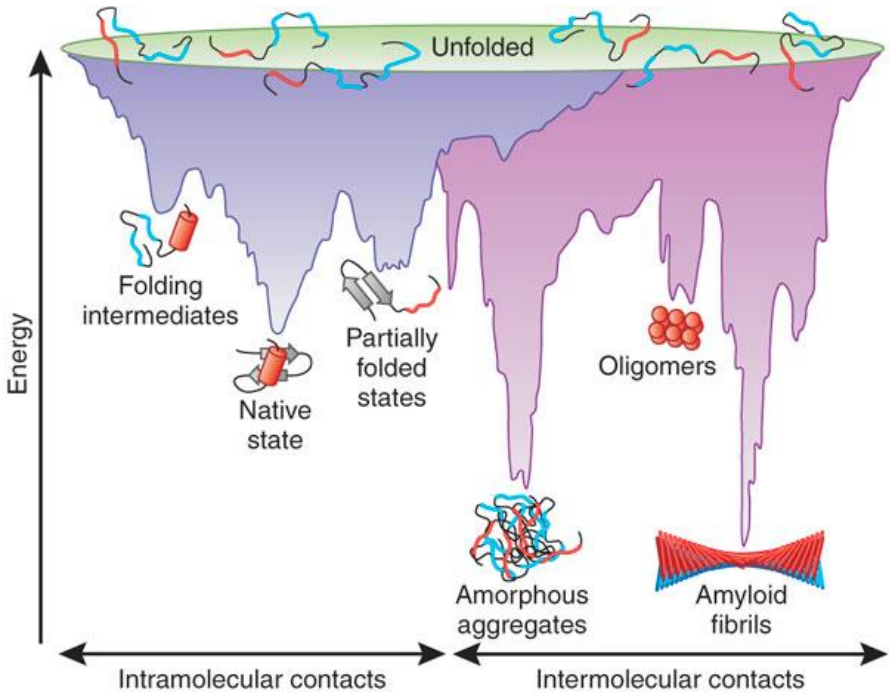

Figure 1.1: Stability diagram depicting the energy level of a protein in a given conformation during the processes of folding and/or aggregation. The protein progresses from an unstructured high energy state to a more energetically favorable compact state. The lowest energy states of a polypeptide are in the aggregate forms. Reprinted by permission from Macmillan Publishers Ltd: [Nature Structural and Molecular Biology]. Hartl, F. U.; Hayer-Hartl, M. *Nat. Struct. Mol. Biol.* **2009**, *16* (6), 574–581, copyright 2009.[14] http://www.nature.com/nsmb/index.html

Amorphous aggregates tend to be large disordered clusters, while the other forms have some distinct structural features. For instance annular oligomers have a circular pattern of proteins while fibrils (including amyloid) have repeating units stacked upon one another, for instance the stacked β sheets of β amyloid[15]. Inclusion bodies, which are of importance in this particular study are one of the lesser understood forms of aggregates, the mechanisms of formation and the state of the contents have not been well defined. Some forms of aggregates are very stable, even more so than the native state.[14]

The aggregation of proteins has been linked to numerous diseases, including many neurodegenerative diseases such as: Parkinson's, Alzheimer's, Huntington's disease, as well as amyotrophic lateral sclerosis (ALS).[15–20] These connections between aggregation and disease have created a great interest in learning more about aggregation, a subject that was largely passed over previously.[13] Aggregation is also of concern for industrial applications of proteins, since many recombinant proteins form IBs when over-expressed in bacteria. Utilizing this aggregation for purification purposes or understanding the factors that direct aggregation may prove useful for a wide range of proteins.[21]

A large field of research is currently focused on developing methods to predict aggregation. Methods can be *ab initio* or empirical, with empirical methods incorporating information from experimental observations in the prediction algorithms. More specifically, Chiti and coworkers have pioneered empirically based methods for determining the relative aggregation propensity of a protein, including upon introducing mutations.[22,23] Other algorithms have been developed such as the TANGO[24] and Zyggregator[25] algorithms which are also

empirically based methods that attempt to predict aggregation-prone regions or structures in a protein by incorporating experimental information. Alternatively, the Waltz method attempts to determine the aggregation prone regions of a protein simply based on a primary sequence.

These methods have been improving and are beginning to show more accurate predictions *in vitro*, however, they are seemingly still inadequate for *in vivo* aggregation prediction and lack consistency between predictions for different proteins. Understanding protein folding both *in vitro* as well as *in vivo* is important*;* information regarding the aggregation of specific proteins in both environments can improve our knowledge of the general principles of folding and our ability to accurately predict protein aggregation. With regards to disease-linked aggregation, an accurate *in vivo* model would be valuable in accounting for the complex surroundings which include the interactions with chaperones and membranes, which an *in vitro* prediction cannot adequately accomplish. This supports experimental observations as an important method of determining if a protein will aggregate. The data from these experiments can be used to improve future protein aggregation prediction algorithms.

1.2.2 Inclusion bodies

There are various types of aggregates that are described using the term inclusion, however, this is not equivalent to the aggregates known as inclusion bodies. Inclusion bodies are one specific form of aggregate in which unfolded or misfolded protein will accumulate to high levels within a cell's cytoplasm and are produced during over-expression in bacteria. The naming for aggregates seen in other organisms (e.g. Humans, mice) is less well defined and the SOD1 aggregates found in humans described here will simply be referred to as inclusions, although other names such as "Lewy-body like" inclusions and hyaline inclusions have been used.[26,27]

Inclusion bodies can be very large (>10 μm in some cases[28]) and usually present like amorphous aggregates, as round with no immediately distinct structure. The IBs are commonly obtained by cell lysis followed by the washing with a gentle detergent such as Triton X-100 [29] (Figure 1.2).

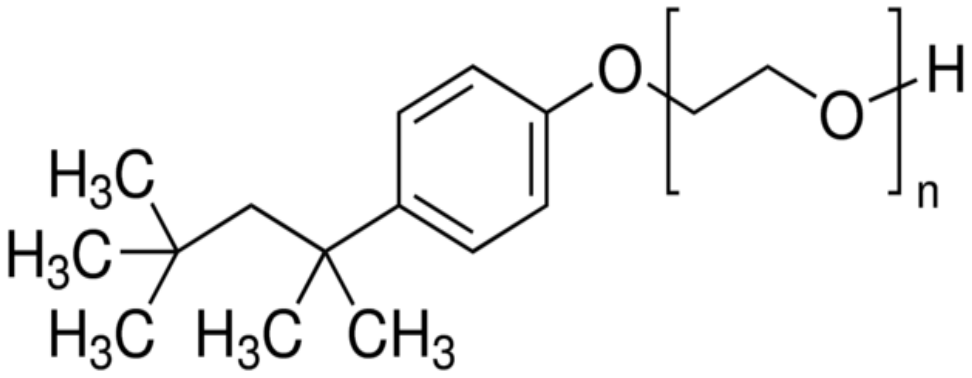

Figure 1.2: Triton X-100 unit, a gentle non-ionic detergent commonly used in inclusion body preparations.

The characteristics of inclusion bodies have been investigated by numerous groups, but there is still much debate regarding their structure and contents. Questions that have been studied include whether IBs are in fact amorphous or contain amyloid, however, the contents may vary depending on the protein[30] and the conditions under which it was produced. The contents of aggregates are more well characterized in bacterial models (e.g. *E.coli*), with Garcia Fruitos et al. reporting up to between 90-95% of the inclusion bodies contents consisting of the over-expressed protein.[31,32] The initial understanding with respect to the structure was that IBs are for the most part structured amorphously, in a way unlike amyloid[13,33], although, this is now in

contention, with studies from Wang et al. observing amyloid like properties of inclusion bodies formed by the secretory human bone morphogenetic protein-2.[34] The reality may be that inclusion bodies do not conform to one defined structure.

Inclusion body formation is generally believed to be concentration dependant, that is, when proteins are produced in large amounts, the cellular folding machinery is not sufficient to aid folding, leaving large amounts of unfolded or partially folded protein in close proximity.[35] Figure 1.3 depicts a number of possible parts that may compose or lead to an inclusion body. To support the mechanism of IB formation, there have been instances of ribosomal RNA and subunits of RNA polymerase identified from inclusions[36], suggesting the protein may not be fully synthesized. Inclusion bodies are commonly found when over-expressing proteins that are not native to the host organism. The inclusions found in cases of disease, such as in ALS[37], described further in section 1.2.2.2, are not as well characterized as those caused by over-expression in bacteria, mainly due to the difficulty of working with low amounts of pathological aggregates from tissue.[38] This is a major factor in determining how to study aggregation associated with ALS. Here we use *E.coli* as a model system, since SOD1 can be over-expressed to form IBs[39] which can be characterized in various ways to define the determinants of aggregation *in vivo*. Knowledge acquired from the study of IBs can provide insights pertinent to the formation of ALS associated inclusions.

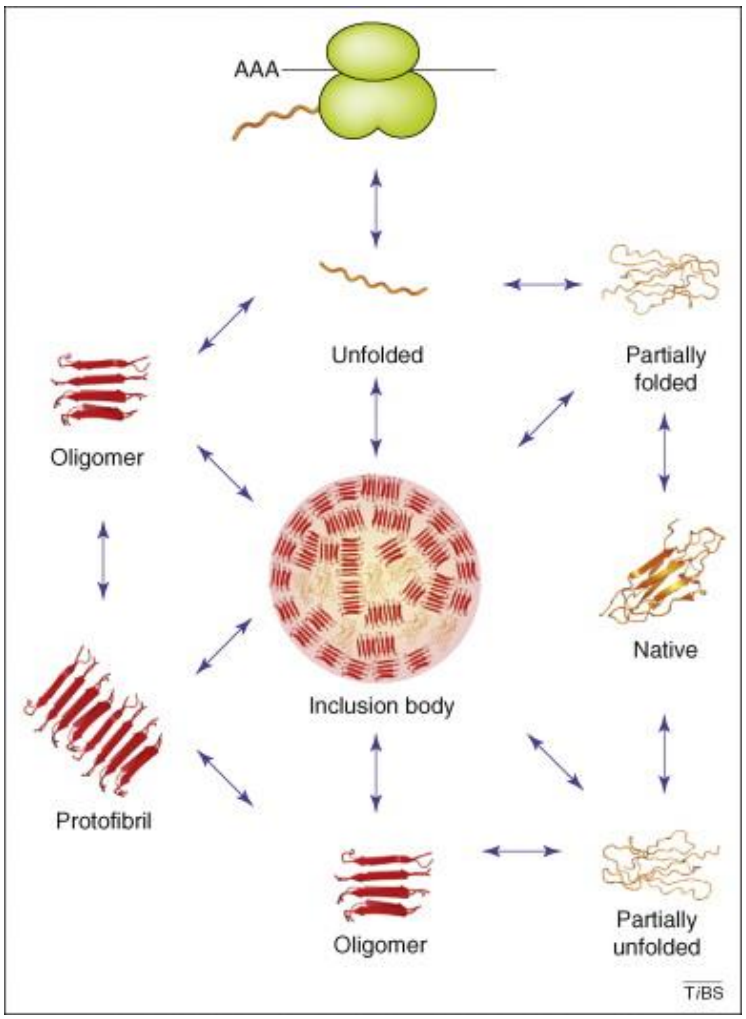

Figure 1.3: Routes of inclusion body formation. From synthesis by the ribosome (top), the initially unfolded polypeptide may attain various levels of structure such as being partially folded or oligomerizing before being incorporated into an inclusion body. Reprinted from Trends in Biochemical Sciences, 34/8, de Groot et al. Amyloids in bacterial inclusion bodies, 408-416, copyright 2009, with permission from Elsevier.[33]
http://www.sciencedirect.com/science/article/pii/S0968000409001236

In more specific examples of previous studies, inclusion bodies have been detected, quantified, and characterized using a wide variety of methods, including but not restricted to: immunoblots (western blots), electron microscopy, atomic force microscopy (AFM), Fourier transform infrared spectroscopy (FTIR), circular dichroism, x-ray diffraction, and fluorescence spectroscopy when reacted with specific dye compounds (Congo red, Thioflavin t etc.) or bound

to fluorescent tags (GFP or YFP)[28,31,33,34,40–42] yet, more analysis is undoubtedly necessary for multiple purposes.

1.2.2.1 Inclusion bodies in industrial applications

Inclusion bodies are of particular interest in nanobiotechnology. They are a common occurrence when overexpressing heterogeneous proteins in bacterial cultures. Certain characteristics of bacterial inclusion bodies have made them more interesting to researchers recently. These characteristics include that their deposition is usually fully reversible and a fraction of the protein found in inclusion bodies may actually be functional[31], as was shown, for example, in studies with dihydrofolate reductase or a form of β-galactosidase[31,43]. This points towards some native-like structure being present in the aggregates.

When looking at the possible uses for this kind of aggregate, some intriguing ideas have been proposed recently. Studies from Wu et al.[44] have highlighted a wide range of enzymes including: green fluorescent protein, β-galactosidase, β-lactamase, alkaline phosphatase, D-amino acid oxidase, polyphosphate kinase 3, and others that have been observed to be produced as active IBs. These enzymes could be used practically, in inclusion body form as natural immobilized enzymes. In this case, the enzymes were produced when the enzyme was fused to another protein. With activities that in some cases rival the native protein[43,45], these inclusion bodies are now of very high interest to not only those studying protein folding, or aggregation related disease, but also those looking to utilize their unique properties and put them to a purpose.

1.2.2.2 Relevance to disease

As mentioned previously, proper protein folding is imperative to an organism's health. Chaperone proteins are among the most abundant proteins in cells[1] which supports the importance of proper folding, and aggregation is clearly linked to numerous diseases. In most of the diseases associated with aggregation, the mechanisms of disease pathogenesis remain unclear. Open questions include the roles of aggregates in a gain of toxic function, in which the mechanism of aggregation may be a synergistic combination of a mutation increasing a proteins propensity to aggregate as well as causing destabilization of the protein[17] or if there are multiple factors, such as other proteins that contribute to the disease. Understanding more about these aggregates may lead to a clearer view on neurodegenerative disease pathology.

1.3 Amyotrophic lateral sclerosis

Amyotrophic Lateral Sclerosis (ALS) is a relatively common and incurable neurodegenerative disease found around the world, which is characterized by the formation of protein aggregates in diseased cells. ALS has a lifetime risk of approximately 1 in 2000 [46], with onset generally seen above the age of 47.[47] It is characterized by various initial symptoms which may include muscle weakness and spasticity in the case of upper or lower motor neuron onset (cervical and lumbar onset respectively), or spastic dysarthria, where the speech is slow or distorted and a loss of the ability to swallow in the case of bulbar onset.[48,49] These three forms of onset are caused by a loss of motor neurons, however, the exact causes of the neuronal death are not well defined.

There are two major classifications of the disease, those being the sporadic form (sALS), accounting for approximately 90-95% of cases, and the familial form (fALS) accounting for the

remaining cases[6,17]. The major causes of the more common sporadic form are still not understood, however a number of heritable factors have been identified as causal for fALS, all of which are associated with some cases of sALS as well, through de novo mutations. The first gene associated with fALS is the SOD1 gene, encoding for the aforementioned protein, which has been studied extensively, and accounts for approximately 20% of fALS cases. Additional genes have been subsequently identified including the most common mutated gene associated with ALS so far, the chromosome 9 open reading frame 72 (C9orf72) which accounts for approximately 40% of fALS cases, in which a hexanucleotide repeat expansion somehow leads to the disease. Mutations in other genes include TARDBP, encoding the TAR DNA-binding protein (TDP-43), and FUS, encoding the Fused in Sarcoma protein. [6,49,50].

Just as amyloid formation is the leading cause of some other neurodegenerative diseases, such as Parkinson's and Huntington's, aggregation is associated with ALS[15–20]. It has been previously proposed that the stability of SOD1 mutants may be compromised leading to aggregation, specifically aggregating in the form of insoluble oligomers termed "Lewy Body Like" hyaline inclusions as well as astrocytic hyaline inclusions[26,27], round aggregates which build up in motor neurons. Fibril type (Skein-like) aggregates have also been reported in some cases[51], and it has also been proposed based on mice and Chinese Hamster Ovary cell studies, that there may also be early forming soluble aggregates[41,51,52]. Detergent-insoluble SOD1 aggregates are found in the late stages of the disease, located throughout the corticospinal tract, however not in the axons[53]. Questions of the aggregate formation still exist, the ubiquitination of inclusions has been observed, which may implicate that the cell is forming inclusions as a defence mechanism, however, ubiquitination is not seen in all cases. [51] The mechanism of

aggregation is still unknown. Answering some of the questions about SOD1 aggregation may be useful for the development of a treatment.

1.3.1 Therapeutic approaches

With only one current drug on the market for the treatment of ALS, Riluzole, showing only slight benefits to the survival of patients [54], there is still a desire to better understand the disease with the goal of developing a more effective treatment. Riluzole itself is believed to have an effect on glutamate metabolism, but this is still not completely clear.[54] Current approaches taken by researchers for the treatment of the disease include aiming at stabilizing mitochondrial stress[55] as well as addressing the disease on the genetic level with stem cell therapy. At least 42 drugs have had negative human studies.[54] Targeting the aggregation has not seemed particularly successful as of yet, however, academics, specifically Ray et al.[56] as well as multiple pharmaceutical companies have taken an interest in that approach. These include Cambria, who had a small molecule compound in development for inhibiting SOD1 aggregation, Reata pharmaceuticals, who have identified a molecule capable of binding to, and stabilizing misfolded SOD1, as well as others.[57]. Studying the aggregation of SOD1 may serve dual purposes, by uncovering more information about inclusion body in general as well as acknowledging possible factors involved in a cause of ALS.

1.4 Superoxide dismutase

1.4.1 Structure

As noted above, proteins play an important role in the life of organisms, they serve a number of purposes from serving a structural function to catalyzing important chemical reactions. One of these important proteins, that has been mentioned above, is superoxide

dismutase. There are several distinct forms of superoxide dismutase found both in eukaryotes and prokaryotes, including three distinct enzymes in humans: a cytosolic Cu, Zn – superoxide dismutase, referred to as SOD1, a manganese binding superoxide dismutase (SOD2) found primarily in the mitochondria[58,59], and a second Cu, Zn – superoxide dismutase found in the extracellular space.[60] The focus in this case has been the cytosolic human Cu, Zn-superoxide dismutase SOD1.

Unlike the homotetrameric SOD2 or SOD3, SOD1 is a 153 amino acid homodimer, with a total molecular mass of approximately 32 kDa (Figure 1.4). Each monomer is composed of a Greek key β-barrel containing 8 β-strands, an electrostatic loop containing a short helical section, and a zinc binding loop, containing histidine residues H63, H71, and H80 as well as aspartic acid D83 which bind to a single zinc ion. The single copper ion is coordinated by four histidines, including H46, H48, H120 and sharing H63 with the zinc ion. The zinc ion plays a structural role in the protein, with the copper ion participating in catalysis. Each monomer also contains 4 cysteine residues, two (C57 and C146) form a disulfide bridge, and two are free cysteines (C6 and C111).[6]

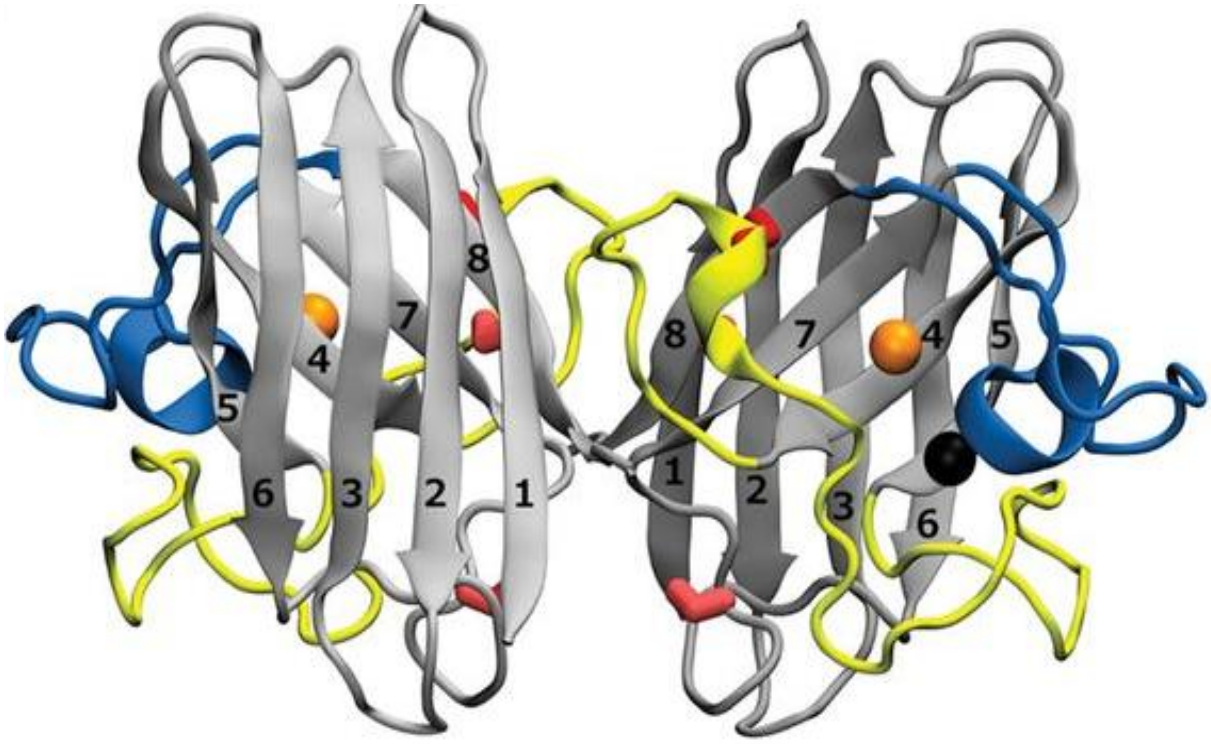

Figure 1.4: Ribbon diagram of the human Cu, Zn-Superoxide dismutase dimer. Each subunit is identical with the Copper (orange) and Zinc (black) ions visible on the right. The two longest loops are the Zn binding loop in yellow and the electrostatic loop in blue. The intrasubunit disulfide bond is seen near the bottom (red stick). Figure adapted from Broom et al.[61] Original PDB 1HL5[62]

1.4.2 SOD1 function

SOD1 is an enzyme that carries out the function of reducing the presence of the harmful radical superoxide. Since superoxide radicals are capable of causing damage within a cell in a number of ways, the removal of superoxide is an important function.[63] The core of the active site of SOD1 includes the copper atom, and the surrounding amino acids to which it is bound, with other structures involved such as the electrostatic loop. When the copper is oxidized those amino acids are the histidines 46, 48, 63, and 120, with His 63 bridging between the copper and zinc

and being released by the copper upon its reduction.[6] The copper is cyclically reduced and then reoxidized during the catalysis. The reaction catalyzed is a disproportionation reaction, with one superoxide ion being oxidized to form an oxygen molecule, and another then being reduced to form hydrogen peroxide. The overall reaction (Equation 1) is as follows[6]:

Eq. 1 $$2\ O_2^- + 2H^+ \rightarrow H_2O_2 + O_2$$

The activity of SOD1 has been studied by various groups, including the Meiering Lab. One main general consensus is that some fALS associated mutations do in fact have an effect on activity, primarily those mutations with metal binding deficiencies. The majority, however, may still retain activity comparable to that of the wild type SOD1 given proper metalation[40,64].

1.4.3 SOD1 in ALS

Due to recent studies showing that the loss of SOD1 function is not likely the cause of the disease, one well supported explanation is that the mutations in SOD1 may cause a gain in toxic function[6,40,49,52,65], which may be associated with a structural change in the protein, or the aggregates. This is supported by the appearance of the inclusions at a later stage of the disease, not immediately. It has also been observed that soluble oligomers may gain a toxic function, possibly related to oxidative stress inside the cell.[66,67] Some of the research in this area has focused on the identification of the products or interacting factors such as mechanisms requiring nitric oxide, or what form of SOD1 is involved, such as those deficient in Zinc, as Zinc is important for the enzymes stability [68,69]. Also, SOD1 has been associated with peroxidase

activity rather than just dismutation, an increase in this activity has been observed with some ALS associated mutations, however, this may be protective[70]. Another change has also been proposed though, involving the auto-oxidation of the enzyme, resulting in the production of O_2^- rather than the consumption of the toxic species.[70] The gain of toxic function idea as a whole, has not yet been adequately explored, leaving key unanswered questions.

Multiple types of mutations in SOD1, including deletions, C-terminal truncations, and, predominantly, point mutations have been implicated in causing the familial form of the disease. Approximately 182 mutations have been identified in patients diagnosed with the disease[71]. These mutations are widespread throughout the protein occurring in a range of locations including the metal binding region of the protein, close to the dimer interface, throughout the β-barrel, and turns/loops (Figure 1.4). Some also show variety in the type of mutation for a single residue, for example mutation to a residue with a different charge, size, or level of hydrophobicity. The mutations have various phenotypes, in particular, variable disease duration (Table 1.1), ranging from more aggressive progression as seen with A4V or G41S mutations, with average disease durations of 1.2 and 1.0 years respectively to longer progression times associated with E21G, G37R, or H46R, with average disease durations of 17.2, 17.0, and 17.6 years respectively[17]. The range includes mutants with average disease durations intermediate between these extremes. These are however averages and there is considerable variation among patients with a given mutation. For instance, individuals with H46R mutations have been observed to have disease progressions as short as 5 years and as long as 47 years.[17]

Table 1.1: The SOD1 mutants studied in this project, along with relevant statistics and information including: the average disease duration, the number of ALS patients that have been identified with the mutation, and the position of the mutation in the proteins structure.

Mutant	Average Disease Duration (years)[17]	Number of Patients [17]	Mutation Position[6]
A4V	1.2	205	β-1 (Dimer Interface)
G16S	N/A	N/A	β-2
G17S	N/A	N/A	β-2 (Dimer Interface)
G37R	17	27	Loop III
G41D	14.1	15	Loop III
G41S	1	16	Loop III
H43R	1.8	12	β-4
L84V	3.2	10	β-5
G85R	6	11	β-5
D90A	8	15	Loop V
G93A	3.1	16	Loop V
G93D	8.8	7	Loop V
E100G	4.7	50	β-6
L106V	1.9	6	Loop VI
I113T	4.3	38	Loop VI (Dimer Interface)
L144F	11.8	15	Loop VII
V148G	2.1	11	β-8 (Dimer Interface)
V148I	1.7	5	β-8 (Dimer Interface)

1.4.4 Wild type and pseudo wild type SOD1

Wild type SOD1 is the form of the protein found naturally in vivo, with no mutations. This form is useful for observing many characteristics such as the aggregation of the protein, however it is unsuitable for some thermodynamic studies. This is due to the necessity for a reversible folding process to obtain stability data through differential scanning calorimetry. The folding of SOD1 is not fully reversible due to the presence of two free cysteines at positions 6

and 111, which may form aberrant disulphide bonds upon denaturing and therefore not allow the protein to refold properly. In order to overcome this obstacle, in many previous experiments conducted by others[72], as well as some experiments described here, the protein is expressed without the two cysteines responsible, changing them to an alanine and serine respectively. This allows the protein to reversibly unfold, allowing for the collection of thermodynamic data. This construct has previously been shown to retain similar catalytic activity and thermodynamic stability compared to the WT as well as other mutant variations and is therefore referred to as the pseudo-wild type (pWT) SOD1, a model comparable to the wild type[40,73].

1.4.5 SOD1 aggregation

The aggregation of SOD1 with relation to ALS has been studied extensively both *in vitro* and *in vivo.* The work that has been published ranges from experiments conducted in *E.coli*, to human embryonic kidney cells, to live mice[19,39,74]. SOD1 aggregation is the major focus of this thesis and as a part of the complex system that is a cell, a few of the many ways to continue studying this protein are explored here. Previous studies have shown that there are many possible pathways by which SOD1 may aggregate, including from the native state, misfolded states, and oligomers, however, the mechanisms are unclear. It is possible that mutant SOD1 may aggregate alongside WT SOD1 which may be misfolded due to oxidative modifications. Some of these misfolded forms may bypass the proteasome or autophagy[49] and how SOD1 aggregates are involved in disease remains unclear.

Some who have focused on the aggregation of the protein in vitro include, from the Meiering lab, Stathopulos et al., Vassall et al. and Broom et al. [40,72,75,76] who have reported the formation of mutant SOD1 fibril type aggregates when the protein is destabilized. Although in

some cases IBs have been shown to exhibit structural characteristics of fibrils[33,34], and in vitro studies have provided information about SOD1 and many mutants, regarding the determination of aggregation propensities and aggregate metalation, in vivo studies also prove constructive.

In vivo studies have also been performed in multiple organisms, notably mice. Mice have been shown to exhibit the symptoms of ALS when fALS-associated mutants of SOD1 are overexpressed[28,77–79]. This makes them a good model for characterizing certain aspects of the disease and SOD1 aggregation. Mice models have various shortcomings though, including a long time period of development of disease (months in many cases), less mutations currently available, and relatively high cost. Therefore, cell culture models may prove to be more tractable in a number of ways, due to fast growth periods with large amounts of expression and, in the case of E.coli, a thoroughly studied host[80].

In terms of inclusion bodies specifically, Leinweber and coworkers, have observed the formation of IBs of A4V SOD1 in E.coli[39]. Also having provided some insight into IB's of SOD1 in mammalian cell cultures were Prudencio et al.[74], who have expressed multiple mutants of SOD1 in human embryonic kidney cells for the determination of aggregation propensities, however, with various important differences to this research, which will also be discussed further below. Finally, inclusion bodies produced in E.coli have been characterized in various ways by Furukawa, with a focus on the redox environment, a factor which is also very important when considering the experiments undertaken in this project[81,82]. All of the studies presented have been influential to the experiments conducted, and much of that work will be discussed in comparison to the results described in this thesis.

1.4.6 SOD1 metallation

The roles of both copper and zinc ions have been investigated in many studies of SOD1, including ones focusing on activity, stability and aggregation. Both metals affect the stability[40], but the metalation of the protein is a complex issue due to the processes that SOD1 may undergo to become metallated. The metal centres of SOD1 are described above in section 1.4.1 and the metals and associated residues are illustrated in Figure 1.5. Structural details have been determined but the mechanism by which metals are acquired are not fully understood. The production of fully metallated SOD1 in E.coli has been shown to require special attention; the lack of the copper chaperone for SOD (CCS) leads to the mismetallation of the protein[39]. Coexpression of the chaperone or another method of copper loading may be applied to increase the level of copper present in the protein[83]. As the metalation of SOD1 is of great interest for both SOD1 aggregation and function/dysfunction, the presence of metals and any characteristic pattern of metalation for mutants may have multiple important implications.

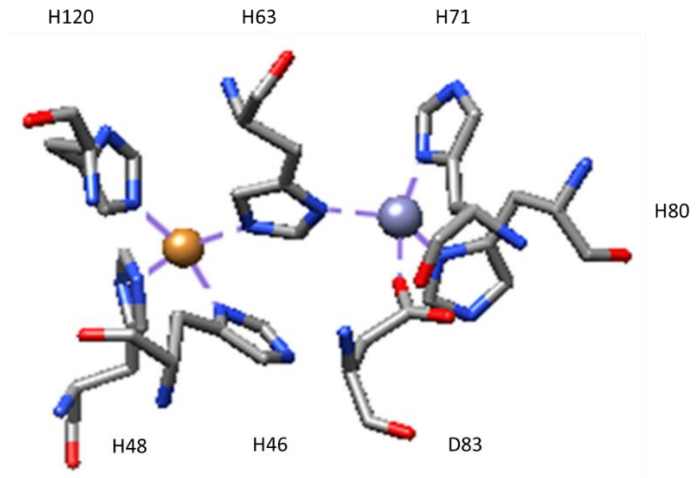

Figure 1.5: Metal centres of SOD1. The copper ion is orange and the zinc ion is blue. Bound to the copper ion are histidine residues H46, H48, H63 and H120. Bound to the Zinc ion are Histidines H63, H71, and H80 as well as aspartic acid D83. Note that Histidine H63 is shared between the two metal ions. Blue lines are nitrogen, red are oxygen, and grey is carbon.

The major chaperone associated with SOD1 in eukaryotic cells is CCS, although there may be others. This chaperone protein, found in the cytosol, assists in the delivery of copper to the protein.[83] The chaperone has three domains, the first is a copper binding domain structurally similar to another copper transporter ATX-1, which delivers copper to the secretory pathway. This first domain is one region of CCS responsible for metallating SOD, however is not absolutely required for SOD1 to gain copper. The second domain has a very similar structure to SOD1, but lacks a metal binding region. This second region is involved in recognition of the SOD1 target for metallation. The third and C-terminal domain is quite short, however, it has a copper binding region and unlike the first domain, is required for the chaperone to transfer metals to SOD1.[84] Although the human SOD1 has been shown to take up copper through an alternative glutathione pathway in yeast cells[85], it exhibits only 25-50% of the activity seen when CCS is present [85]. There has not been any chaperone identified for zinc and its mode of delivery to the protein is not known. It has been shown in previous studies that the amount of Zn in the protein varies depending on the expression system.[79,86]

The role of metals in IB formation by SOD1 has received little attention to date, and is of interest for numerous reasons. Given that SOD1 in many studies is purified in the soluble form before experimentation discerning the metalation characteristics of the mutants, an open pathway of experimentation is the observation of metalation in mutant SOD1 aggregates formed in vivo, in this particular case, without the copper chaperone, which may lead to various partially metallated states[39]. This may also provide insight into the general characteristics of inclusion bodies. As mentioned in section 1.2.2., residual activity of inclusion bodies may be of interest for a large variety of reasons. Since such a large portion of proteins are metalloproteins, expanding our knowledge of inclusion body metalation could be key to their effective use in functional

applications. Two methods of metal analysis will be used here, specifically a recently developed procedure using the chelator 4-pyridylazo resorcinol (Figure 1.6), and inductively coupled plasma atomic emission spectroscopy, both of which have been used to measure the metalation of SOD1 previously[87–89].

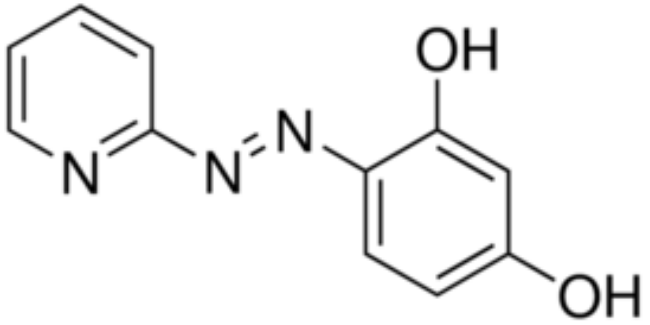

Figure 1.6: Molecular structure of 4-pyridylazo-resorcinol (PAR). A metallochromic indicator, the molecule consists of a heterocyclic nitrogen group, an azo group, and an orthogonal hydroxyl group[90].

PAR is a metallochromic indicator for a number of metal ions. When free of metal ions in solution, PAR has a maximum absorbance at approximately 416 nm.[91] When bound to metals, the absorbance shifts to a longer wavelength creating a shoulder peak. The maximum of the shoulder depends on the metal bound. Spectrophotometrically, the concentration of a metal in solution can be determined by the PAR-metal complex absorbance.[89,91]

1.5 Research objectives

Following extensive SOD1, research described in this thesis aims to expand our knowledge of mutant SOD1 aggregation in cells, using IB formation in *E.coli* as a model system. New information can be discovered which will complement the work of others, and lay a foundation for continued research. Here, the aggregation propensity of a set of chemically

diverse mutations distributed throughout the structure of SOD1 (Figure 1.7) are characterized. New characteristics will be revealed and may be compared to other information known about the mutations such as thermal stability, kinetic folding rate, and disease duration. It may also improve aggregation propensity prediction algorithms. By observing the metal status of the aggregates produced, a more detailed picture of the effects of mutations on SOD1 folding and metal binding can be developed.

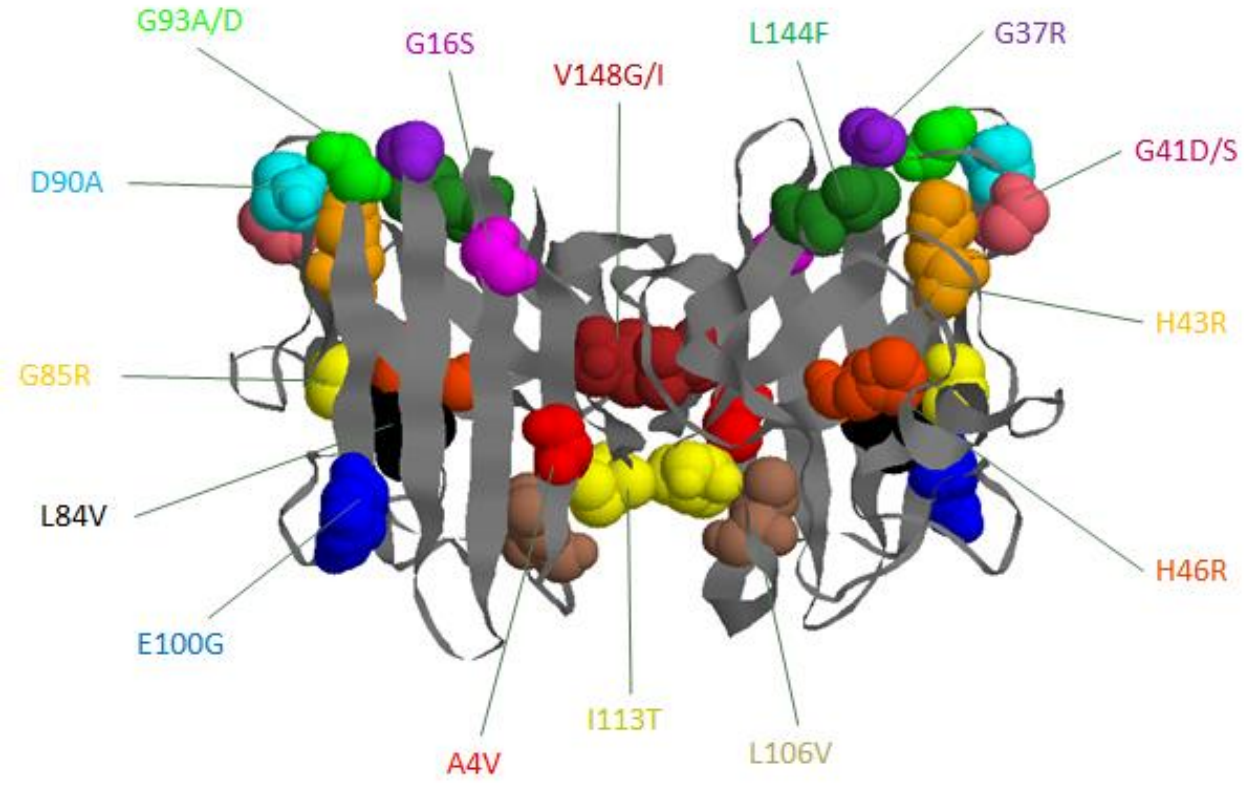

Figure 1.7: Ribbon diagram depicting the SOD1 dimer with sites of mutations expressed in this project highlighted as space filling residues. Each mutation location can be seen on each subunit of the protein. Figure adapted from Strange et al.[92] PDB No. 2C9V

2.0 Methods

2.1 Pseudo wild type (pWT) SOD1 expression and purification

ALS-associated mutations in a pseudo wild type (pWT) background were prepared using the pHSOD1ASlacIq vector (A pBR322 derivative) in an E.coli cell line, known as $SOD^{-/-}$ cells, devoid of the bacterial manganese and iron superoxide dismustases[93]. Cells were transformed as described by Miller[94] with electroporation using an Eppendorf Eporator electroporation apparatus. $SOD^{-/-}$ cells stored in glycerol at -80°C were thawed and placed on ice. In a 0.1 cm electroporation cuvette, pre-chilled on ice, 40 µL of cells were mixed with 1 µL of a diluted DNA stock (5µg/mL). The cells were then electroporated at 1.80V. The cells were immediately suspended in 1 mL of sterile growth media containing tryptone, yeast extract, NaCl and glucose, then transferred to a tube and incubated at 37°C in an Isotemp Incubator (Fisher Scientific) for an hour. The cells were then concentrated by centrifugation ~0.9 mL of the supernatant was removed, the cells were resuspended and plated on LB-agar plates supplemented with chloramphenicol (30 µg/mL), ampicillin (100 µg/mL), and kanamycin (30 µg/mL), then once again placed in the incubator to grow overnight at 37°C.

A single colony was taken from the plate and used to inoculate 5 mL of LB broth supplemented with antibiotics, chloramphenicol (30 µg/mL), ampicillin (100 µg/mL), and kanamycin (30 µg/mL). The tube was incubated overnight at 37°C and at 200 rpm in an Innova 4330 refrigerated shaker (New Brunswick Scientific). The next morning, 1 mL of the overnight culture was transferred into a 4 L flask with 1 L of sterile 2TY media (16 g/L Tryptone, 10 g/L yeast extract, 10 g/L NaCl in water) with the same antibiotics, chloramphenicol (30 µg/mL), ampicillin (100 µg/mL), and kanamycin (30 µg/mL). These cultures were incubated in the shaker

until the optical density (O.D.) at 600 nm reached between 0.6 and 0.8. At this point, the cultures were induced with 0.25 mM isopropyl-β-D-thiogalctopyranoside (IPTG), and both $CuSO_4$ and $ZnSO_4$ were added to final concentrations of 0.5 mM and 0.01 mM respectively. The cultures were incubated with shaking for a further 8 hours.

Once the cells had been expressing SOD1 for 8 hours, they were transferred to 500 mL centrifuge bottles and pelleted by centrifuging at 4000g for 15 minutes at 4°C in a Beckman Coulter Avanti J-E centrifuge; the supernatant was discarded. An osmotic shock procedure adapted from Liochev et al.[95] was used to obtain the periplasmic fraction. The cells were resuspended in 150 mL of 20 mM Tris at pH 7.5, 120 mL of 40% Sucrose, and 18 mL 250 mM ethylenediaminetetraacetic acid (EDTA). For some experiments, the EDTA solution was replaced by a nitrilotriacetic acid (NTA) or Diethylene triamine pentaacetic acid (DTPA) solution, the reasons for which will be described further in Section 4.4.1. The cells were gently shaken for 20 minutes on ice before being centrifuged again at 4000g for 25 minutes. The cell pellet was resuspended in 120 mL of MilliQ water and shaken again on ice for 20 minutes. The cells were finally centrifuged at 4500g for 45 minutes and the supernatant removed, flash frozen in liquid nitrogen and stored at -80°C.

. The supernatant recovered from the osmotic shock was thawed and diluted in 20 mM Tris pH 8 and MilliQ water. Copper sulphate solution (100 mM) was added to a final concentration of 1.4 mM and the solution was heated in a 70°C water bath for 20 minutes. The tubes were cooled slowly at room temperature and the precipitate was centrifuged at 10000 g for 20 minutes. Ammonium sulphate was added to the supernatant 30% w/v. The supernatant was then loaded onto a Waters column packed with Poros 20 micron HP2 resin using a Bio-rad Biologic Duo Flow chromatography system. A gradient program is run from 25% ammonium

sulphate to 45%. While observing the UV scan of the eluate, the fractions with any significant absorbance signal were collected and analyzed for SOD1 content by SDS-PAGE. The fractions containing SOD1 were pooled and dialyzed using 12-14 kDa Spectra/Por against 4 exchanges of MilliQ water. The protein solution was concentrated by ultrafiltration using a 10 kDa YM10 (Amicon) membrane. Once concentrated to 3-10 mg/mL the solution was filtered using a 0.2 µm filter, flash frozen in liquid nitrogen and stored at -80°C. The concentration was determined by measuring the absorbance at 280 nm using a monomeric molar extinction coefficient of 5400 M^{-1} cm^{-1},[96] and the purity assessed by SDS-PAGE (15%), using the procedure in Section 2.3.

2.2 pWT activity and melting temperature assays

Multiple assays were conducted to assess the metallation purified samples of pWT mutants of SOD1. These included a pyrogallol assay (adapted from Marklund and Marklund)[97] to determine the activities of each mutant and differential scanning calorimetry (DSC) to determine the melting temperatures. The pyrogallol assay was conducted by initially generating a reference scan using bovine liver catalase in potassium phosphate buffer (50 mM, pH 7.5), with 8 mM pyrogallol, and assay buffer (50 mM Tris, 1 mM DTPA, pH 8.2). The solutions were brought to 25°C before mixing, once mixed in a polystyrene cuvette, the absorbance at 420 nm was measured for 2 minutes. Once the reference scan is obtained, an inhibition scan is generated by mixing catalase with the assay buffer, then adding a volume of the purified SOD1 solution and measuring at 420 nm for 2 minutes. The concentration of SOD1 to add is determined by trial and error to achieve approximately 50% inhibition of the activity.

Samples were prepared for DSC by mixing the purified SOD1 solution with Hepes buffer (20mM) and water. A reference solution containing the flowthrough of the proteins

concentration is also prepared. Both the sample and the reference solution are degassed before use. The DSC experiments were conducted on a VP-DSC microcalorimeter. The scans began at 25°C and ramped up at a rate of 1°C/minute to a maximum of 100°C. The resulting data was taken to be analyzed using Origin software (OriginLab Corp.). After the subtraction of the refolding transition from the unfolding transition, the peak of the endotherm and melting temperature T_m was determined.

2.3 Mutant SOD1 in wild type background expression and sample preparation

ALS-associated mutations of SOD1 were generated in the wild-type background, and expressed using the pET 21 vector together with the pLysS vector in the BL21 DE(3) E.coli cell line[98], kindly provided by W. Colón. The pET vector encoded for SOD1 as well as the production of β-lactamase to provide ampicillin resistance. The pLysS plasmid encodes for the production of T7 lysozyme, which lowers background expression of target genes under control of the T7 promotor. The pLysS plasmid also confers chloramphenicol resistance. The cells were prepared two different ways, one smaller scale procedure was used for the determination of the SOD1 aggregation propensities described in Section 2.3, the other preparation, on a larger scale, was used to produce SOD1 for experiments for analyzing the metalation state of SOD1 inclusion bodies, described in Section 2.4.

For the small scale production, the cells were grown from cell stocks by using the frozen cell stock to directly inoculate 10 mL of LB media supplemented with 100 µg/mL Ampicillin and 30 µg/mL chloramphenicol. The culture was then grown at 37 °C shaking at 200 rpm overnight, then a portion of this overnight culture was used to inoculate 50 mL of LB media containing the same final concentrations of antibiotics as the starter cultures. These flasks were

incubated with shaking at 25°C. When the cultures reached an optical density at 600 nm (OD_{600}) between 0.7 to 0.8, IPTG was added to a final concentration of 0.1 mM. The flasks were then incubated at the same temperature and shaking speed for 4 hours. Samples of 1 mL were taken before the induction, at 2 hours of induction and at 4 hours of induction. These samples were run on an SDS PAGE gel to observe the expression over time. After the results of the first expression experiment were obtained, the sampling times were adjusted to be at 4 h, 6h, and 24h of induction time.

The 1 mL samples were centrifuged using an Eppendorf microcentrifuge at 12000 rpm for 2 minutes and 970 µL of supernatant was discarded. The cell pellet was then resuspended in the 30 µL of remaining media and 10 µL was removed for analysis as the whole cell fraction. The remaining 20 µL was then centrifuged again at 12000 rpm for 2 minutes. The supernatant was discarded and at this point the cell pellets were usually frozen at -80° C. When preparing the pellet for lysis, the pellet was resuspended in 30 µL of 10 mM Tris, 100 mM NaCl, and 0.1 mM EDTA (TEN buffer) at pH 8.

The lysis of the small fractions involved a series of freeze-thaw cycles. For the first freeze-thaw, the Eppendorf tube containing the sample was placed in liquid nitrogen for one minute, followed by placing it in a 37°C water bath for 5 minutes. Lysozyme and DNase1 were then added to the sample and the tube incubated in a refrigerator at 4°C for one hour. Finally, the tube was subjected to two additional freeze-thaws by the same method as the first. The sample was centrifuged at 12000 rpm for 10 minutes, then the supernatant was removed and analyzed by SDS-PAGE as the soluble fraction. The insoluble portion was resuspended in another 30µL of TEN buffer. To prepare the samples for gel electrophoresis, 15 µL of each of the soluble and insoluble fractions was mixed with 15 µL of gel loading buffer, and then mixed with 3 µL of 2-

mercaptoethanol (BME). The samples were then boiled for 10 minutes and immediately centrifuged at 14000 rpm for 1 minute. The 10 µL whole cell fractions were prepared at the same time, using 10µL of loading buffer and 2 µL of βME, boiled and spun as above.

The 12% SDS-PAGE gels were made and 10 or 15 µL of each sample was loaded in its respective well; initially the gels also included a lane with MW standards and they always included a 10 µg standard of previously purified pWT SOD1, necessary for densitometry calculations. The running of the gels is described in the next section. Variations of this cell growth protocol for sample preparation included cells grown in minimal media to observe metal free aggregation propensities, as well as expressing the proteins in LB at 37°C or 18°C to observe the effect of temperature on aggregation.

The metal analysis experiments required much more protein and so, the larger scale growths mentioned above were necessary. Following the same initial overnight growth period, the starter cultures were used to inoculate 1L of LB media in 4L Erlenmeyer flasks supplemented with chloramphenicol and ampicillin, which were then grown at 25°C to an optical density between 0.6-0.8 at 600 nm. IPTG was added to a final concentration of 0.1 mM and the growth was continued overnight. The cells were harvested the next day by centrifugation at 5000 g in a Beckman Coulter Avanti J-E centrifuge. For each litre of cells collected, the pellet was then resuspended in 15 mL 20 mM Tris/100 mM NaCl buffer pH 7.1.

The resuspended cells were then lysed using an Avestin Emulsiflex E5 emulsifier. The lysates were passaged three times using a minimum pressure of 17000 psi. The samples were centrifuged at 20000 g for 25 minutes at 4°C. The supernatants were discarded and the pellets were resuspended in a 0.5% (v/v) Triton X-100 solution, mixed and incubated for 30 minutes at

4°C. This sample was centrifuged at 20000 g for 25 minutes and the washing step was repeated, then the pellet was resuspended in 20 mM Tris, 100 mM NaCl, pH 7 buffer followed by centrifugation at 20000 g for 25 minutes to remove any residual Triton X-100. The pellets were flash frozen in liquid nitrogen and stored at -80°C until metal analysis, described in section 2.4 below.

2.4 Analysis of soluble protein expression in *E.coli* by gel densitometry

Electrophoresis was performed using a Hoefer Mighty Small II and Fisher Scientific power source gel running system at 120 V. The 12% SDS-PAGE gels were run for a time of approximately 2 hours and thirty minutes. Once the electrophoresis was completed, the gel was stained using Coomassie Brilliant Blue (62.5% MilliQ water, 30% methanol, 7.5% Acetic acid, 1 g/L Coomassie Brilliant Blue), then destained in 62.5% MilliQ water, 30% methanol, 7.5% Acetic acid, with rotation and a kimwipe to absorb excess dye.

Images of the gels were obtained using either a BIS303PC gel documentation system or an Alpha Innotech FluorChem FC2 imaging system, and analysed using the Total Lab TL100 analysis software, using the 1D gel analysis function. Lanes were manually defined as were the SOD1 bands. Once this was complete, the standard pWT band was labelled with the known amount added (typically 10 µg) and the program normalized the values based on pixel density to obtain the mass of protein in the sample SOD1 bands. The background density of the gel itself was subtracted using a "rolling ball" method which involves the program determining peak limits by using a moving baseline. In the rare case that the software was unavailable for use due to the facilities computer maintenance, the program ImageJ[99] was also used to determine the

relative pixel densities of bands on a gel, with the primary difference being that baseline of the band was determined manually.

2.5 Determination of SOD1 aggregation propensity

Once the amount of protein from the soluble and insoluble fractions of a given sample was known, they were compared. The total amount of SOD1 was determined by adding the amounts for the soluble and insoluble fractions together. The proportion of the protein that was soluble was then determined by comparison to the total (Equation 2.1).

$$\left(\frac{mass\ of\ SOD1\ in\ supernatant}{(mass\ of\ SOD1\ in\ supernatant + mass\ of\ SOD1\ in\ pellet)}\right) * 100 = \%\ of\ SOD1\ which\ is\ soluble$$

Eq. 2.1

The percentage of SOD1 which was soluble was used as the measure of aggregation propensity. Therefore, those with a lower percentage soluble given the same conditions had a greater propensity to aggregate.

2.6 Analysis of metal content of SOD1 inclusion bodies

The washed inclusion bodies were analyzed for metal content using two different methods: 1) a spectrophotometric assay using the chelator 4-pyridylazo-resorcinol (PAR), and 2) inductively coupled plasma atomic emission spectroscopy (ICP-AES). The former method was optimized for pWT and mutant SOD1s in the Meiering lab by a previous student[100]. The PAR assay utilizes a denaturant to initially unfold the protein and release bound metal to the chelator. The latter experiments required optimization including acid digestion to prepare the protein for the ICP instrument.

2.6.1 PAR assay for metal analysis of inclusion body samples

Necessary solutions for the assay were prepared beforehand, these included 8 M Guanidine Hydrochloride, a 400µM 4-pyridylazo-resorcinol working stock solution in 200 mM HEPES pH 8, 25 mM $CuSO_4$ and $ZnSO_4$ standard solutions and the sample solutions, consisting of Triton X-100 washed SOD1 mutant inclusion bodies. Inclusion bodies resuspended in 20 mM Tris/ 100mM NaCl buffer were added to the 8M guanidine hydrochloride solution and were left to unfold for at least an hour, as this was the average time at which brown inclusions were no longer observed and light scattering was not further reduced by extending the time.

When the unfolding was considered to be complete, PAR solution was mixed with the guanidine/protein solution or a guanidine/metal standard solution in a cuvette. The samples were scanned from 200 to 700 nm using a Cary 300 Bio UV/Visible spectrophotometer. The data were then analyzed using the program SpLab, developed by Dmitri Davydov (University of California San Diego) for spectral decomposition[101]. The two standard solutions spectra were used to calculate the portions of the protein spectra comprised of those metals and therefore the concentrations of those metals in their respective protein samples.

2.6.2 Inductively coupled plasma atomic emission spectroscopy metal analysis of inclusion body samples

Sample preparation for the ICP-AES instrument calls for the sample to be fully soluble so it does not clog or stick to any tubing the instrument uses. The solubilising of the inclusion bodies was achieved by acid digestion. Samples of inclusion bodies resuspended in MilliQ water (5 mL) were placed in volumetric digestion vessels (Environmental Express) and concentrated Nitric acid (70%) was then added (at least 5 mL). Reflux caps were placed on the tubes and they

were then put in an aluminum block on top of a hot plate located in a fume hood and heated to approximately 100-105°C. The solution was refluxed for 3 hours, with more acid added if it was necessary to avoid the sample drying out. Once the samples were digested in the heating block, the tubes were removed and left to cool in the fume hood for approximately half an hour or until they were cool enough to hold. The volume was then made up to 20 mL using MilliQ water. The samples were filtered by plunging 2 µm FilterMate filters (Environmental Express) to the bottoms of the tubes. At this point, the tubes were capped. Controls were prepared in the same manner, along with a method blank lacking the inclusion body sample.

The High Dispersion Prodigy ICP-AES instrument (Teledyne Leeman Labs) was turned on and heated up to a temperature of 34°C the night before use to ensure a stable chamber temperature. The instrument is supplied a constant flow of nitrogen through an oxygen trap. The SALSA program was used to run the instrument and analyze data. Basic maintenance needs were dealt with as necessitated by the software, including making sure there was enough cooling liquid flowing in the instrument. Essential solutions prepared by the instrument technician (Ralph Dickhout, Chemical Engineering) were checked to make sure there are adequate volumes for the use of the instrument. These solutions included an internal standard solution of Yttrium (10 ppm), a rinse solution of MilliQ water, standard solutions of metals including Cu and Zn and also containing Na, Ca, Fe, K, Ni, Pb, Mn, and Mg in the same solution (although only Cu and Zn were measured), ranging in concentration from 3.2 mg/L to 160 mg/L for all metals, and a manganese peaking solution (10 mg/mL).

Once the instrument was ready to be used, Argon tanks were opened to supply the instrument and the flow rate was set to 1.0 L/min. The chiller was turned on and the standard solutions were placed in sample test tubes in a rack alongside tubes with rinse solution and the

manganese peaking solution. This rack was then loaded onto an autosampler. The inclusion body digests were then also loaded into test tubes in a rack and placed next to the standards. The samples were organized each time to avoid having the same samples next to each other, including the random placement of the controls and method blank to avoid any bias introduced by the preceding samples.

Once the samples were in place, the lines were locked against the pump. The method used was multiscan 20 IS in SALSA. The elements selected for measurements were Cu, Zn, and Y. The method was set to integrate 3 measurements of each sample. The plasma was started and the injector positioned to the manganese solution for peaking at 257.610 nm to detect the area of maximum ICP discharge and determine the optimum viewing angle of the ICP discharge. The instrument was then aligned to each of the standard metals using the 10 mg/mL solution, giving manual confirmation that each element's maximum emission was present on the detector. The sample sequence was then run and the autosampler pumped each standard and sample to the plasma flame and the emission at 324.754 nm (Cu) and 202.548 nm (Zn) was recorded.

The concentrations of the metals of interest were determined by the program from a curve of the standards (Cu and Zn at concentrations of 3.2, 9.6, 16, 32, 80, and 160 mg/L. An example of the quadratic fit used for the standard curve is shown in section 3. Results were given in ppm along with deviations and relative standard deviations. These values of metal content in the solutions were then corrected for dilutions and compared to the protein concentration values of the original solutions obtained using densitometry data to determine the level of metallation of the SOD1 inclusion bodies.

3.0 Results

3.1 SOD1 variants in pWT background

3.1.1 Protein expression and purification

The pseudo wild-type mutants produced included A4T, L38V, L84V, and D90A. After growing and purifying the cells as described above, the purity was assessed by SDS PAGE of the final product and the yield by the UV absorbance at 280 nm. In each case, the only band observed for the gels of the final purified fractions was that for SOD1 (Figure 3.1).The yields were adequate for completing all further experiments with all three mutants. When A4T was purified using various chelators in place of EDTA, the results had little variation. The experiment when conducted with NTA provided slightly less yield than those with EDTA and DTPA. However, all three were capable of assisting the osmotic shock process and provided protein for analysis in another students experiments analysing the metal content of these mutants.

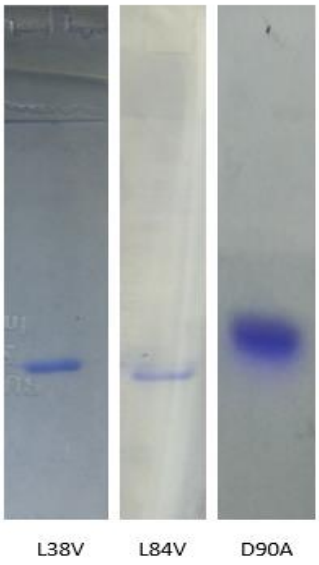

Figure 3.1: SDS-PAGE gel lanes of purified pWT SOD1 mutants. No contaminant proteins are apparent in the final solutions of purified protein.

To measure the activity of the purified protein, a pyrogallol assay was conducted as described in Section 2. The pyrogallol assays for the mutants all yielded similar results with activity (Figure 3.2) being close to that of the pWT SOD1 activity. The mutants had activities either higher or slightly lower than the typical pWT value of approximately 1800 units/mg[40]. The mutants D90A and L38V had activities of 2059.11 and 2053.33 units/mg respectively, while L84V was slightly lower at 1715 units/mg.

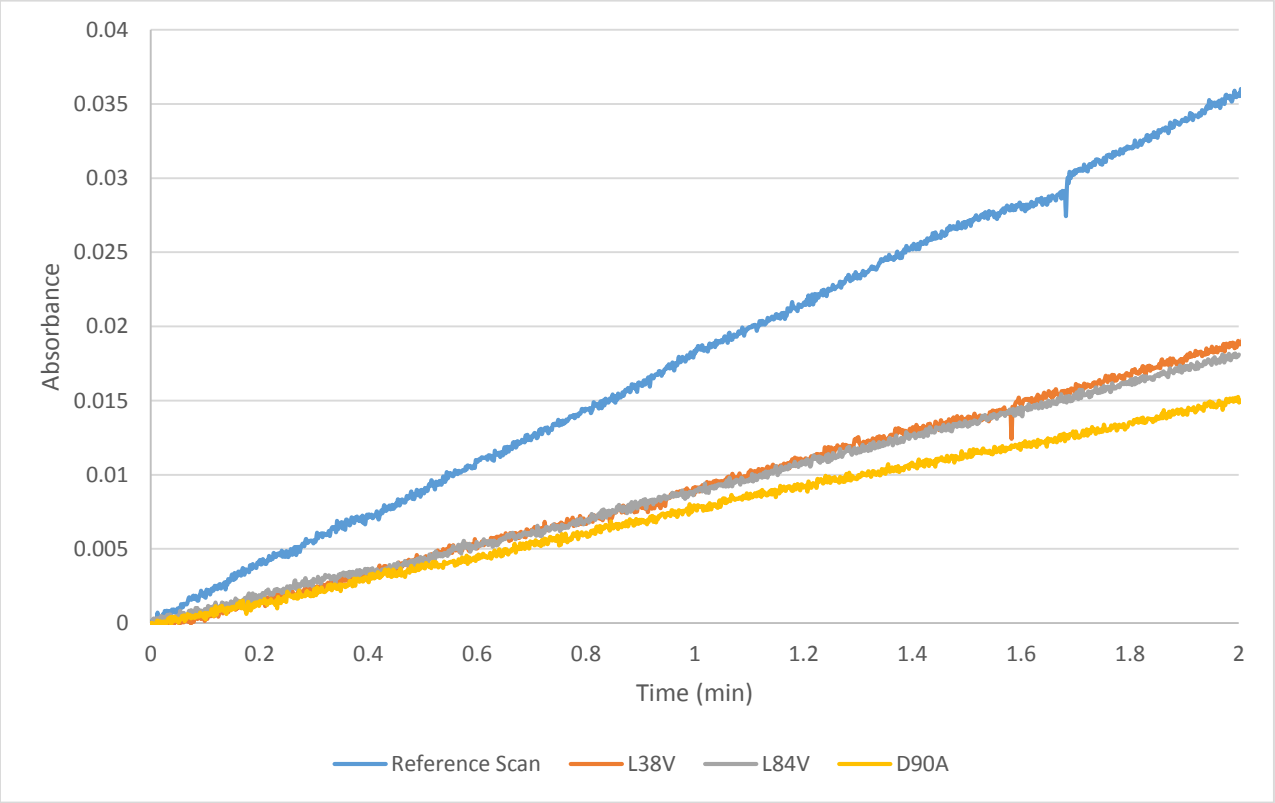

Figure 3.2: Kinetics scans of the pyrogallol assay reaction. An amount of each mutant was used to achieve an approximately 50% inhibition of the reference scan, meaning each mutant showed significant levels of activity in inhibiting pyrogallol oxidation. From this data, the level of activity of a given amount of protein was determined.

3.1.2 pWT mutant melting temperatures

Melting temperatures were measured using, differential scanning calorimetry for the mutants L38V and L84V. Adequate unfolding and refolding thermograms were obtained for both mutants (Figures 3.3 and 3.4). The most defined unfolding transition of the 20 Scans was taken and the following refolding transition subtracted. Apparent melting temperatures were taken from the peak of the endotherms for L38V and L84V. The apparent melting temperatures were determined to be 88° for L38V and 85° for L84V. The slight shoulder in the L38V thermogram may be due to some of the protein not properly metallated.

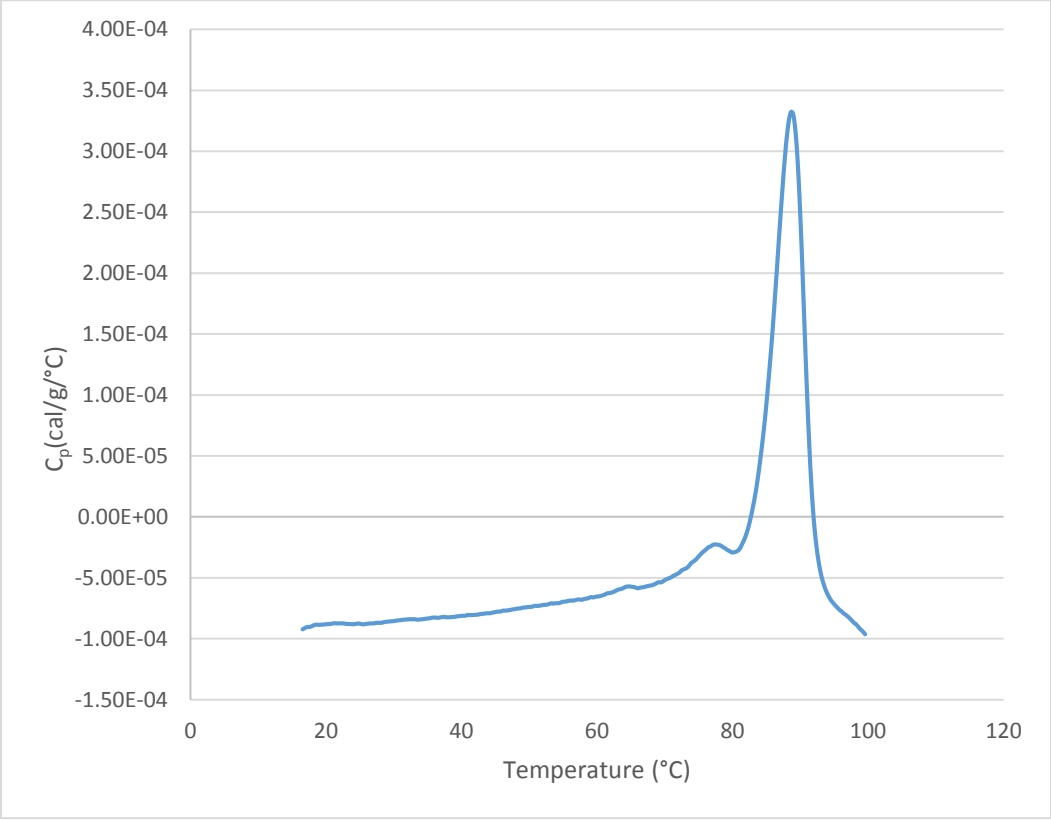

Figure 3.3: Differential scanning calorimetry thermogram of SOD1 mutant L38V (0.5 mg/mL) in 20 mM HEPES. The apparent melting temperature is 88°C.

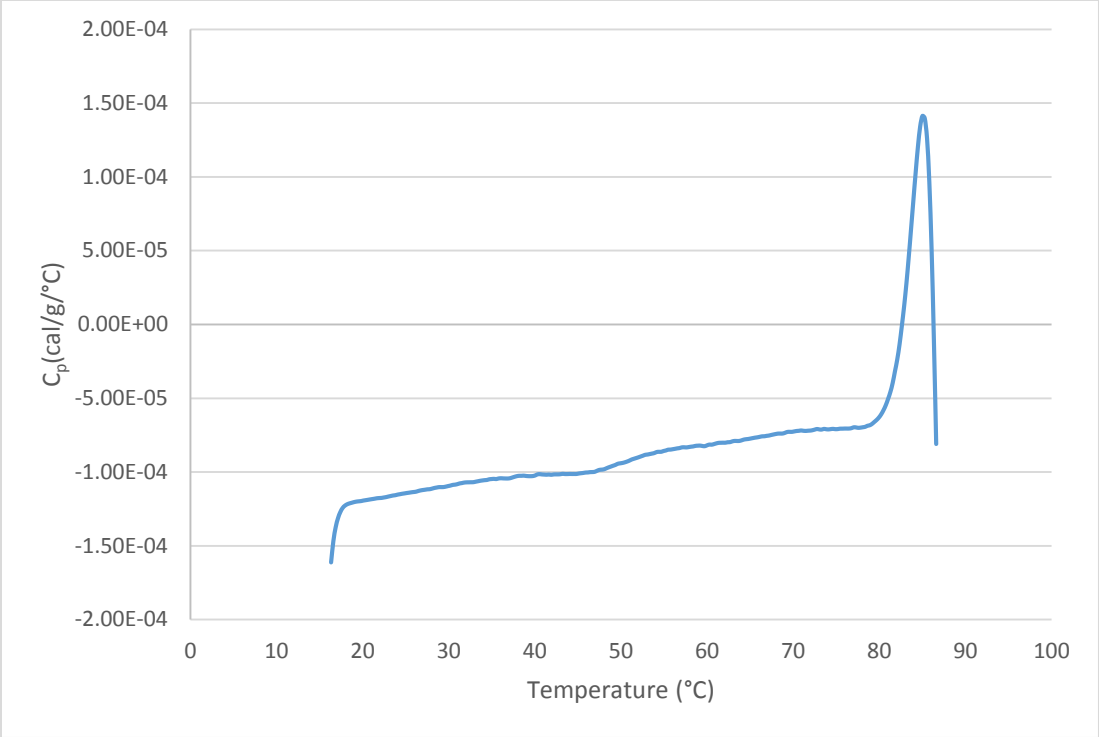

Figure 3.4: Differential scanning calorimetry thermogram of SOD1 mutant L84V (0.5 mg/mL) in 20 mM HEPES. The apparent melting temperature T_m was determined to be 85°C.

3.2 SOD1 variants in WT background

3.2.1 Expression of WT mutants

The expression levels of WT SOD1 and its mutants were all quite similar to each other, as determined by SDS-PAGE, throughout the experiments conducted. Representative results are shown in Figure 3.5. The expression time was optimized to yield a band of suitable intensity for quantitation by densitometry to be feasible with most mutants. The total amount of SOD1 produced was approximately 9 to 12 µg per mL of cell culture at the 4 hours of induction time point (25°C); from 10 to 15 µg/mL at 6 hours of induction; and from 15 to 20 µg/mL at 24 hours of induction. When grown in minimal media, the cells that were able to grow had greatly varying

amounts of growth and expression, with final SOD1 yields between 1 to 9 µg after 4 hours of induction, depending on the mutant.

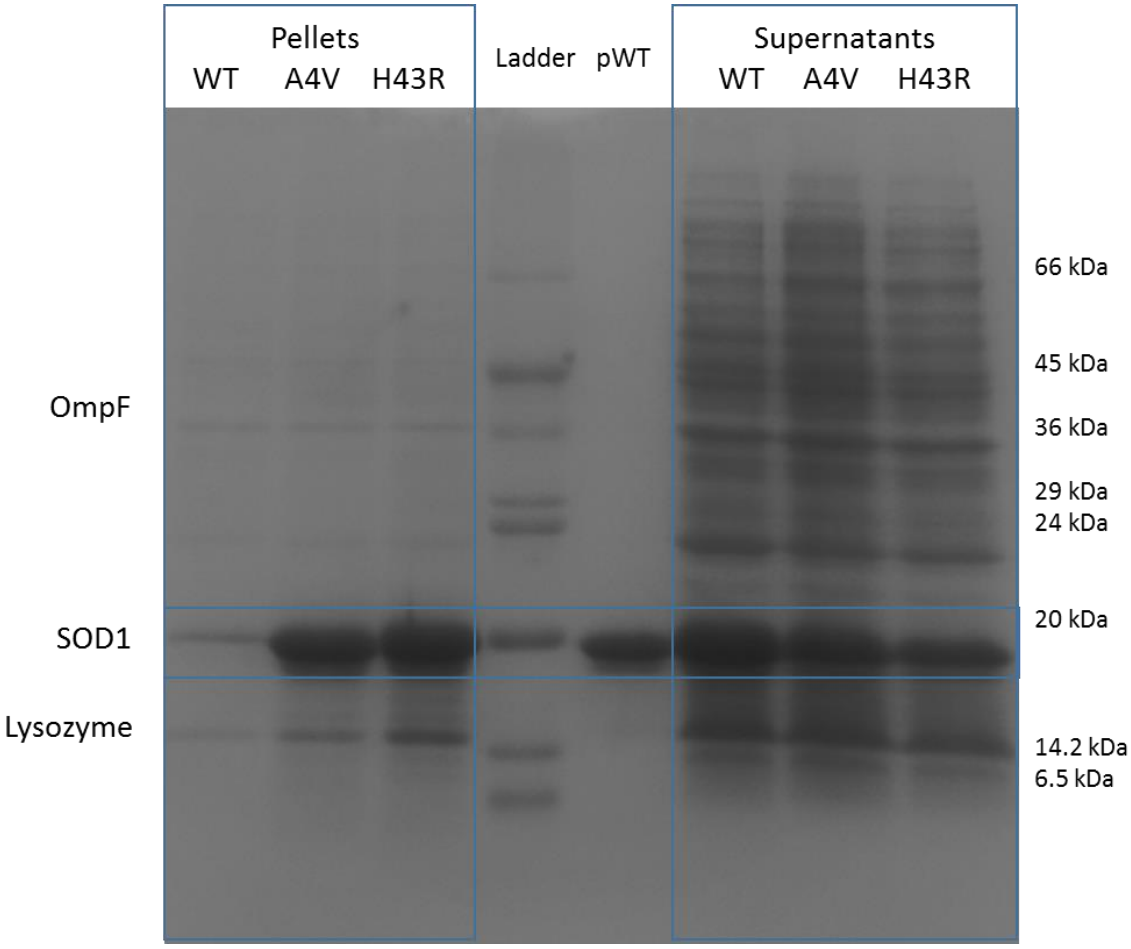

Figure 3.5: SDS-PAGE gel with pellet and supernatant fractions of three examples of SOD1 (WT, A4V, H43R), although the propensity of each to aggregate is different, the total expression of each was similar, based on the total SOD1 mass of supernatant and pellet fractions. The standard is purified pWT SOD1. Other significant sample components that can be seen here are lysozyme which is added during the lysis and what is likely the *E. coli* outer membrane protein OmpF[39].

3.2.2 Preparation of WT variants for metal analysis

The washings of WT mutants described in section 2, yielded varying results in terms of amount of protein and quality. When produced on a large scale, a variety of coloration in the inclusion bodies pellet could be observed. When washed with Triton x-100, minimal changes were seen in the final product when run on a gel (Figure 3.6). Very few bands (proteins) were removed during the washing process. However, the size and coloration of the pellet had changed, the pellet was slightly smaller and usually became a paler brown colour. The proportion of protein lost was usually qualitatively similar for all bands, therefore SOD would be lost to a similar extent as any other remaining proteins. The change in the size of the pellet, however, implies the removal of other fractions of the cell not visible by SDS-PAGE.

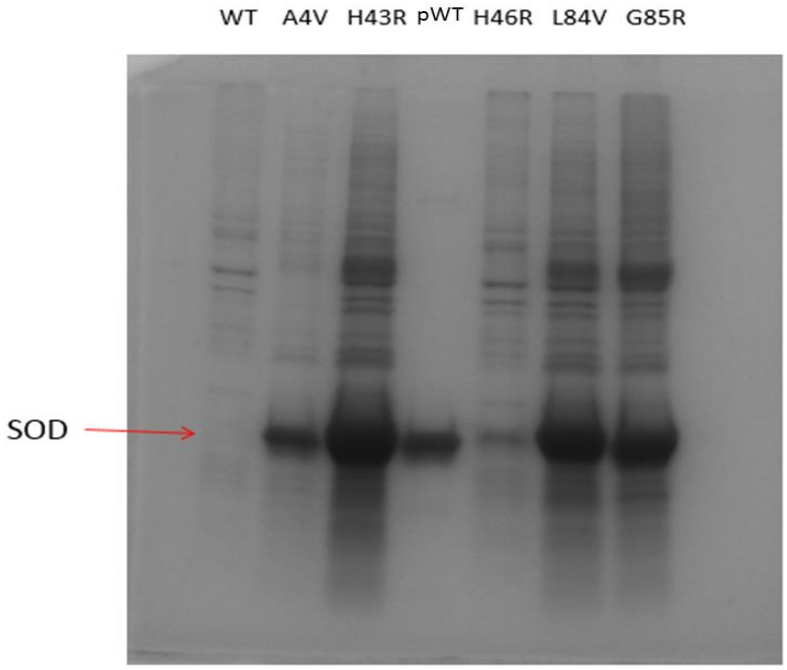

Figure 3.6: Gel of Triton X-100 washed pellets from *E.coli* cells expressing each mutant. Note the low level of SOD1 in the insoluble fractions of cells expressing WT SOD1 and H46R SOD1, two instances where SOD1 is largely found in the soluble fraction of the cell lysate. The standard sample of purified pWT SOD1 is 10 µg.

The inclusion body samples of WT SOD1 mutants described here contained predominantly SOD1 but also somewhat variable levels of contaminant proteins. Various steps were taken, however, to minimize contaminating proteins as well as separate the SOD1 from non-protein components of the cells. Several proteins with molecular weights of approximately 23, 36, and 37 kDa proved recalcitrant to removal; these may be outer membrane proteins, such as OmpF, which was identified in the similar experiments by Leinweber and coworkers.[39] Although attempts were made to eliminate OmpF from the samples, this protein was consistently observed in the inclusion body fraction. Various speeds of centrifugation (Figure 3.7) as well as other detergents (Triton X-100, NP-40, Deoxycholate, SDS) did not separate the OmpF from the SOD1.

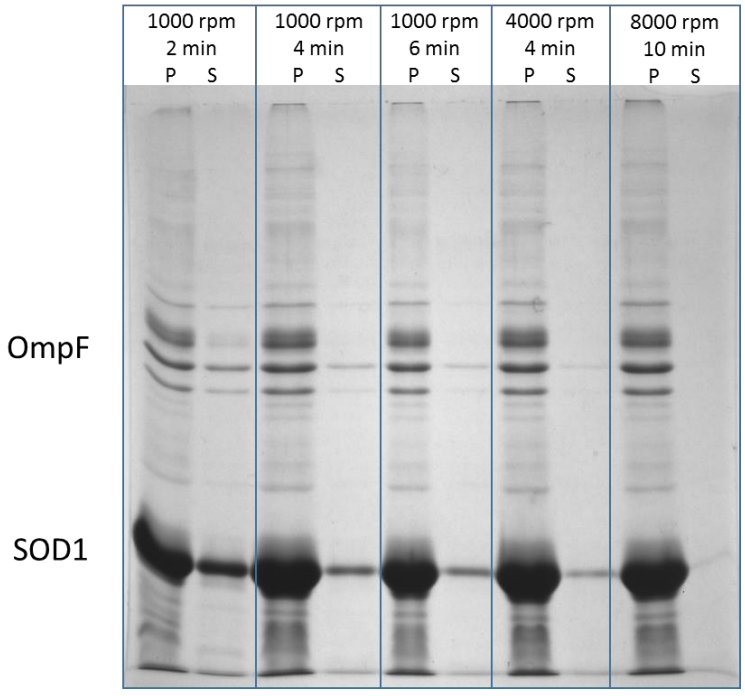

Figure 3.7: SOD1 mutant V148G inclusion body samples in TEN buffer, centrifuged at different speeds for various amounts of time to assess if the E.*coli* OmpF could be separated from the SOD1. At lower speeds, as more SOD1 is left remaining in the supernatant after centrifugation, more of the contaminant proteins are as well. P indicates the pellet fraction, S is the supernatant.

The fraction of insoluble material that was SOD1 in the large scale cultures, was variable depending on the mutant, and consistent with the results of the small scale aggregation propensity experiments below (section 3.2.3). The solubility of the SOD1 mutants when grown at 25°C in the small scale cultures, was consistent with the solubility when grown in the large scale cultures. The more soluble SOD1 mutants made up a smaller fraction of the total protein in the insoluble pellet compared to less soluble mutants, since there was a constant amount of other remaining proteins in the insoluble pellet.

3.2.3 WT variant aggregation propensities

Initially, six mutants were chosen for the investigation of aggregation propensities. These mutants were characterized using various methods to optimize the experimental conditions for quantitation of IB formation. At 37°C, all mutants with the exception of I113T were predominantly (>95%) insoluble. This made 4 of the mutants (A4V, H43R, L84V, and G93D) essentially indistinguishable in terms of their propensity to aggregate (Figure 3.8). When the growth temperature was reduced to 25°C, a greater range of aggregation propensity for mutants was observed (Figure 3.9). The variability in O.D. at the induction time was also reduced at 25°C relative to 37°C, where the induction time was more difficult to predict and keep consistent as the cell growth passes through the logarithmic growth stage quickly in small culture volumes. When the cells were grown at 18°C, however, the cell growth was variable and unpredictable, with some cultures not growing to the necessary levels for induction. If induction was successful at 18°C, it was also very low, and not suitable for densitometry.

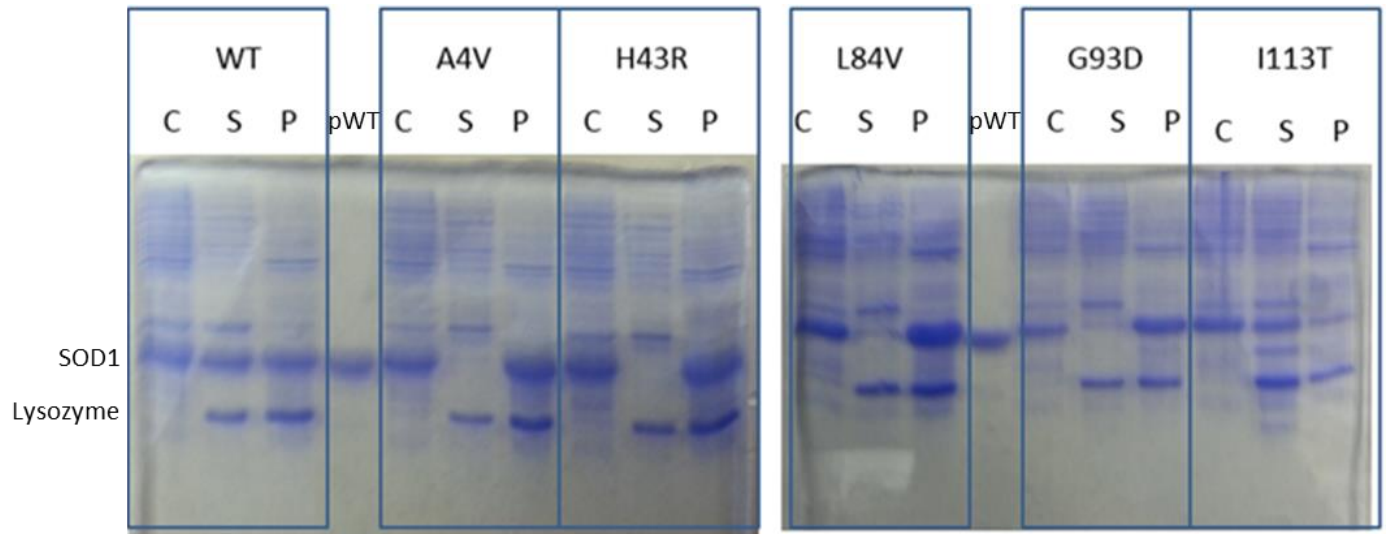

Figure 3.8: SDS-PAGE gels of whole cell (C), soluble (S), and pellet (P) fractions of *E.coli* cells expressing SOD1 mutants at 37°C for 4 hours. The majority of SOD1 is found in the pellet fraction with the exception of WT and I113T. The intensity of the band corresponding to SOD1 was quantitated with reference to the standard of 10 µg of purified pWT.

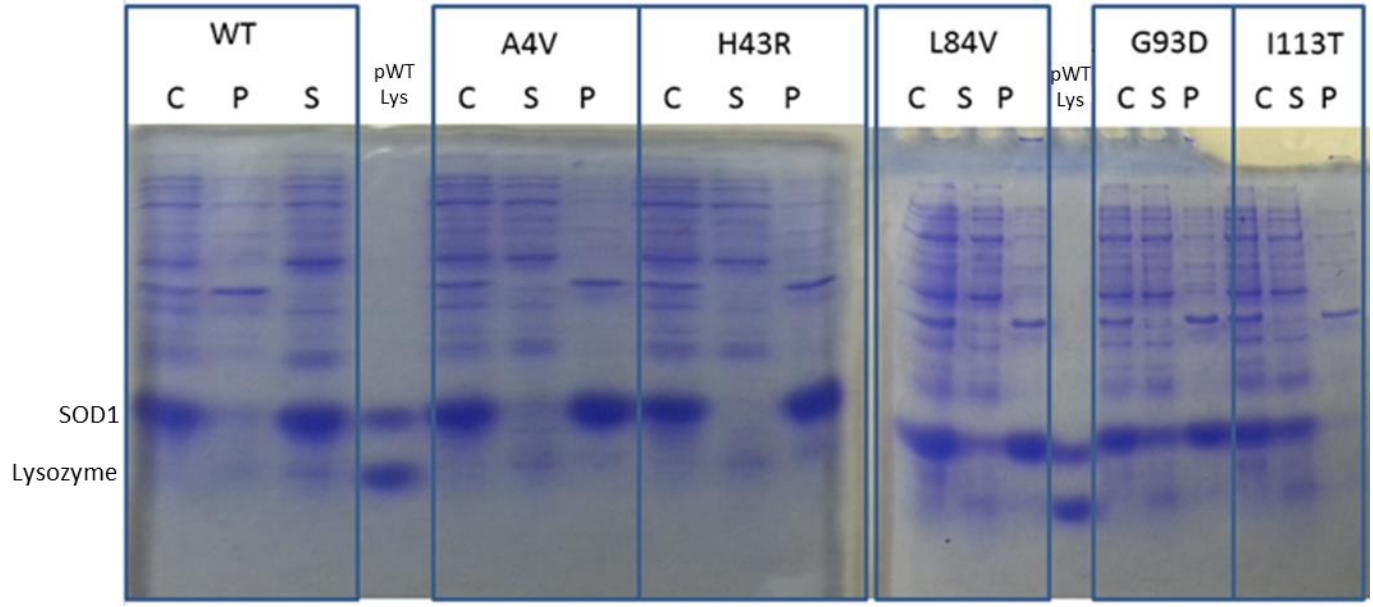

Figure 3.9: SDS-PAGE gels of whole cell (C), soluble (S), and pellet (P) fractions of *E.coli* cells expressing SOD1 mutants at 25°C for 4 hours. Mutants are more easily distinguishable by the fractions of soluble and insoluble SOD1 at 25°C compared to those grown at 37°C. The WT and I113T mutant are mostly soluble while G93D, L84V, and A4V have various amounts in either fraction and H43R is the most insoluble. The intensity of the band corresponding to SOD1 was quantitated with reference to the standard of 10 µg of purified pWT.

Initially, the final concentration of IPTG used was 1 mM in culture solutions, however it was of interest to see the effect that lowering IPTG concentration may have had on the solubility. IPTG concentration has been identified as a factor in the formation of inclusion bodies, since it is the molecule that initiates the over-expression of a non-native protein. By reducing the IPTG concentration in the growth procedure we can determine to what extent it affects SOD1 solubility.[102] The results (Figure 3.10) showed no clear change in solubility after a ten-fold decrease in IPTG concentration.

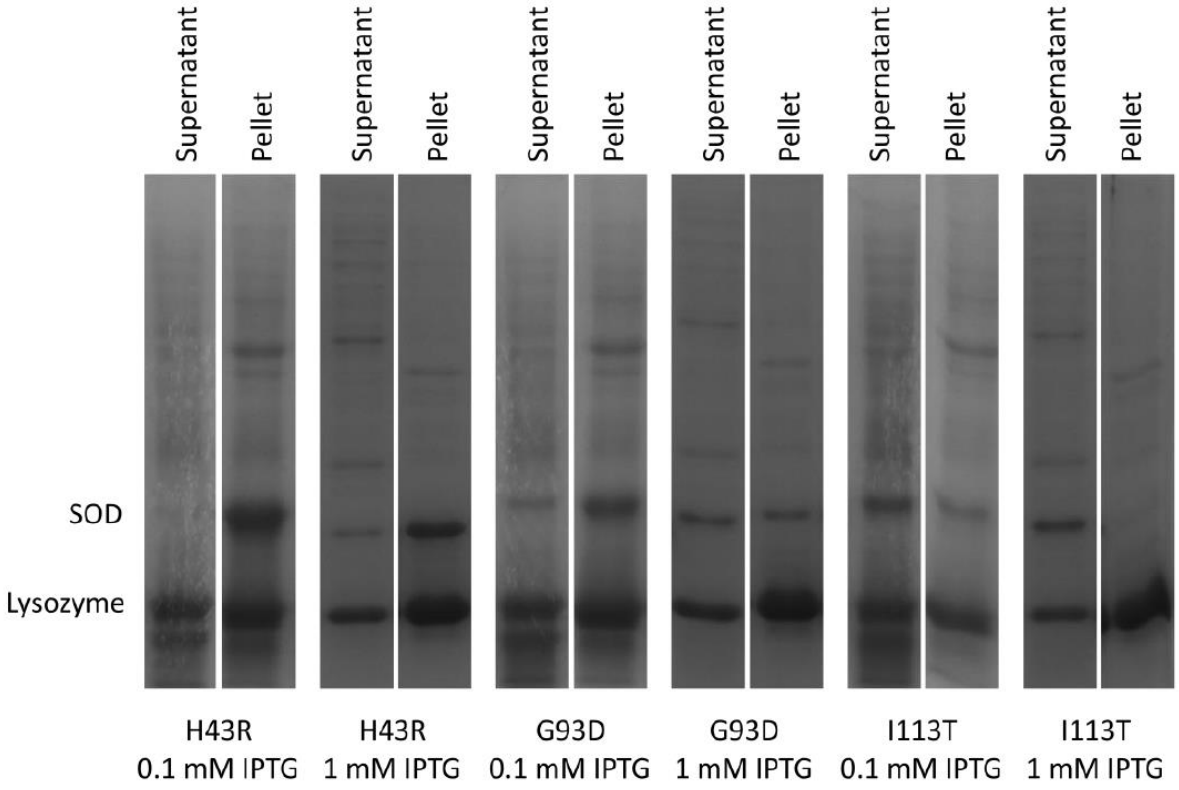

Figure 3.10: Cell lysate fractions of samples grown at 25°C with two different final concentrations of IPTG during induction, 0.1 and 1 mM.

In total, 19 mutants of SOD1 and the WT were analyzed for soluble expression at 25°C. The results of a minimum of 3 independent culture growths were averaged to determine the

aggregation propensity, with many more for some mutants. The averaged results for the aggregation propensities at 4, 6, and 24 hours of induction are illustrated in Figure 3.11 and listed in Table 3.1 along with other mutant properties which are compared to in section 4. Some independent cultures were also grown and analyzed by student Yi Yang, these values have been included in the data presented below.

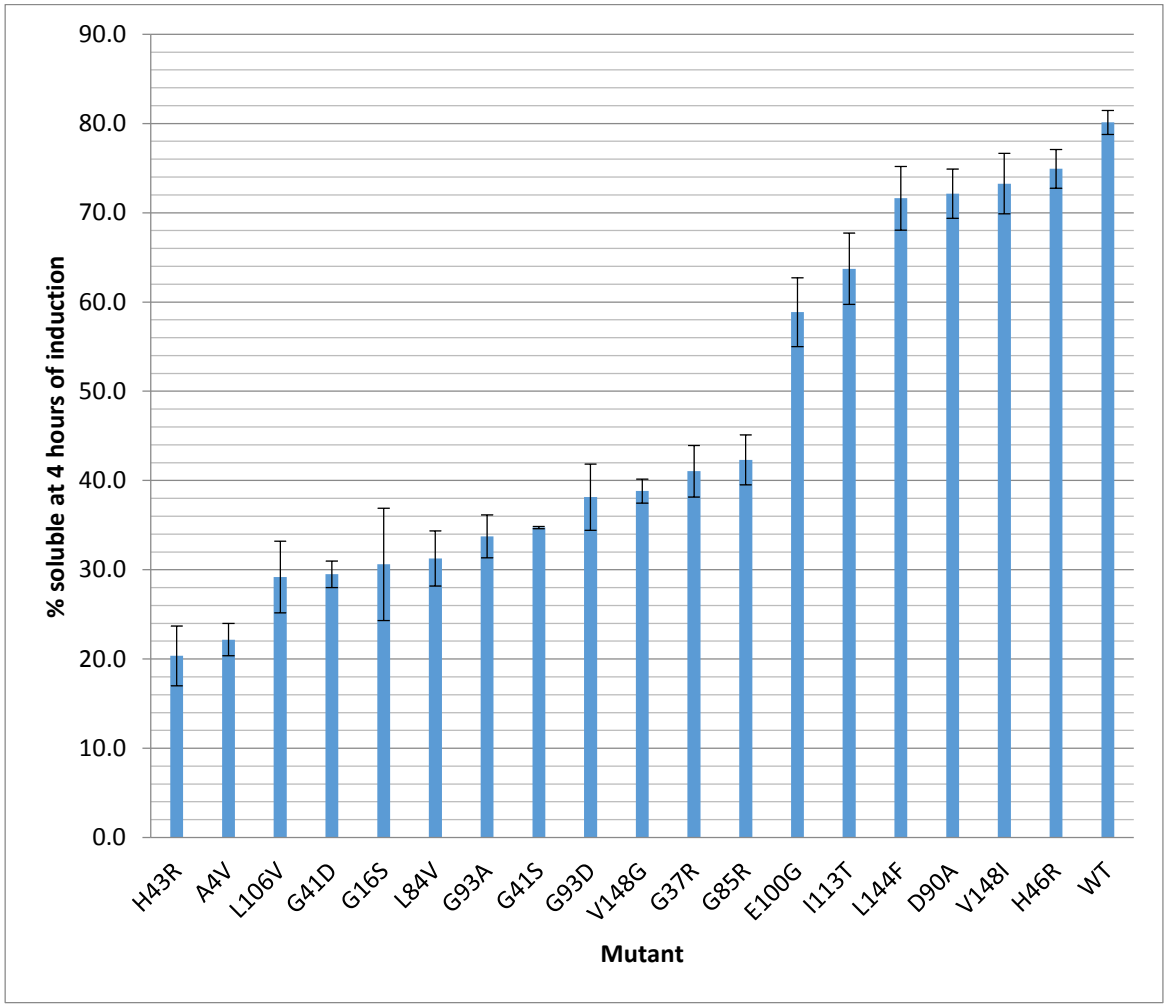

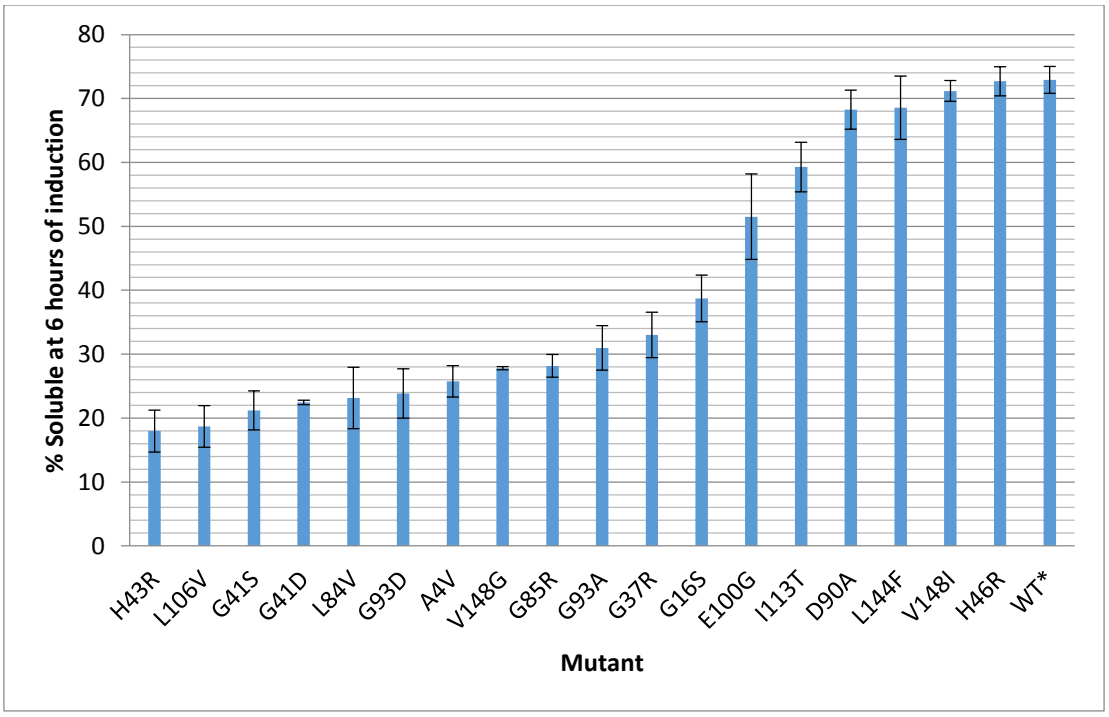

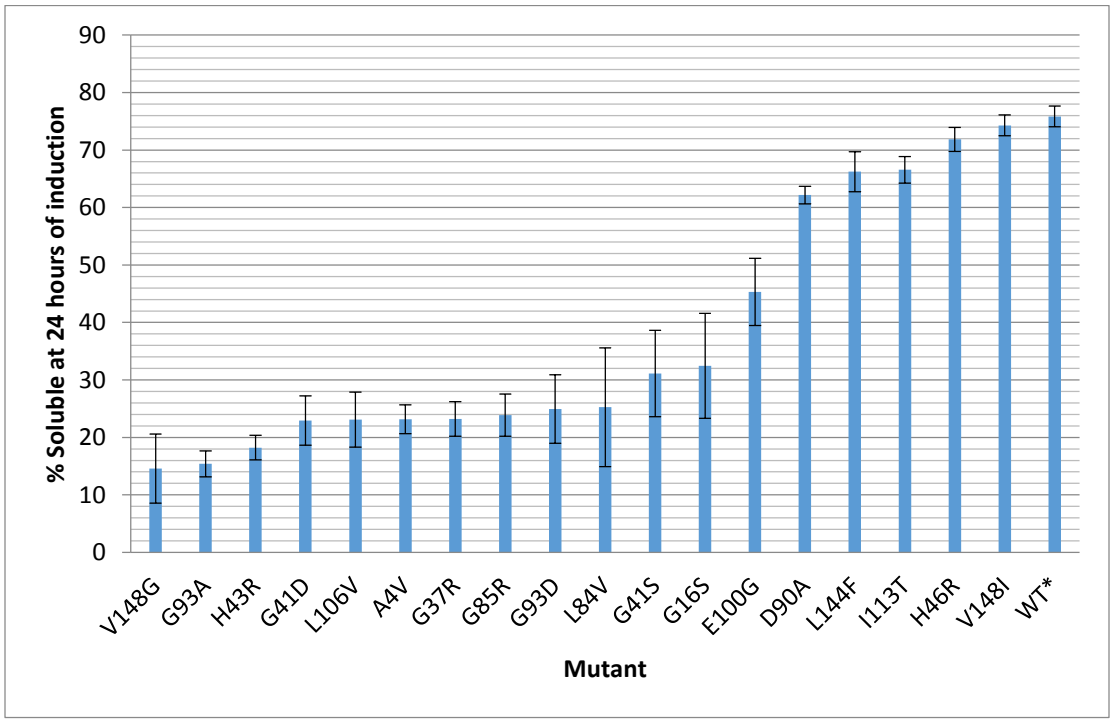

Figure 3.11: Average % soluble of SOD1 mutants at 4, 6, and 24 hours of induction (top, middle, bottom respectively) at 25°C. The error bars are the standard error of the mean for the replicate experiments. A higher % soluble means a lower propensity to aggregate. Some variation is seen between time points. A wide range of aggregation propensities were observed.

Table 3.1: The WT background SOD1 mutants average % soluble after 4 hours of induction at 25°C along with melting temperatures of the pWT background mutants in various metallation and disulphide statuses. Also included are folding rate constants. *includes some unpublished data.

Mutant	Region of Mutation	Avg. % Soluble	Holo T_m (°C)[87]*	Apo-Oxidized T_m (°C)[88]	Apo-Reduced T_m (°C)[75]	Folding rate constant k_f [103]
WT/pWT	N/A	80.11	92.7	59.1	47.6	0.04365
A4V	β-1 (Dimer Interface)	22.17	86.7	50.7	36.3	0.10715
G16S	β-2	30.61				
G37R	Loop III	27.01		50.1	33.5	
G41D	Loop III	41.04	86	45.2		0.04365
G41S	Loop III	29.50	84.4			0.01514
H43R	β-4	34.73	86.3	48.1	35.4	0.04365
H46R	β-4	20.36		55.6	52.6	0.04571
L84V	β-5	74.92				0.02399
G85R	β-5	31.26	77.5	54.7	40.7	0.02344
D90A	Loop V	42.30				0.02884
G93A	Loop V	72.13	87.7	47.9		0.04365
G93D	Loop V	33.74	85.1	45.6		
E100G	β-6	38.14	86.2	51.2	33.2	0.03090
L106V	Loop VI	58.85				0.01995
I113T	Loop VI (Dimer Interface)	29.20	88.2	47.1		0.02884
L144F	Loop VII	63.72				0.05248
V148G	β-8 (Dimer Interface)	71.62	86.9	49.3	34	
V148I	β-8 (Dimer Interface)	73.26	92.7	60.5	51	

In Figure 3.11, a clear trend is evident, with mutants exhibiting a spectrum of solubility when overexpressed in *E.coli*. Only minor changes in % soluble are observed between repeated experiments. The % soluble generally decreases from 4 hours to later time points and is usually around a 5% change. In all cases, the WT SOD1 has the lowest propensity to aggregate, with the largest fraction remaining soluble. At the 4 and 6 hour time points of induction, the mutant with the largest insoluble fraction and therefore greatest aggregation propensity is H43R. This changes at 24 hours of induction though, as V148G, becomes increasingly more insoluble with increasing time of induction, dropping from an initial % soluble at 4 hours of induction of 38%, to 14% at 24 hours. The experimental uncertainties may be a factor in this distinction; it is generally larger at the later time points, and for a few mutants (V148G, G93D, L84V, G41S, G16S and E100G).

3.4 Metal analysis of mutant SOD1 inclusion bodies

3.4.1 4-Pyridyl-azo-resorcinol (PAR) measurements of metal in mutant SOD1 inclusion bodies

In order to investigate if inclusion body formation was influenced by metal binding by SOD1 and to explore whether the aggregates may have metals necessary for activity, the metal content determination using a spectrophotometric PAR assay was explored. The first series of experiments using the PAR assay produced results that gave highly variable data when analysed, with seemingly no methodical reason. The initial unfolding procedure yielded a clear colorless solution with no particulates seen in the cuvette. This was consistent for all of the SOD1 mutant washed inclusion body preparations. When the 4-pyridyl azo-resorcinol was added to these solutions, various amounts of colour were seen, ranging from no change in the metal-free yellow

PAR, to orange and red. At this point all solutions still appeared to be clear, with nothing solid observed in the cuvettes.

The absorbance spectra obtained (Figure 3.12) exhibited a slight increase in signal beginning at ~330 nm and increasing with decreasing wavelength. This may indicate some scatter from particulate matter in the sample, however, this was highly variable for each mutant. As a control, samples, once mixed and scanned were transferred to a small tube, centrifuged, and then scanned again. After the centrifugation, nothing was observed at the bottom of the centrifuge tubes, so there was no reason to assume any large amount of protein was lost from the sample, or that there were residual inclusion bodies. This also did not affect the slight incline associated with the spectra. Thus, no sedimentable aggregates were apparent in this experiment

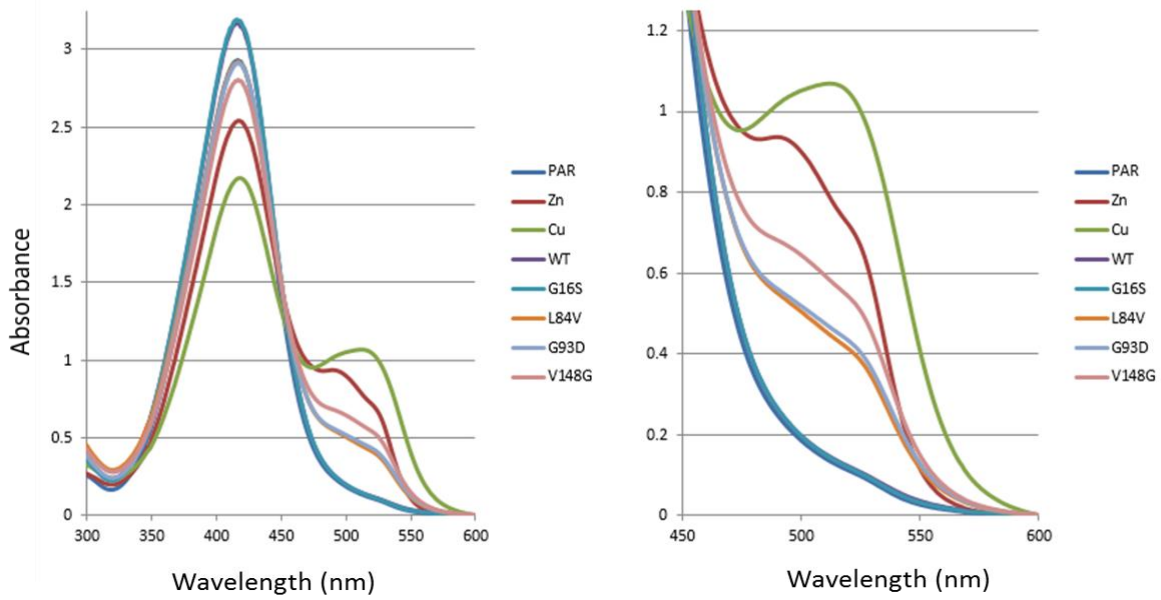

Figure 3.12: (Left) Spectra of PAR, metal standards complexed with PAR, and mutant SOD1 resolubilized inclusion bodies with PAR. All samples contained 90 µM PAR, 45 mM HEPES buffer, with varying concentrations of protein. The large peak between 325 and 475 nm is due to uncomplexed PAR. When a sample containing metals is added, this peak is reduced and peaks ranging from 475 to 575 nm arise. (Right) A closer view of the metal bound PAR portion of the spectra, where copper has a maximum absorbance at approximately 535 nm, zinc at approximately 495 nm with a shoulder and the mutants with various levels of metals present.

The spectra were analysed for metal content using SpLab software (figure 3.13), and among the mutants initially analyzed, A4V, had very little to no metal content, with WT seemingly having the most, and the other mutants H43R, H46R, L84V, and G85R having a range of metal concentrations in between. In the first trial, all mutants had larger amounts of copper than zinc, with anywhere from 1.25 times as much Copper compared to zinc (A4V), to about 25 times more copper than zinc (H43R). The PAR assay works to varying levels of accuracy depending on what proportion of the sample is SOD1, and is accurate if SOD1 is the main source of metals in the sample. PAR also has spectral changes upon binding other divalent metals (e.g. Cd^{2+}, Co^{2+}, Ni^{2+})[104], however, these are not expected to be present in significant amounts whereas copper and zinc have been added in excess to the growth media.

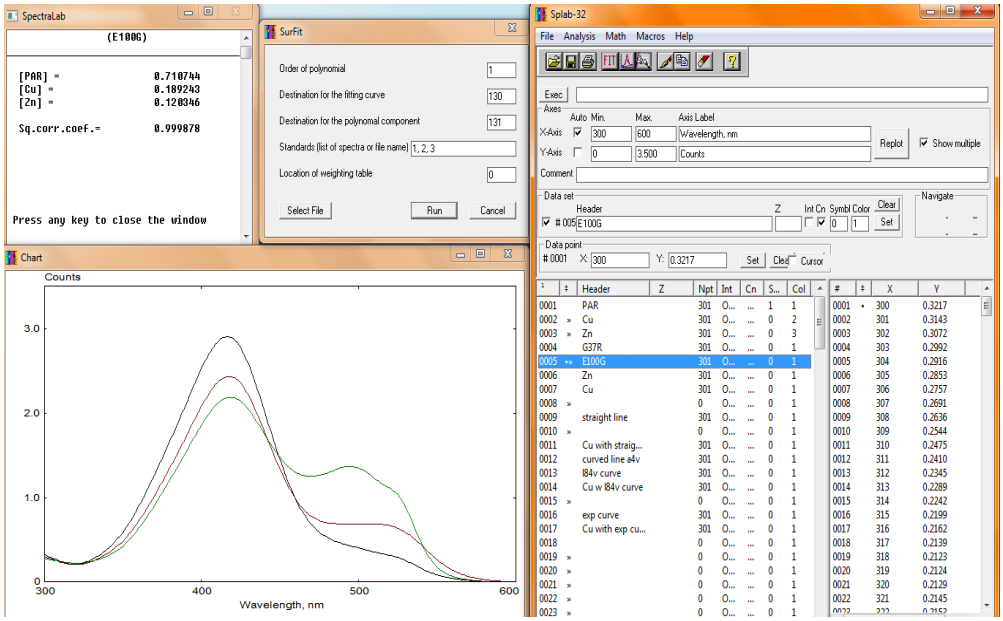

Figure 3.13: SpLab results for metal analysis. The main window (right) with sample list and spectra data, spectra (bottom left), results window (top left) containing the amount of metal and PAR absorbance relative to the amounts of the standards, and fit parameters window (top center) where the order of polynomial is chosen and the standard spectra for reference. The panels shown are the analysis for a sample of E100G inclusion bodies. The protein spectrum in blue is analysed using the green 10 µ Zn standard spectrum and the red Cu standard spectrum to determine the amount of each metal present in the protein sample.

Significant problems presented themselves upon the repetition of the experiment, with re-growths of the same mutants. After having been prepared and analysed by the exact same method as the first trial, inconsistent results were obtained. The ratios of metal to protein subunit were vastly different between the two experiments. The values in the second experiment were for the most part much larger for Zn, and while some copper values were higher, for instance H43R had about twice as much copper, some values were also so low or fit so poorly that negative values were obtained. Interestingly, some values were now above a 1:1 ratio of metals to protein subunits. This implied, given accurate concentrations, that there was excess metal present in the sample, possibly from another metal binding protein, or that the metals are binding in non-native positions around or inside the inclusion bodies.

The experiment was repeated again for fresh growths of *E. coli* expressing the same mutants under the same conditions several times to eliminate the possibility that one set of results was due to a mistake made during one preparation. The results were that the metalation of the inclusion bodies was still highly inconsistent. The range of the values obtained for either metal, copper or zinc, in any of the mutants, was never consistent between any 2 trials in 5 separate trials. It was soon after the completion of these experiments that small insoluble particles were observed, capable of binding PAR and forming a red pellet. Also observed after longer incubation was a clear gel-like substance in the sample Eppendorf tubes (Figure 3.14). These gel-like aggregates were resistant to disruption by a pipette, boiling, or the addition of SDS. However, the addition of a reducing agent, such as βME or tris (2-carboxyethyl) phosphine (TCEP) dissolved the aggregates.

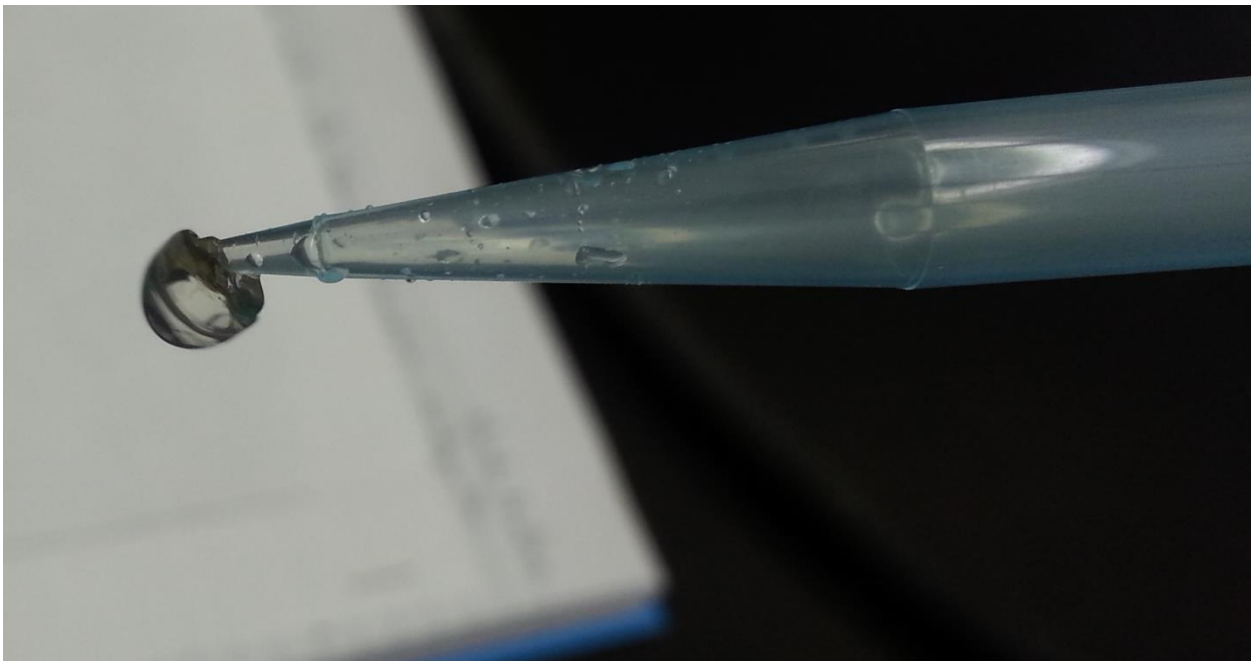

Figure 3.14: Gel-like aggregate are removed from a 1.5 mL tube in which A4V inclusion bodies had been dissolved in GdnHCl as described in section 2.6.1. This particular gel was found after the sample had been sitting overnight and was approximately 2.5-3 mm long. The clear colourless gel was difficult to see in solution and was discovered when pipetting the solution.

Unfortunately, due to interactions between PAR and the reducing agents, the determination of accurate metal concentrations was unachievable. Both reducing agents above were tested with PAR to observe the effect on the spectrum. Some results can be seen below in Figures 3.15-3.17. Both of the reducing agents caused reductions in the metal-PAR complex absorbance for zinc and copper. In PAR assays conducted by Atanassova et al.[105], TCEP had been shown to influence the relative intensity of Fe^{2+} and Fe^{3+} peaks, however, it was unknown if it would influence the peak height of copper and zinc PAR complexes or how it would do so. Since we did not find a reliable way to remove and measure the metals from the SOD1 gels using PAR, we explored measuring metal content using another method, ICP-AES.

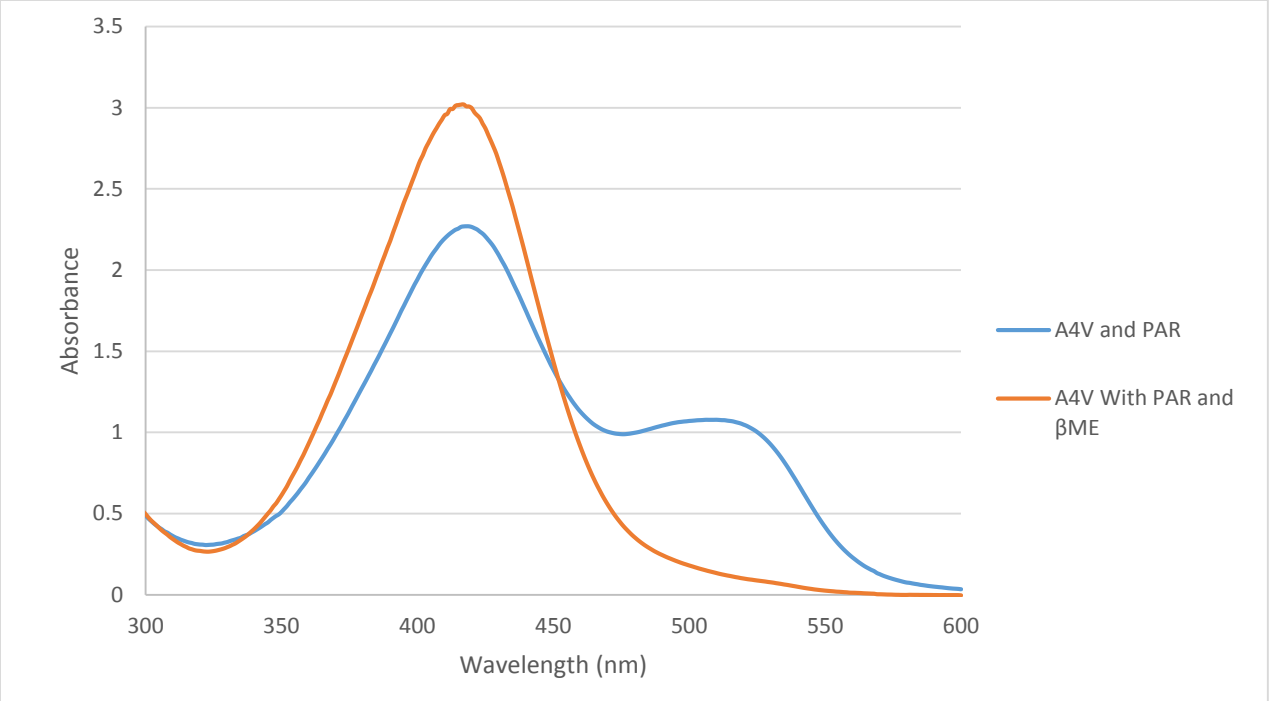

Figure 3.15: UV/Visible spectra of A4V inclusion bodies in 90 µM PAR and 45 mM HEPES (blue), and the same sample after βME has been added to a final concentration of 0.1%. The absorbance for the metal-PAR complex from 500 nm to 550 nm is no longer observed upon addition of the reducing agent.

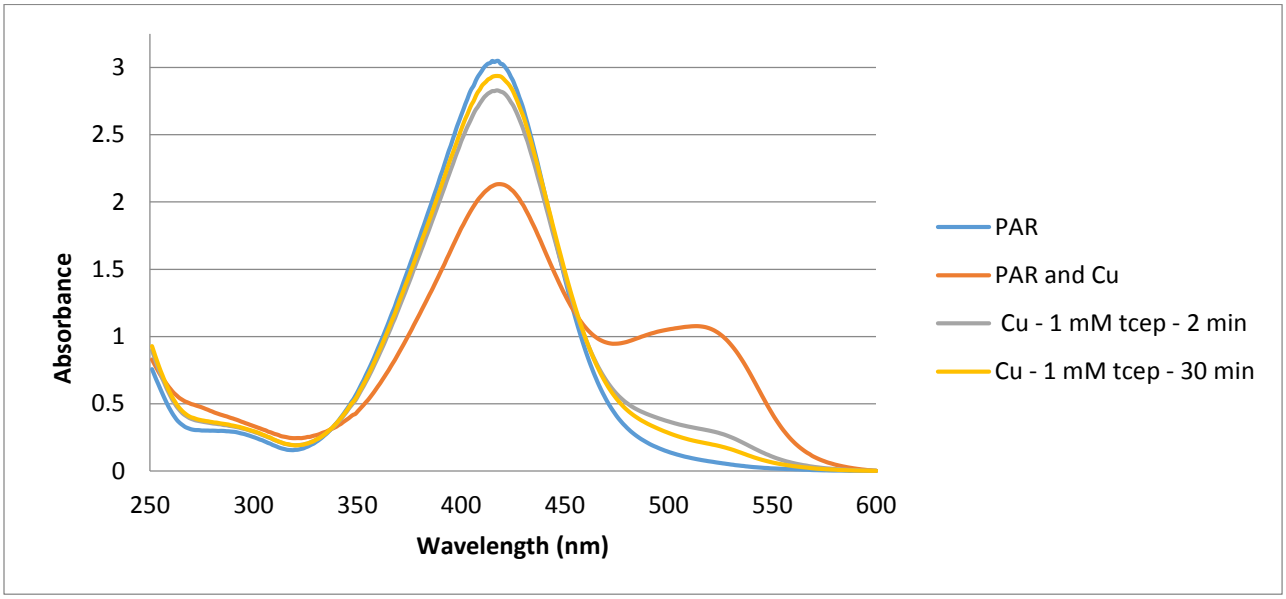

Figure 3.16: UV/Visible spectra of PAR-Cu standard solution (25 µM $CuSO_4$, 90µM PAR, and 45 mM HEPES) and with the same solution when TCEP is added at different time points of incubation.

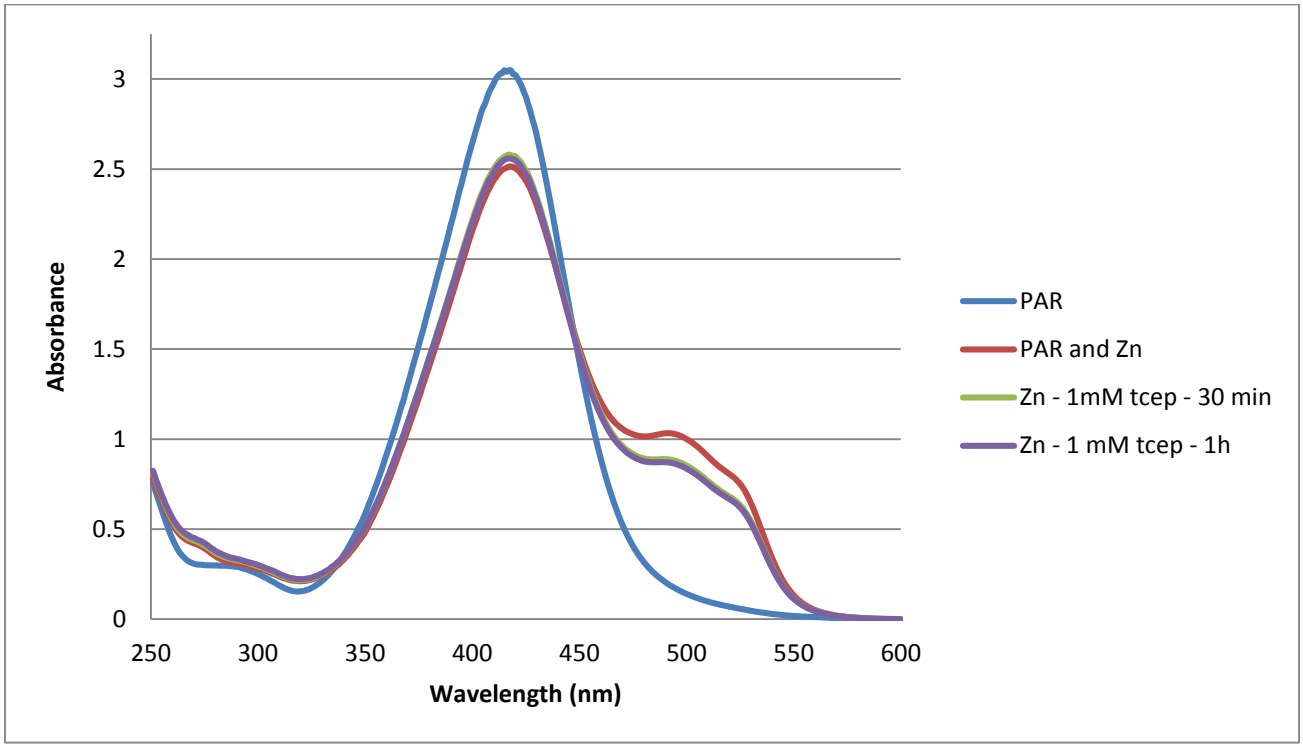

Figure 3.17: UV/Visible spectra of PAR-Zn standard solution (10µM $ZnSO_4$, 90 µM PAR, and 45 mM HEPES) and with the same solution when TCEP is added at different time points of incubation.

3.4.2 Inductively coupled plasma atomic emission spectroscopy (ICP-AES) measurements of SOD1 inclusion body metal content

Acid digestion was chosen to dissolve the aggregates due to its previous use in protein sample preparation for ICP-AES[106] and its ability to oxidize organic compounds, including proteins.[107] The acid digestion conducted, from a visual observation, was capable of eradicating the gel-like aggregates. After approximately 4 hours of digesting, no solids were detected remaining in the solution, even upon centrifugation. To confirm this, a portion of the digestate was removed, neutralized using NaOH, and run on an SDS-PAGE gel. After staining, no bands

were observed from the digested sample, where as a control sample not digested but diluted to the same volume had clear bands observed. This gel indicated that the digestion was complete in breaking down all protein in the sample as was expected. After filtering the digested solution in the reflux tube, visual inspection of the filter also showed no signs of any buildup of solids.

As with the PAR experiments, multiple experiments were conducted in an attempt to obtain reproducible data. There were clear problems in the initial experiments, primarily associated with SOD1 variants with the lowest aggregation propensities. These included the WT SOD1 and the mutant G37R. The analysis values for both were extremely high for copper, and the WT was also extremely high in Zn. The amount of metals when compared to the amount of protein for WT SOD1 were 2674% metallated for copper and 147% metallated for zinc. Other mutants, including G16S, G41D, L84V, and L106V also indicated levels of metals that were higher than expected, however, not as extreme as those obtained for the WT and G37R samples. The copper levels for these four mutants were all between 117% and 206% metallated for copper with zinc levels between 80% and 127% Zn per subunit (Figure 3.18). These variants, unlike WT and G37R, do not immediately stand out based on their aggregation propensities. The remaining mutants (A4V, G41S, H43R, H46R, G93D, and V148G) yielded the lowest values between 1% and 63% metallation, for either Cu or Zn.

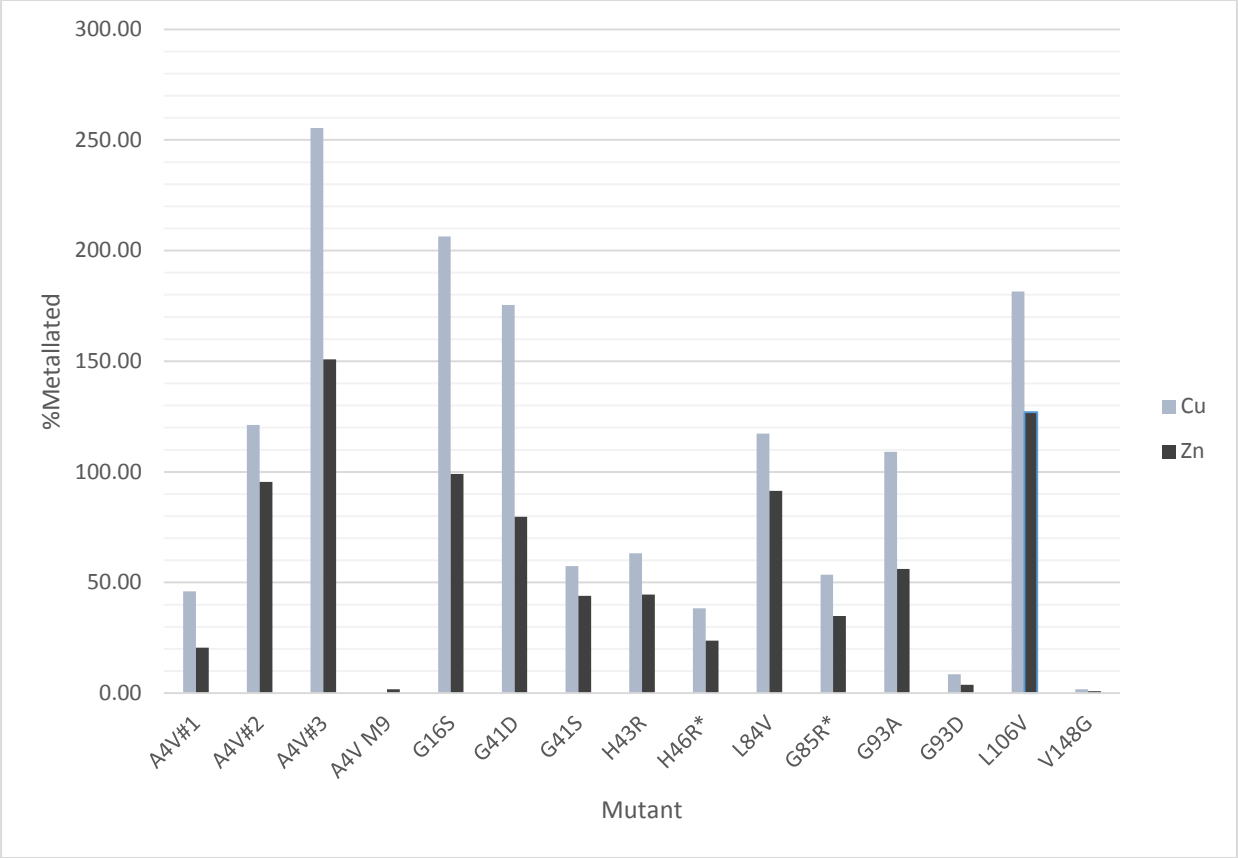

Figure 3.18: ICP-AES metal analysis for acid digested inclusion body preparations of SOD1 mutants. 100% metallated corresponds to a 1:1 ratio of metal: protein subunit, for Cu or Zn. The amount of metal varies markedly, between mutants and for repeated experiments (for example A4V#1,2 and 3). A4V expressed using M9 minimal media had no copper present and a very small amount of Zinc. Metal binding mutants, G85R and H46R are indicated with a *.

When the experiments were repeated, they were focused on one of the most aggregation prone mutants, with no known effect on metal binding, A4V. Two more experiments were conducted, each with new growths and expressions of A4V, following the same procedure as the first experiment. There were also controls grown alongside these growths. The main controls were cells grown under the same conditions but with no inducing agent (IPTG) added to the media during the growth, and induced cells grown in M9 minimal media with no added metal. The former control was designed to determine whether the washed insoluble fraction of the cells,

grown in LB with metals present, contains detectable metal. If the insoluble fraction contains metals but no SOD1, this would have to be either accounted for in the experiments where SOD1 is expressed. The purpose of the latter control is to determine if there is any other source of metal in the experiment; the observation of inclusion bodies in a metal free culture would suggest that metals detected in the original experiments were from the LB media and added metal. Two additional mutants, G93A and G85R, were also grown for comparison, with one of the mutants, G85R, having known metal binding deficiencies.

The results of the repetitions for A4V were surprising in that, like the PAR data, they were still inconsistent. The initial results for A4V were that the metalation was 46% metallated for copper and 20% metallated for zinc. The repetitions, gave very different results, with the first repeat experiment yielding A4V inclusion bodies that were 121% metallated for copper and 95% metallated for zinc, and the second repeat experiment yielding A4V inclusion bodies that were 255% metallated for copper and 150% metallated for zinc. All of these experiments were conducted under the same conditions, with the exact same methods used for growth, lysing, washing, protein concentration determination, and metal analysis. Given the identical conditions of the experiment, the results were surprising.

The controls also provided interesting information. First, in the control of cells grown in LB media with no IPTG added to the growth, there was no SOD1 expressed in the cells, which was confirmed by SDS-PAGE. The procedure was continued, to lyse the cells, isolate the insoluble fraction (there was low levels of insoluble material), and analyze the metal content. The results showed that there was approximately 1 ppm copper and 0.2 ppm Zn in the control sample. Given that the metal content of SOD1-containing samples in many cases was over 10

ppm under the same conditions, this means that less than 10% of copper and less than 2% of the Zinc in the samples is attributable to remaining cell portions not associated with the SOD1

Inclusion bodies. The metal free controls, using M9 minimal media, confirmed that the procedure used, including the tubes, buffer solutions, and acid digestion, added no further metals. The sample, once analyzed, had negligible amounts of both copper and Zn.

The results of the two new mutants included were similar to those obtained previously for some of the other mutants. The G93A sample had significant levels of metal corresponding to 109% copper and 56% Zinc. Given the results from the previous experiments, this was not out of the ordinary; for a mutant with no previous indication of metal binding problems, the copper and zinc levels were comparable to the other mutants. In contrast, the G85R mutant inclusion bodies, however, showed signs of lower levels of metals compared to most other mutants, as expected. The mutant showed 53% copper and 34% zinc. These numbers are comparable to those for H46R, another known "metal binding mutant" in which mutation of the Cu liganding residue H46 markedly decreases metal binding[6]. The only other mutant that showed similar and actually lower levels of metalation is A4V. The initial results showing A4V with very low levels of metalation, however, were not observed in the repeat experiments, and showed large variability. These results are summarized in Table 3.2.

Table 3.2: ICP-AES metal analysis for digested inclusion body preparations of SOD1 mutants. 100% metallated corresponds to a 1:1 ratio of metal: protein subunit, for Cu or Zn. Also listed is the mass of SOD1 in the inclusion body sample analysed.

Mutant	Cu (%)	Zn (%)	Mass of SOD1 analyzed (mg)
A4V	46.08	20.51	87
A4V 2	255.40	150.89	31.4
A4V M9	-0.01391	1.708239	111.9
G16S	206.37	99.14	16.3
G41D	175.39	79.68	79.5
G41S	57.39	43.95	78.2
H43R	63.19	44.52	87.35
H46R	38.39	23.76	4.05
L84V	117.34	91.39	64
G85R	53.57639	34.91376	145.7
G93A	109.1329	56.08563	126
G93D	8.52	3.81	64.05
L106V	181.52	127.01	69
V148G	1.71	0.92	68.2

4.0 Discussion

4.1 SOD1 mutants in the pWT background

4.1.1 Melting temperatures of L38V and L84V SOD1 variants

The SOD1 mutants L38V, L84V and D90A in the pWT background had no previous stability data from this lab, however, melting temperatures for L38V (apparent T_ms of 56.5, 72.5, and 80.2 °C) and D90A (apparent T_ms of 59.8, 75.5, and 82.9°C) in the wild-type background were found in multiple metalation states [96] and apo apparent melting temperatures for L38V (apparent T_m of 42.96°C) and L84V in the wild-type background (apparent T_m of 41.80°C) were reported by Rodriguez et al.[108] The methods used by Rodriguez and coworkers differ from those used in the Meiering lab. Rodriguez and coworkers prepared mutants in the wild-type background using insect cells which produces proteins containing the natural N-terminal acetylation but generally incomplete metallation. This results in observation of multiple endotherms in thermograms owing to multiple forms of the protein that vary in metal content. This means a stage of deconvolution and analysis of what each peak represented had to be undertaken, with assumed relative stabilities that were in some cases supported by experiments on homogeneous samples of metalation states. In some cases, mutants had different numbers of endotherms, with some having three distinct peaks and others four.[109] Other important factors are that the experiments conducted by Rodriquez and coworkers were conducted in phosphate buffer, which has been shown to decrease the apparent melting temperature by ~10°C, and since the wild-type background does not allow for reversible unfolding, the T_ms are apparent, whereas the pWT background results in highly reversible unfolding.[87]

The values reported by Rodriguez *et al*. that are of interest in this case are the highest temperature endotherms, which would often correspond to the fully metallated holo form of the protein. For L38V the highest value was the "T_{m3}" or third endotherm, with a melting temperature of 80.2°C, for D90A, the highest endotherm recorded was 82.9°C. Although some mutants in the Rodriguez experiments obtained "T_{m4}", ranging from 88.9 to 91.6°C for the "WT like" mutants, neither of these two mutants exhibited a fourth peak at this higher temperature[96]. In the experiments conducted here, the melting temperature obtained for L38V was 88°C, closer resembling a T_{m4} of the previous studies. This possibly indicates that the melting temperature of a fully metallated species was not originally characterized but is here. As D90A has not yet been analysed by DSC here, this may give reason to do so, as it seems likely a fully metallated melting temperature of that mutant may also not have yet been characterized.

4.1.2 pWT background SOD1 enzyme activity

The results of the activity assays are an indication that the protein purified was well metallated. This means the major endotherms observed in the DSC experiments are most likely for the fully metallated species. This is also supported by how high the melting temperatures are compared to the pWT and other mutants previously characterized by members of the Meiering Lab[87], as well as the T_{m3} values reported by Rodriguez *et. al.*[96] The melting temperatures indicate a slight loss in thermostability of the mutants here compared to pWT (T_m of 92°C at 0.5 mg/mL, which increases with increasing protein concentration[87]) , however, they are still very stable compared to other mutants, in particular compared to more destabilizing mutations in metal binding regions. [86]

4.2 Expression of fALS associated SOD1 variants in the WT background in *E.coli*

4.2.1 Sample preparation of insoluble SOD1

Examples of the mutant expressions from the Colon lab, from where the cells used in these experiments were obtained, were very similar to the levels observed when the cells were grown and induced under the same conditions in this lab. In these experiments all 19 mutants had similar levels of expression at 4 hours of induction, and this was consistent for each temperature tested. The growth however, was variable when cells were grown in minimal media. The cultures did not all grow and if they did, they did not necessarily grow at the same rate from one experiment to the next. This limited the ability to compare the results for any metal free growths with those for metal supplemented rich media.

Not all problems were associated with growth in minimal media, another issue described in Section 3 was the inability to remove contaminant proteins from the SOD1 IBs. Ideally, the contaminant protein OmpF would have been removed, however, as this proved difficult, its presence was tolerated because OmpF is a porin that transports small hydrophobic molecules[110] and has not been found to bind metals. The end result still produced samples where the most aggregation prone SOD1 mutants constituted greater than 80% of the insoluble proteins isolated from the cells. Although OmpF was initially a concern, it may have revealed more about the composition of bacterial inclusion bodies. Regardless of the centrifugation speed used for obtaining the insoluble portion, or the type of detergent (Triton X-100, NP-40, Deoxycholate, SDS) used for the wash steps, SOD1 and OmpF were consistently found together. This may indicate that OmpF is either integrated into the inclusion bodies, or stuck to them in some way.

Previous studies have reported that outer membrane protein expression is increased during cell stress[111,112]. This may in itself cause those outer membrane proteins to misfold and aggregate along with the overexpressed protein of interest. In another experiment conducted in the Meiering lab, centrifugation was able to separate the inclusion bodies of another protein domain expressed in *E. coli* from OmpF by adjusting the centrifugation speed, however, this was not effective for SOD1. Thus, it may be specific properties of SOD1 that allow the OmpF to stick to or be included in their inclusion bodies.

4.2.2 Aggregation propensity analyses for SOD1 variants; predicted and measured propensities and relationships with ALS disease characteristics

When comparing the aggregation propensities for SOD1 variants in *E.coli* to various other characteristics of SOD1 and or ALS, a number of interesting correlations arise. Many characteristics of SOD1 mutants have been reported by many different research groups. Some that are of interest here are the melting temperatures of SOD mutants in various metallation states, in order to attempt to connect the thermal stability of a given mutant to its aggregation propensity. Others include the kinetic folding rate of the mutants, the average disease durations, and in the following sections, the metallation state of the SOD1 IB's.

The information revealed by the aggregation propensity data itself is a prime example of the effects that different mutations may have on a protein. Although the range of propensities was measured at one specific temperature to maximize observed differences between mutants, this method highlights that mutations may cause marked differences in protein characteristics. Although mutations promoting aggregation has already been observed and compared with stability for other proteins, for example HypF-N[113], observing the aggregation propensities of

SOD1 mutants *in vivo* had been limited to few studies. These include the study of A4V mutant inclusion bodies in *E. coli* [39] and the formation of IB's by many different mutants in human embryonic kidney cells[74]. The study conducted by Prudencio et al.[74] has multiple differences from the studies described here. For example, the kidney cell line may have important cellular machinery (such as the copper chaperone for SOD1) for folding SOD1 that E.coli lacks. Another difference is their choice of sonication as a cell lysis technique. Using sonication with SOD1 which still has the free cysteines present has been shown to cause aggregation.[76] This may make all mutants seem more aggregation prone than they actually are.

When the aggregation propensities measured here are compared to multiple thermal stability data sets (Summarized in Table 3.1 and shown in Figure 4.1), some trends with each data set are observed. In the correlations generated here, each set of thermodynamic data shows a clear relationship to the aggregation propensity. The available thermodynamic data differs somewhat for the different forms of the protein, with 13 mutants oxidized apo melting temperatures known, 12 for holo, and 9 for reduced apo melting temperatures having been determined as of now, however, all available data was used in order to observe any trends. When using all available data, the thermodynamic data set with the greatest correlation to aggregation propensity, is that of the reduced apo melting temperatures, with a squared correlation coefficient (r^2) of 0.609 and a P value of 0.013, significant at $P < 0.05$. The oxidized apo melting temperatures when compared to the aggregation propensities also show a clear trend, ($r^2 = 0.5094$, $P = 0.00615$), with the holo comparison having the worst r^2 at a value of just over 0.3 and a P value of 0.062 (not significant at $P < 0.05$).

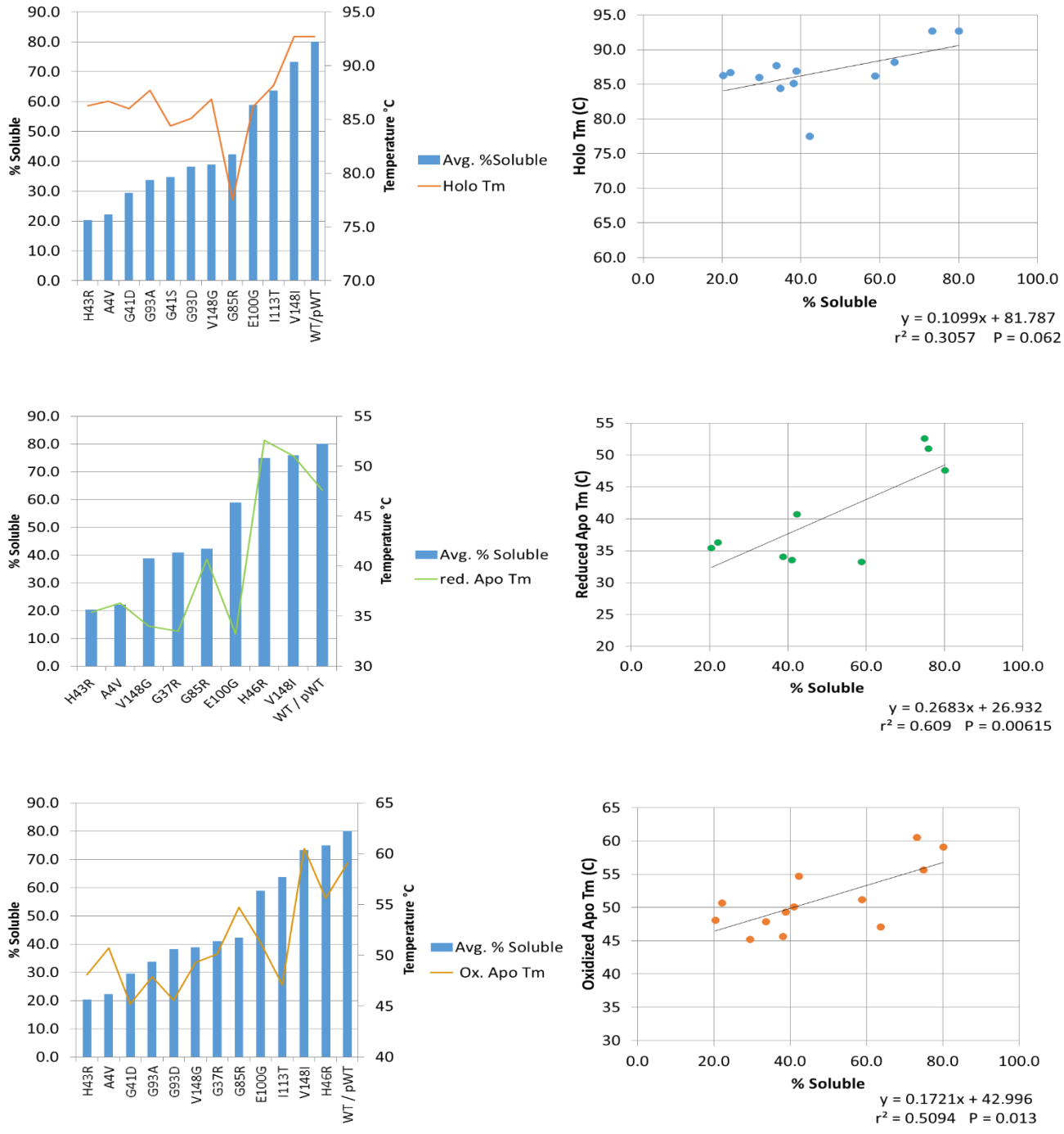

Figure 4.1: Comparisons (left) and correlations (right) of the aggregation propensities determined here to previously measured melting temperatures of SOD1 mutants with various metalation and disulfide statuses. (Top) The holo SOD1 mutant melting temperatures, (middle) the reduced apo melting temperatures, and (bottom) the oxidized apo melting temperatures compared to aggregation propensities.

An interesting outlier is found in the holo correlation plot, the mutant G85R. This mutant in particular, has been identified to alter metal binding. When that data point is removed from the plot (Figure 4.2), the r^2 increases to 0.61. The remaining plots with the G85R mutant removed, also see an improvement, however, the reduced apo is still the most correlated.

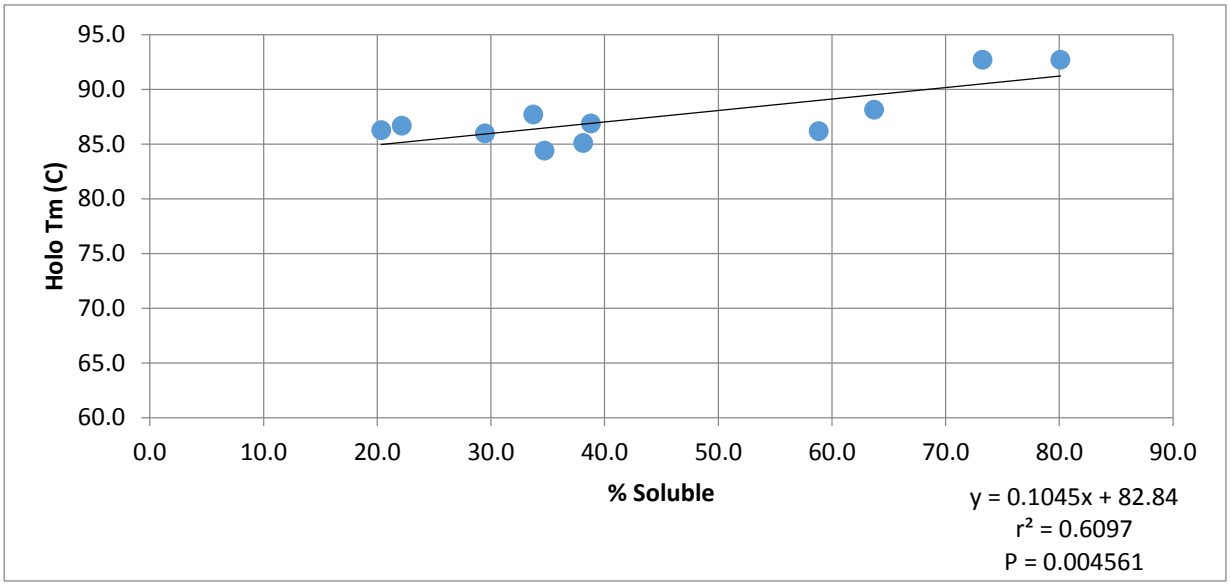

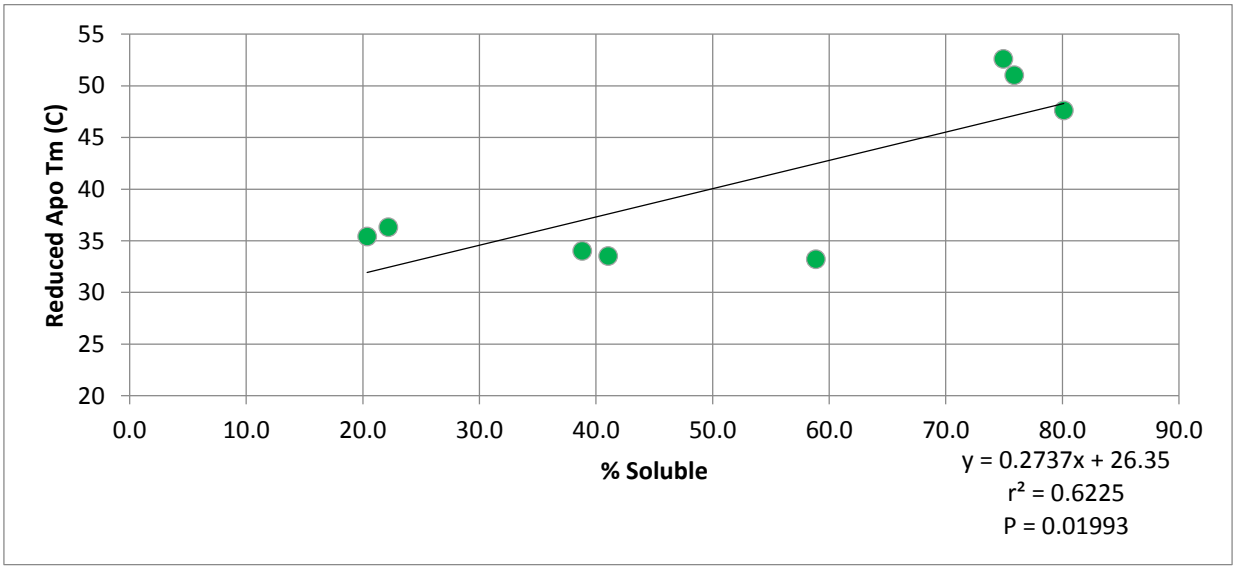

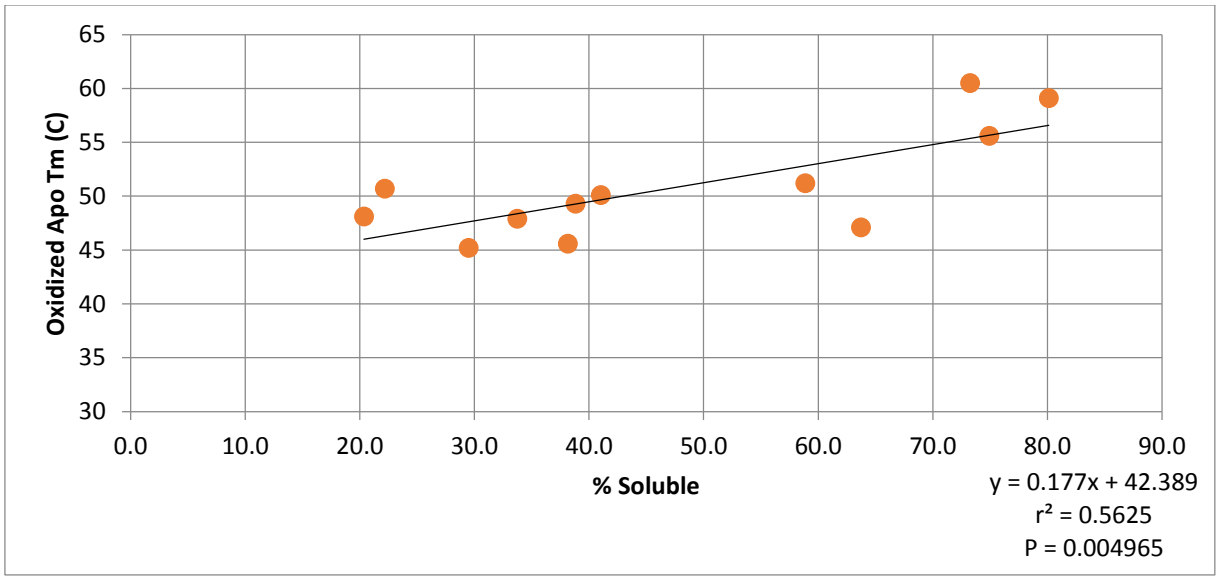

Figure 4.2: Correlation of aggregation propensity to melting temperatures with the removal of metal binding mutant G85R.

A final question regarding the ability to properly coordinate the DSC obtained data to the aggregation propensities, is whether they change substantially in the presence of the proper chaperone for copper metalation. If the copper chaperone assists the mutants to different degrees, some mutants may change position in the correlation. Determining if this is a factor may have implications for the study of aggregation with other metalloproteins. This could be an interesting direction for future research.

With these correlations, a number of new questions arise. Some of these include, whether the aggregation propensities better match the thermodynamic data of a certain metalation state (e.g. Apo or holo), how much can we determine from comparing a characteristic obtained *in vivo* to one that was observed *in vitro*, and whether any correlations hold true for multiple proteins from other studies. Other proteins that have been studied for similar characteristics include the N terminal domain of the *E. coli* HypF (HypF-N)[113] and some of its mutants, the spectrin SH3

domain (SPC-SH3) and some its mutants[9], Interleukin-1β and some of its mutants, as well as the human p53 core domain (p53C) and its mutants.[114]

In comparing to the other studies mentioned above, a consensus is not reached. Although Mayer et al. do not report the % soluble for their protein of interest, they conclude that the level of soluble protein is decreased with decreasing thermodynamic stability, as this was the case with the p53 core domain.[114] Castillo et al. show results supporting that aggregation propensity is controlled by thermodynamic stability based on the data produced using the SPC-SH3 domain model.[9] Finally, Chrunyk et al. state their observation of no strong correlations of the Interleukin -1β inclusion body formation to thermodynamic or thermal stability.[115] This final study is in contrast to the others, as well as to the correlation observed here with SOD1. Therefore, although there are multiple studies supporting the correlation between aggregation propensity and thermal stability, this may not be true for all proteins.

The rate of folding for mutant SOD1s has been studied previously by members of the Meiering lab and others.[103,116] Comparing the kinetic folding rates to the aggregation propensities (figure 4.3), there is a clear outlier, A4V. The folding rate constant for A4V at >0.1 s^{-1} is much larger than the next highest value; this has been observed independently by both the Meiering and Oliveberg groups. Whether A4V is included or not, no significant correlation is observed between the folding rate and the aggregation propensity of SOD1 mutants expressed here.

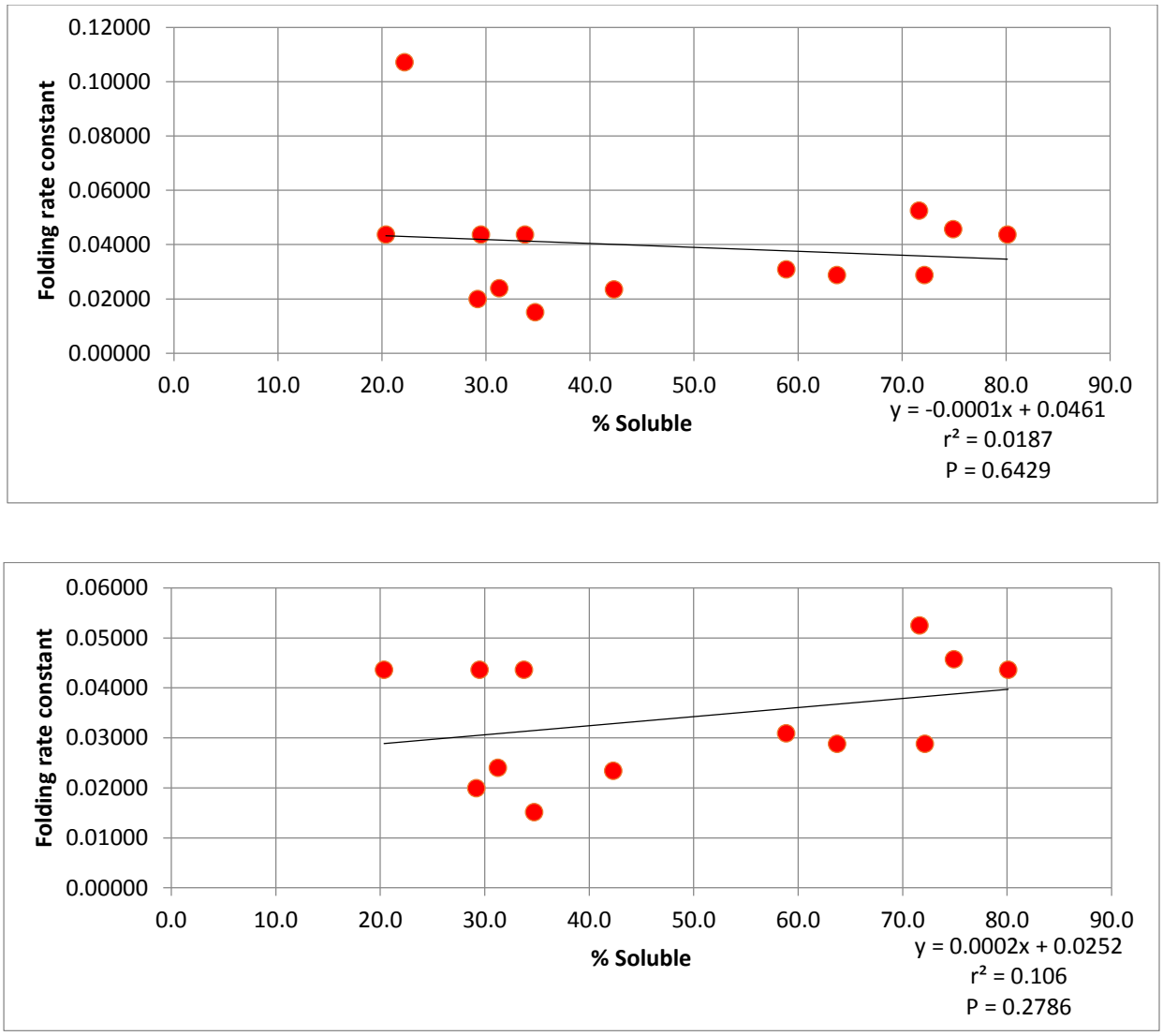

Figure 4.3: Comparison of the kinetic folding rates to the aggregation propensities of SOD1 mutants. Top: with A4V. Bottom: with A4V removed.

It has been noted that different SOD1 mutations are associated with different disease durations[17] and the relationship between disease duration and mutant SOD1 aggregation propensity has been investigated in the studies mentioned above by Wang et al.[17] and Prudencio et al.[74] Using the % soluble data obtained here, there may be a trend that disease duration increases with increasing variant solubility (Figure 4.4), however, the r^2 of 0.1302 and P value of 0.1548 are relatively low values and the trend is not significant. As seen in section 3 the data

obtained here shows a lack of correlation between the average disease duration and the aggregation propensity of the fALS associated SOD1 mutants. The results obtained here are roughly in line with the results of Wang et al.[17] or Prudencio et al.[74] The study from Wang et al. had compared the disease duration in a more complex model, including both protein stability and a calculated aggregation propensity obtained from a recalibrated version of the Chiti-Dobson equation. The authors concluded that this method revealed a correlation with disease duration, reporting an R value of 0.58 (R^2 = 0.34). The study from Prudencio et al. showed that when grouped into relatively loose categories (low, moderate, high, and extreme measured aggregation propensities), mutants with a high aggregation propensity have a shorter disease duration, however, when all considered together, like the data presented here, no statistically significant correlation was observed.

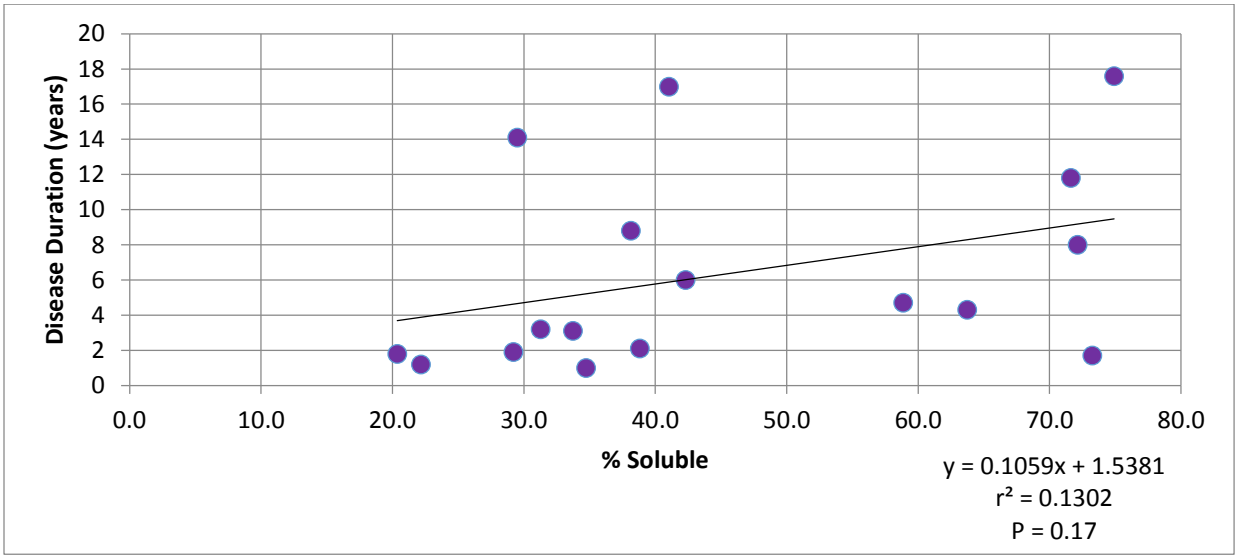

Figure 4.4: Comparison of the average disease duration and aggregation propensity of fALS associated SOD1 mutants.

Differences in the methods between the study from Prudencio et al. and the experiments reported in this thesis have been mentioned above, however the extent to which those differences

affect the aggregation propensity is not clear. A comparison between the same mutants used in the two studies shows differences with many mutants relative to each other. For example, in the experiments conducted here, H43R and A4V had the highest propensities to aggregate, yet, in the Prudencio study, mutants such as L84V, G41S, V148G and E100G all had greater aggregation propensities than either A4V or H43R. On the other hand, similar results for aggregation propensities were observed for some mutants, including V148I and L144F, which in both cases were among the least likely to aggregate.[74] Overall, it seems the two studies provided somewhat different results. There could be multiple reasons for this arising from differences between *E. coli* and human cells, and experimental protocols used to express and analyze the SOD1 variants. This raises questions about what can be done in further studies to provide the most useful information for understanding the results and their relation to ALS characteristics, such as expressing the CCS in *E.coli*.

One shortfall of the average disease duration data is the lack of large patient sample sizes. Various researchers have reported their results on the disease duration of specific mutations they have investigated, and although some have attempted to combine data from others reports, the numbers may not be large enough yet to have a good idea of the actual average disease duration for those mutants. This is especially evident looking at the work of Wang et al.[17] versus the work of Andersen et al. where both have looked at 15 patients with the D90A mutation (with the information of 2 patients from Andersens study also taken into account in the Wang report). Andersen reported an average disease duration of over 14 years[117]. However, Wang reported an average disease duration of 8 years[17]. Thus, limitations in patient data are a significant limiting factor in identifying clear correlations with SOD1 characteristics.

There are a number of possible additional explanations for the absence of a clear correlation of patient disease duration with protein solubility measured here. A major possibility is that the fully formed insoluble aggregates of SOD1 are a byproduct, or only one further stage in the disease ALS.[118] Keller et al. have reported evidence that many mutant proteins in various genes that are associated with ALS are involved in the larger system of RNA metabolism, as evidenced by the co-localization of ALS-mutant TDP-43 and FUS in cytoplasmic inclusions.[119] Other studies have focused on the involvement of soluble oligomers as the cause of disease.[41,120–122] Studies by Banci et al.[41] Redler et al.[121] and Grad et al.[122] have attempted to identify and characterize the early stages of SOD1 oligomerization, with the hope of identifying a soluble oligomer with characteristics that may reveal more about the disease progression. Grad et al. have proposed that these misfolded mutants or soluble aggregates may efficiently propagate misfolding between cells.[122] These ideas do not completely rule out that the insoluble inclusions are still a factor in the disease. The relationship of the level of large soluble aggregates formed in model cellular systems, such as *E. coli* and human cell culture, to the types of aggregation occurring in disease is complex and not yet well understood.

As mentioned above, the aggregation propensity data used by Wang et al.[17] was predicted using an algorithm, which is based on physical properties of the proteins amino acid sequence (such as hydrophobicity, charge and secondary structure propensity). In the past decade, many algorithms have been developed to attempt to predict whether a mutation may alter a protein's propensity to aggregate. This may be by analysing the sequence surrounding a mutation or by the chemical differences presented by the change of an amino acid. Some of these include the previously mentioned Chiti-Dobson equation[23] and the related Wang-Agar adaption[17], as well as Zyggregator[25], Ztox[25], fold-amyloid[123], Pasta[124], Tango[24], Waltz[125], and

Profile 3D[126]. All of these algorithms have been used previously to analyze SOD1 mutants with values calculated and normalized by Heather Primmer.[127] Comparison of the predictions (Table 4.1) with the levels of aggregation measured here (Figure 4.5), shows that none of the predicted propensities correlates strongly with the experimental data.

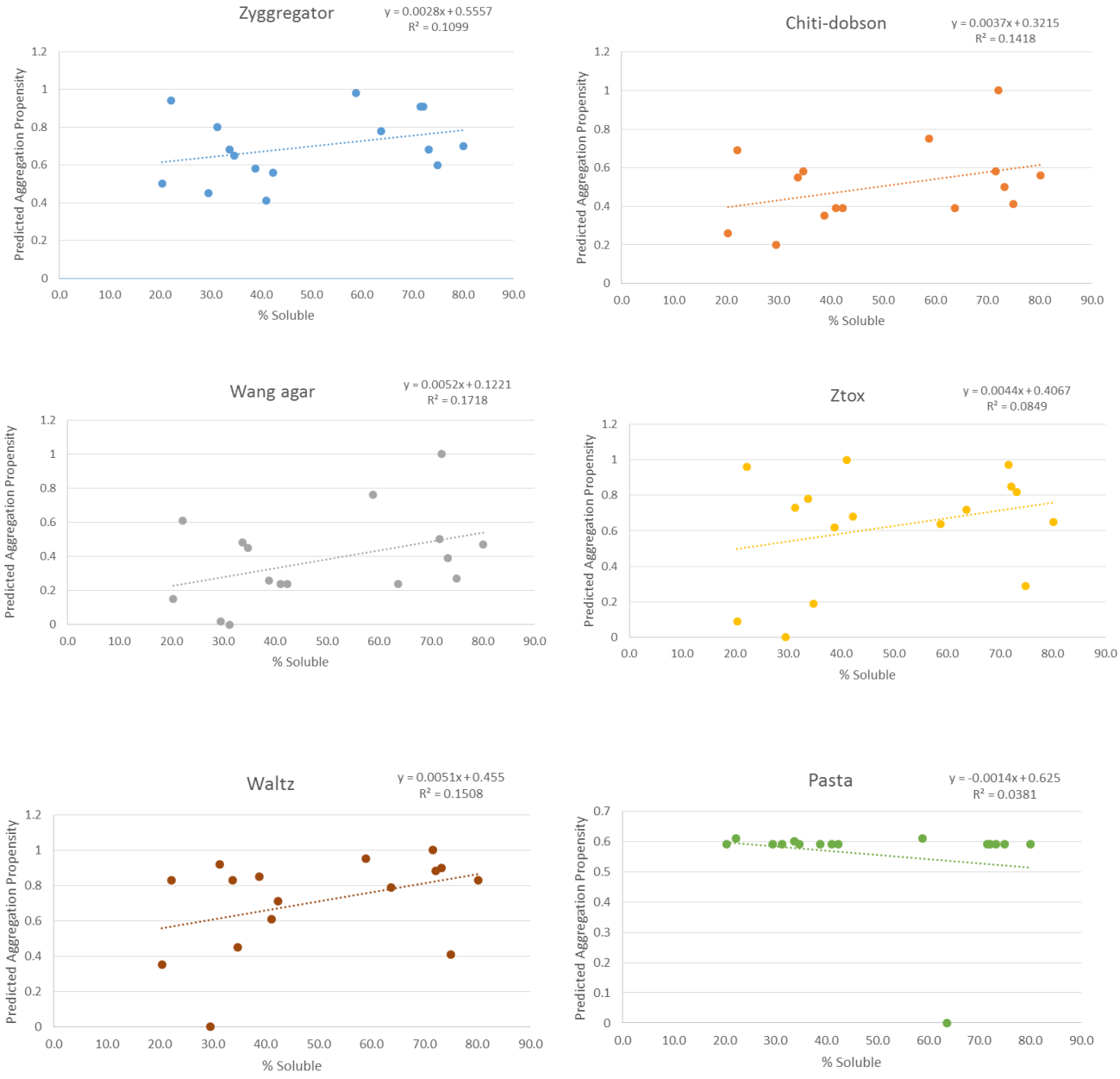

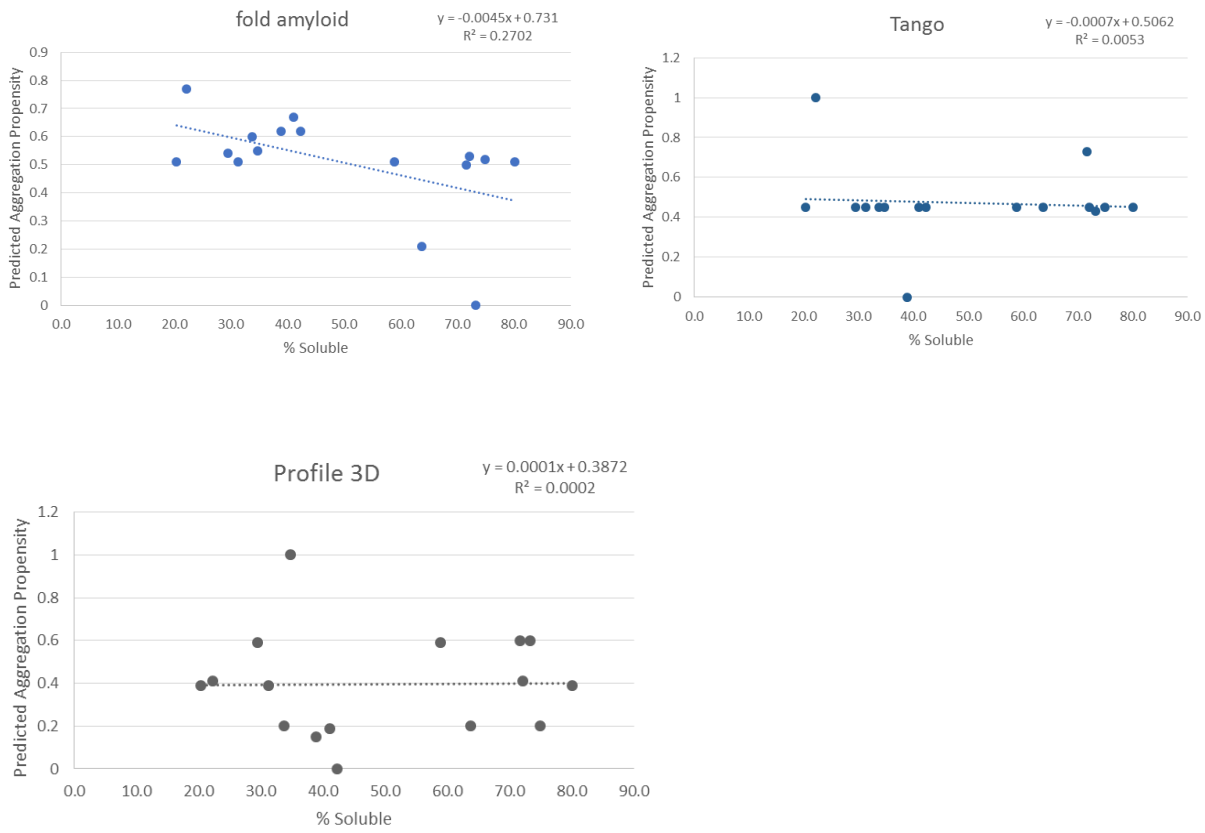

Figure 4.5: Aggregation propensities of selected SOD1 mutants as determined by various prediction algorithms vs. the aggregation propensity as determined by inclusion body formation in E.*coli*. A table of the normalized aggregation prediction values is shown in Appendix 1.

With respect to expanding our knowledge of inclusion body formation in general, the data obtained are also quite interesting. Although stages of the optimization process, such as temperature control have already been thoroughly studied[13,128,129], the wide range in different aggregation propensities given single point mutations, specifically in SOD1 has shown how small changes in a protein can yield a full spectrum of results. Ideally, identifying the underlying factors that lead a specific mutation to a specific result would lead to more control in protein design. For example, designing a protein to be very insoluble, yet active. When we look closely at the mutations in SOD1 studied here, there are many examples of various changes, such as

mutations in the metal binding regions (G85R, H46R), in the dimer interface (A4V, V148G/I), as well as throughout the rest of the protein.

Different mutations at the same location in SOD1 have shown here to have varying effects. For example, the multiple mutations at the 41st, 93rd, and 148th amino acid positions have shown some interesting variations. The two mutations at the 41st position, G41D and G41S have similar aggregation propensities, as do two mutations at the 93rd position, G93A and G93D. Unlike those mutations, V14G and V148I have very different propensities to aggregate, with V148G being much more insoluble after 4 hours of induction at 25°C. Although this is a small sample size, it further supports the hypothesis that different mutations, even at the same position can have variable effects, which would be of interest to investigate further. One study that has focused further on this question is from Pratt et al.[130] specifically on mutations in the 93 position, labelled as a "hot spot" with 6 different mutations associated with fALS. Each of those mutations presented with a distinct clinical phenotype and the aggregation of each was observed with a small-angle x-ray scattering assay to determine the aggregation propensity *in vitro*. Looking at a single position in a complex protein simplifies comparisons of the effects of mutations between regions of SOD1 (metal binding, dimer interface, etc.). While the Pratt study concluded once again that there was a correlation between mutant aggregation and disease, the results here suggest that a different "hot spot" may give a different range of effects than ones at another position. This is simply analysing the effects of the mutations themselves, the resulting changes to the protein from mutations or the process of aggregation, such as the loss of, or partial binding of metals is also a major aspect of interest.

4.3 Metal analysis of SOD1 inclusion bodies

4.3.1 PAR spectrophotometric analysis of metal content of SOD1 inclusion bodies

All of the results obtained by PAR became questionable upon the discovery of transparent gel-like substances in the guanidium hydrochloride / inclusion body samples. After allowing samples of A4V to sit at ambient temperature overnight, one of these clear colorless gels became apparent when the sample was pipetted. It was very flexible and would not break up easily with intense pipetting or vortexing. Multiple methods were used in an attempt to break up the gel-like aggregates, as described in Section 3.4.1, including: mixing vigorously with a pipette, vortexing, boiling, and boiling with added SDS. Those attempts only resulted in smaller pieces of the gel. It was not until the addition of reducing agents that the gel dissolved, revealing that the gel was most likely formed from aberrant disulphide crosslinking.

After searching the literature, it was apparent that similar gels have been observed in other studies with SOD1, however, none of these described the gels in detail or analyzed their structure. Lindberg et al.[131] reported gels in their *in vitro* studies of SOD1 variants. They did not describe structural details of the gel, but the aggregates did not stain with the amyloid binding dyes thioflavin T or Congo red. Based on the experiments conducted here, these gels likely retain some bound metals. At the later time points of incubation with PAR, there were very small insoluble pieces that showed signs of metal binding. These were only apparent upon closer observation and became a red colour in contrast to the more yellow background of the PAR solution (Figure 4.6). There is a possibility that these were portions of the original inclusions that may not have been dissolved in the guanidine due to disulphide crosslinks. This seems unlikely though due to the great majority of the inclusion mass dissolving in the guanidine, and the inclusions being formed in the reducing environment of the E.*coli* cytoplasm[132]. It seems likely

that upon incubation of the IB sample in denaturant, after protein was solubilized, it may have oxidized to form a gel, perhaps by adding to small particles of undissolved material.

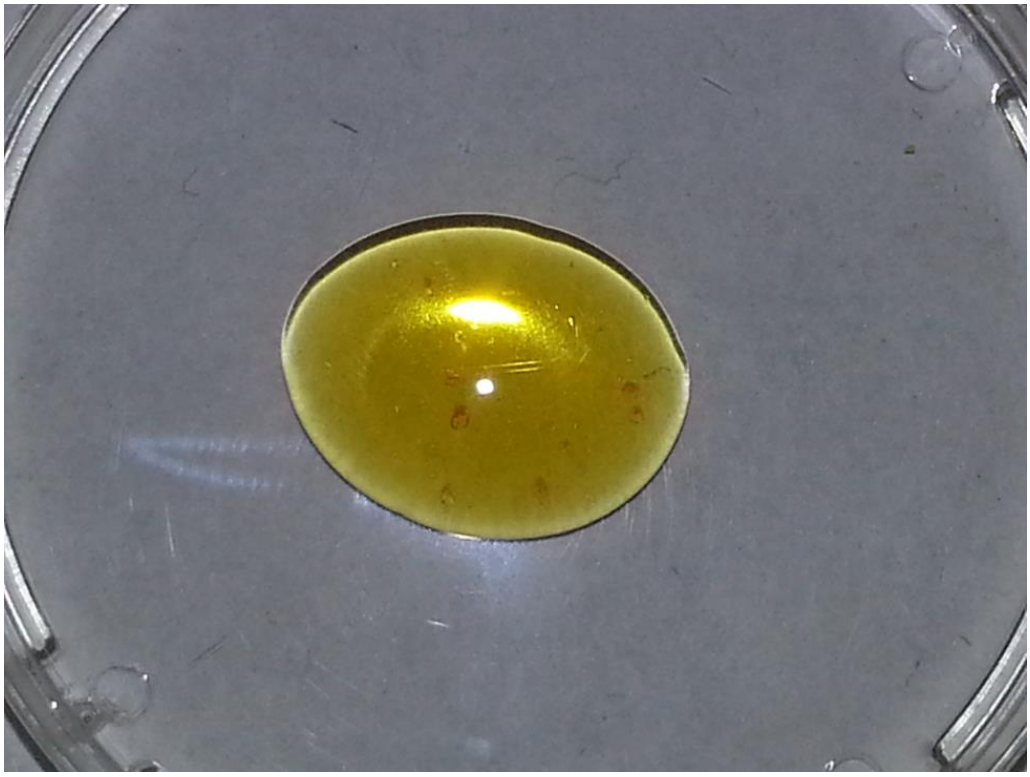

Figure 4.6: Sample A4V inclusion bodies denatured in 5.4 M GdnHCl with 90 µM PAR, and 45 µM HEPES. Samples was denatured overnight. After the addition of PAR, small pieces of insoluble material become apparent as the more deeply coloured orange/red compared to the yellow solution when bound to PAR. This colour change may be expected if PAR is binding to metals that have a higher concentration inside the particles than in solution.

It has been reported in multiple studies that wild-type and mutant SOD1 can aggregate due to the formation of intermolecular disulphide bonds involving the free cysteines Cys 6 and Cys 111, although these bonds do not appear related to the disease.[39,131–136] The experiments conducted are also consistent the ability of the protein to form intermolecular disulphides and gel-like aggregates either within inclusion bodies or from the unfolded state in guanidine, on the

approximate time scale of hours. This imposes limitations on the quantitative analysis of metals using PAR.

As the experiments here are a new application of the PAR assay, it was important to identify any possible cause of error. The procedure initially used by Crow et al. [89] involved the use of PAR along with other chelators (NTA and EDTA) to analyze the metal content of SOD1. The purposes of the chelators were to specifically bind and sequester either Cu or Zn from binding PAR in order to enable specific analysis of both metals. This method was adapted by Colleen Doyle in the Meiering lab[100] to eliminate the other chelators, and instead use the spectral decomposition software SpLab to fit the components of absorbance arising from free PAR and PAR complexed with Zn or Cu. The results for the new PAR method were compared to results of the same samples analyzed by ICP-MS. Notably, residual EDTA from the purification procedure interfered in the PAR assay such that it decreased the apparent levels of Zn compared to the ICP-MS values. Attempts were made to overcome this obstacle in the experiments described here, specifically the purification of the pWT SOD1 mutants. This was the reason that some of the purifications used NTA or DTPA as described in section 2.1. Unfortunately neither of the alternative chelators was a suitable replacement, with both still sequestering some metal from PAR. EDTA is a common component in cell lysis buffers and other solutions used during protein sample preparations, and it is known to also bind very tightly to SOD1[137]; thus the presence of EDTA is very important to take into account when analyzing metal content of proteins, in particular SOD1, using PAR.

Due to large variations in the apparent metal content of IB samples as measured by PAR, the insoluble gel-like aggregates, and the inability to use reducing agents due to their interference with the PAR spectra, another technique was deemed necessary to analyze the inclusion body

metalation. What had been consistently been used by others previously to determine the metal content of SOD1, was ICP-AES.[82,106] More on the details of this technique are discussed below, however, the PAR technique was also revisited. To validate results obtained from PAR, the PAR experiments were conducted using the sample preparation method also used for the ICP-AES procedure. Differing from the technique of using denaturant as in the Crow[89] and Doyle[100] assays, this sample preparation method was the acid digestion described in Section 2.6.2. When the solution was neutralized to not affect the PAR spectra, the results loosely agreed with those obtained from using the ICP-AES. A comparison of the techniques is continued in sections 4.4.3 and 4.4.4

4.3.2 ICP-AES analysis of SOD1 IB metal content

The results of the ICP-AES experiments clearly showed that the inclusion body samples of SOD1 contained at least some metals, in agreement with the PAR assay results. With a more reliable method of denaturing the inclusion bodies by simply acid digesting them, ICP-AES provided results unimpeded by the hydrogel type aggregates unveiled during the PAR experiments. Unfortunately, the experimental method showed increased relative uncertainties for SOD1 mutants with lower aggregation propensities. The numbers were severely skewed in the direction of large amounts of metal per subunit of SOD1 when the mutant expressed was mostly soluble and there was consequently smaller absolute and relative amounts of SOD1 in the inclusion body sample. This could be in large part due to excess metals binding other remaining portions of the cell. Normally, when SOD1 comprises the majority of the insoluble sample, the fractions of the cell remaining after washing have much less effect. This may change when the amount of SOD1 in inclusion bodies is very low, the majority of the pellet is then other protein and likely other cell material. Due to the same washing procedure being used for all samples in a

given experiment, this does not account for instances where 2 samples of the same mutant prepared by the same procedure showed different metalation.

One case where this was in fact a problem was with 2 separate samples of the mutant A4V. In two separate trials of determining the metalation of A4V inclusion bodies, one result had a relatively low level of metalation, with approximately 40% Cu, and 18% Zn, and a second sample prepared later yielded 120% Cu and 95% Zn. With the entirely same procedure, two very different results were obtained. This may be an indication that the procedure has a major flaw; on the other hand the PAR results also showed high variability. Thus, it is very likely that the level of metalation of inclusion bodies is truly variable.

4.3.3 Comparison of Techniques

Due to the large variability in the initial PAR experiments, and the new procedure being used, it is important to validate the technique. Both the PAR assay and ICP-AES have benefits and shortcomings for determining the metal content of SOD1 aggregates. Comparing the results of the two techniques for SOD1 samples can give information also for their general applicability to analyze metal content for other protein aggregates.

The most inconvenient aspect of ICP-AES for this purpose, in these experiments, was obtaining the necessary large amount of protein (at least ~30 mg of SOD1 per sample). This is due to the volume of digested sample necessary to run the machine (at least 10 mL with minimum metal concentrations of 2.9 mg/L Cu and 1.3 mg/L Zn, as well as the extent of the inclusion body formation. Due to some SOD1 variants forming lower levels of inclusion bodies, more culture is needed. In comparison, the PAR assay required 100 fold less protein.

Although the acid digestion preparation of the samples for ICP-AES was augmented in order to utilize the PAR assay on the WT background SOD1 mutants, the PAR assay is still ideal to be conducted on proteins with no ability to form aberrant disulfide bonds in chemical denaturant, including the pWT SOD1 mutants[100]. For ICP-AES is important to avoid high levels of salts in solution, some may cause reductions in the signal of the metal of interest if they cool the flame, for example high sodium can have this effect (1 g/L can cause a decrease in Cu signal intensity by 15%) .[138,139] In terms of flexibility of sample preparation, this may be an argument in favour of using the PAR technique.

ICP-AES was convenient for analyzing multiple samples. Here, it was necessary to analyze a large number of samples, where several mutants of SOD1 were analyzed and compared to each other. Having the ability to use an instrument that accommodates a program to analyze multiple samples in succession with minimal time between sample readings without extra interaction is beneficial. This is in contrast to the PAR assay, in which, taking the time to properly clean the cuvette used is an important factor, as residual metals may affect the next sample. This involved continually washing with nitric acid and thoroughly rinsing with MilliQ grade water between each sample. Both techniques, however, provided inconsistent results.

4.3.4 Metallation of SOD1 Mutants

When comparing the results of both techniques used here, there were some similarities as well as some differences. The inconsistency in trials was one similarity between the two techniques. This could have indicated either an inherent problem with the procedure itself or the inclusion bodies were binding very different amounts of metals seemingly at random but perhaps relating to the circumstances of the growth and expression. This variability is not likely arising

from the instrument since when the same sample was analyzed by both PAR and ICP-AES after acid digestion, similar results were obtained (Figure 4.7)

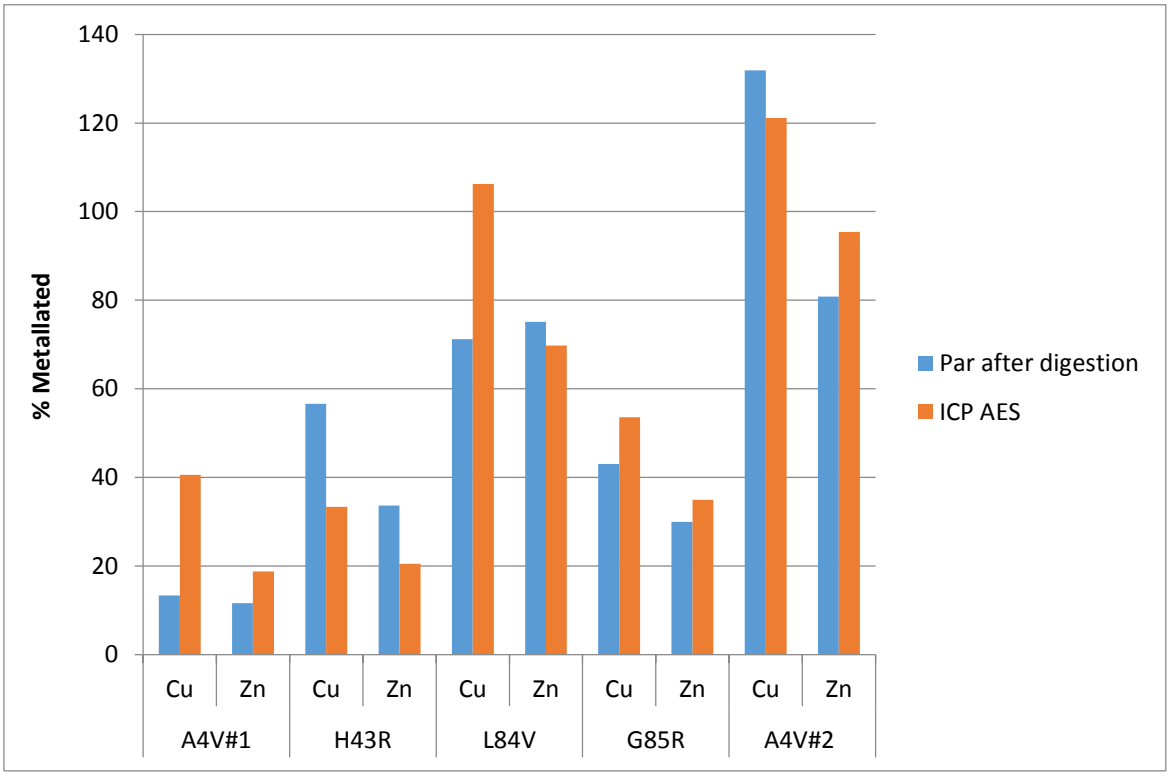

Figure 4.7: PAR and ICP-AES metalation results of the SOD1 mutant acid digested inclusion body samples. A4V#1 and #2 were samples prepared from repeated culture growths.

The results of both PAR and ICP-AES experiments indicate that the SOD1 IBs contain some metal. When assessing the possibility that metals could bind in the inclusion bodies, a number of factors were taken into consideration. The first was residual structure of the protein. As mentioned in section 1, IB's had generally been considered amorphous[34,140]. More recently, the internal structure of inclusion bodies has been characterized in further detail. The observation of amyloid like structure[33,34,140] as well as residual activity in some inclusions[128,141] has raised many more questions about not only the process of IB formation, but also possible uses for IB's. The presence of metals in IB samples here, suggests exploring studies to determine levels of

residual activity in mutant SOD1 inclusions. Since the levels of aggregation for each mutant have been determined, by continuing with the characterization of activity, the mutant with the highest activity to inclusion body yield could be identified. This may be useful for applications requiring an insoluble or immobilized superoxide dismutase catalyst.

If the binding of the metals is not regulated by chaperones or the other cellular components normally found in human cells, it may be reasonable to predict mismetallation in *E.coli*. As mentioned in Section 1.4.6, SOD1 normally utilizes the CCS protein for proper Cu metalation[82,84,85]. If this chaperone is not present, it is highly unlikely that the SOD1 grown in E.coli will reach a fully metallated state. This may affect the level of copper observed in some of the IB's. However, the large amount of copper and zinc present in the media may cause metals to "stick" to the inclusion bodies. In regards to the metal content of inclusions in humans, there are no direct analyses, however, copper has been found to be elevated in the cerebrospinal fluid of ALS patients.[142]

Finally, it is worth noting that a significant source of error for the accuracy of either technique is likely the determination of protein concentration. The error associated with the densitometric protein determination can be high if care is not taken. The differences in the experiments for A4V however appear to be larger than the experimental uncertainties as estimated from analyzing many samples; this suggests that there is likely real variation in the levels of metal content.

The study of the misfolding and aggregation of fALS-associated mutant SOD1 is still a very active field. The studies here support why that is, with the observation of correlations between the thermal stability and aggregation propensities of SOD1 variants in *E.coli* and

supporting the possibility that mutant SOD1 IB's may bind metal. Questions still remain regarding how metals are bound to aggregates, as well as how much the differing aggregation propensities of mutants has to do with disease. It would also be interesting to investigate how the presence of CCS may affect SOD1 IB formation in E.*coli*. The results discussed here may help future generations with the many remaining questions regarding the aggregation of SOD1 in ALS, while also providing insights into IB formation for protein production and the design of functional insoluble biocatalysts.

ELSEVIER LICENSE
TERMS AND CONDITIONS

Aug 27, 2015

This is a License Agreement between Johnathan Almey ("You") and Elsevier ("Elsevier") provided by Copyright Clearance Center ("CCC"). The license consists of your order details, the terms and conditions provided by Elsevier, and the payment terms and conditions.

All payments must be made in full to CCC. For payment instructions, please see information listed at the bottom of this form.

Supplier

Elsevier Limited
The Boulevard,Langford Lane
Kidlington,Oxford,OX5 1GB,UK

Registered Company Number

1982084

Customer name

Johnathan Almey

Customer address

University of Waterloo

Waterloo, ON N2L 3G1

License number

3695551389918

License date

Aug 24, 2015

Licensed content publisher

Elsevier

Licensed content publication

Trends in Biochemical Sciences

Licensed content title

Amyloids in bacterial inclusion bodies

Licensed content author

Natalia S. de Groot,Raimon Sabate,Salvador Ventura

Licensed content date

August 2009

Licensed content volume number

34

Licensed content issue number

8

Number of pages

9

Start Page

408

End Page

416

Type of Use

reuse in a thesis/dissertation

Portion

figures/tables/illustrations

Number of figures/tables/illustrations

1

Format

both print and electronic

Are you the author of this Elsevier article?

No

Will you be translating?

No

Original figure numbers

Figure 2

Title of your thesis/dissertation

Inclusion body formation of familial amyotrophic lateral sclerosis associated Cu Zn superoxide dismutase mutants in Escherichia coli

Expected completion date

Sep 2015

Estimated size (number of pages)

90

Elsevier VAT number

GB 494 6272 12

Permissions price

0.00 CAD

VAT/Local Sales Tax

0.00 CAD / 0.00 GBP

Total

0.00 CAD

Terms and Conditions

INTRODUCTION

1. The publisher for this copyrighted material is Elsevier. By clicking "accept" in connection with completing this licensing transaction, you agree that the following terms and conditions apply to this transaction (along with the Billing and Payment terms and conditions established by Copyright Clearance Center, Inc. ("CCC"), at the time that you opened your Rightslink account and that are available at any time athttp://myaccount.copyright.com).

GENERAL TERMS

2. Elsevier hereby grants you permission to reproduce the aforementioned material subject to the terms and conditions indicated.

3. Acknowledgement: If any part of the material to be used (for example, figures) has appeared in our publication with credit or acknowledgement to another source, permission must also be sought from that source. If such permission is not obtained then that material may not be included in your publication/copies. Suitable acknowledgement to the source must be made, either as a footnote or in a reference list at the end of your publication, as follows:

"Reprinted from Publication title, Vol /edition number, Author(s), Title of article / title of chapter, Pages No., Copyright (Year), with permission from Elsevier [OR APPLICABLE SOCIETY COPYRIGHT OWNER]." Also Lancet special credit - "Reprinted from The Lancet, Vol. number, Author(s), Title of article, Pages No., Copyright (Year), with permission from Elsevier."

4. Reproduction of this material is confined to the purpose and/or media for which permission is hereby given.

5. Altering/Modifying Material: Not Permitted. However figures and illustrations may be altered/adapted minimally to serve your work. Any other abbreviations, additions, deletions and/or any other alterations shall be made only with prior written authorization of Elsevier Ltd. (Please contact Elsevier at permissions@elsevier.com)

6. If the permission fee for the requested use of our material is waived in this instance, please be advised that your future requests for Elsevier materials may attract a fee.

7. Reservation of Rights: Publisher reserves all rights not specifically granted in the combination of (i) the license details provided by you and accepted in the course of this licensing transaction, (ii) these terms and conditions and (iii) CCC's Billing and Payment terms and conditions.

8. License Contingent Upon Payment: While you may exercise the rights licensed immediately upon issuance of the license at the end of the licensing process for the transaction, provided that you have disclosed complete and accurate details of your proposed use, no license is finally effective unless and until full payment is received from you (either by publisher or by CCC) as provided in CCC's Billing and Payment terms and conditions. If full payment is not received on a timely basis, then any license preliminarily granted shall be deemed automatically revoked and shall be void as if never granted. Further, in the event that you breach any of these terms and conditions or any of CCC's Billing and Payment terms and conditions, the license is automatically revoked and shall be void as if never granted. Use of materials as described in a revoked license, as well as any use of the materials beyond the scope of an unrevoked license, may constitute copyright infringement and publisher reserves the right to take any and all action to protect its copyright in the materials.

9. Warranties: Publisher makes no representations or warranties with respect to the licensed material.

10. Indemnity: You hereby indemnify and agree to hold harmless publisher and CCC, and their respective officers, directors, employees and agents, from and against any and all claims arising out of your use of the licensed material other than as specifically authorized pursuant to this license.

11. No Transfer of License: This license is personal to you and may not be sublicensed, assigned, or transferred by you to any other person without publisher's written permission.

12. No Amendment Except in Writing: This license may not be amended except in a writing signed by both parties (or, in the case of publisher, by CCC on publisher's behalf).

13. Objection to Contrary Terms: Publisher hereby objects to any terms contained in any purchase order, acknowledgment, check endorsement or other writing prepared by you, which terms are inconsistent with these terms and conditions or CCC's Billing and Payment terms and conditions. These terms and conditions, together with CCC's Billing and Payment terms and conditions (which are incorporated herein), comprise the entire agreement between you and publisher (and CCC) concerning this licensing transaction. In the event of any conflict between your obligations established by these terms and conditions and those established by CCC's Billing and Payment terms and conditions, these terms and conditions shall control.

14. Revocation: Elsevier or Copyright Clearance Center may deny the permissions described in this License at their sole discretion, for any reason or no reason, with a full refund payable to you. Notice of such denial will be made using the contact information provided by you. Failure to receive such notice will not alter or invalidate the denial. In no event will Elsevier or Copyright Clearance Center be responsible or liable for any costs, expenses or damage incurred by you as a result of a denial of your permission request, other than a refund of the amount(s) paid by you to Elsevier and/or Copyright Clearance Center for denied permissions.

LIMITED LICENSE

The following terms and conditions apply only to specific license types:

15. **Translation**: This permission is granted for non-exclusive world **English** rights only unless your license was granted for translation rights. If you licensed translation rights you may only translate this content into the languages you requested. A professional translator must perform all translations and reproduce the content word for word preserving the integrity of the article. If this license is to re-use 1 or 2 figures then permission is granted for non-exclusive world rights in all languages.

16. **Posting licensed content on any Website**: The following terms and conditions apply as follows: Licensing material from an Elsevier journal: All content posted to the web site must maintain the copyright information line on the bottom of each image; A hyper-text must be included to the Homepage of the journal from which you are licensing

athttp://www.sciencedirect.com/science/journal/xxxxx or the Elsevier homepage for books athttp://www.elsevier.com; Central Storage: This license does not include permission for a scanned version of the material to be stored in a central repository such as that provided by Heron/XanEdu.

Licensing material from an Elsevier book: A hyper-text link must be included to the Elsevier homepage at http://www.elsevier.com . All content posted to the web site must maintain the copyright information line on the bottom of each image.

Posting licensed content on Electronic reserve: In addition to the above the following clauses are applicable: The web site must be password-protected and made available only to bona fide students registered on a relevant course. This permission is granted for 1 year only. You may obtain a new license for future website posting.

17. **For journal authors:** the following clauses are applicable in addition to the above:

Preprints:

A preprint is an author's own write-up of research results and analysis, it has not been peer-reviewed, nor has it had any other value added to it by a publisher (such as formatting, copyright, technical enhancement etc.).

Authors can share their preprints anywhere at any time. Preprints should not be added to or enhanced in any way in order to appear more like, or to substitute for, the final versions of articles however authors can update their preprints on arXiv or RePEc with their Accepted Author Manuscript (see below).

If accepted for publication, we encourage authors to link from the preprint to their formal publication via its DOI. Millions of researchers have access to the formal publications on ScienceDirect, and so links will help users to find, access, cite and use the best available version. Please note that Cell Press, The Lancet and some society-owned have different preprint policies. Information on these policies is available on the journal homepage.

Accepted Author Manuscripts: An accepted author manuscript is the manuscript of an article that has been accepted for publication and which typically includes author-incorporated changes suggested during submission, peer review and editor-author communications.

Authors can share their accepted author manuscript:

- – immediately
    - via their non-commercial person homepage or blog
    - by updating a preprint in arXiv or RePEc with the accepted manuscript
    - via their research institute or institutional repository for internal institutional uses or as part of an invitation-only research collaboration work-group

- directly by providing copies to their students or to research collaborators for their personal use
- for private scholarly sharing as part of an invitation-only work group on commercial sites with which Elsevier has an agreement

- after the embargo period
  - via non-commercial hosting platforms such as their institutional repository
  - via commercial sites with which Elsevier has an agreement

In all cases accepted manuscripts should:

- link to the formal publication via its DOI
- bear a CC-BY-NC-ND license - this is easy to do
- if aggregated with other manuscripts, for example in a repository or other site, be shared in alignment with our hosting policy not be added to or enhanced in any way to appear more like, or to substitute for, the published journal article.

Published journal article (JPA): A published journal article (PJA) is the definitive final record of published research that appears or will appear in the journal and embodies all value-adding publishing activities including peer review co-ordination, copy-editing, formatting, (if relevant) pagination and online enrichment.

Policies for sharing publishing journal articles differ for subscription and gold open access articles:

Subscription Articles: If you are an author, please share a link to your article rather than the full-text. Millions of researchers have access to the formal publications on ScienceDirect, and so links will help your users to find, access, cite, and use the best available version.

Theses and dissertations which contain embedded PJAs as part of the formal submission can be posted publicly by the awarding institution with DOI links back to the formal publications on ScienceDirect.

If you are affiliated with a library that subscribes to ScienceDirect you have additional private sharing rights for others' research accessed under that agreement. This includes use for classroom teaching and internal training at the institution (including use in course packs and courseware programs), and inclusion of the article for grant funding purposes.

Gold Open Access Articles: May be shared according to the author-selected end-user license and should contain a CrossMark logo, the end user license, and a DOI link to the formal publication on ScienceDirect.

Please refer to Elsevier's posting policy for further information.

18. **For book authors** the following clauses are applicable in addition to the above: Authors are permitted to place a brief summary of their work online only. You are not allowed to download and post the published electronic version of your chapter, nor may you scan the printed edition to

create an electronic version. **Posting to a repository:** Authors are permitted to post a summary of their chapter only in their institution's repository.

19. **Thesis/Dissertation**: If your license is for use in a thesis/dissertation your thesis may be submitted to your institution in either print or electronic form. Should your thesis be published commercially, please reapply for permission. These requirements include permission for the Library and Archives of Canada to supply single copies, on demand, of the complete thesis and include permission for Proquest/UMI to supply single copies, on demand, of the complete thesis. Should your thesis be published commercially, please reapply for permission. Theses and dissertations which contain embedded PJAs as part of the formal submission can be posted publicly by the awarding institution with DOI links back to the formal publications on ScienceDirect.

Elsevier Open Access Terms and Conditions

You can publish open access with Elsevier in hundreds of open access journals or in nearly 2000 established subscription journals that support open access publishing. Permitted third party re-use of these open access articles is defined by the author's choice of Creative Commons user license. See our open access license policy for more information.

Terms & Conditions applicable to all Open Access articles published with Elsevier:

Any reuse of the article must not represent the author as endorsing the adaptation of the article nor should the article be modified in such a way as to damage the author's honour or reputation. If any changes have been made, such changes must be clearly indicated.

The author(s) must be appropriately credited and we ask that you include the end user license and a DOI link to the formal publication on ScienceDirect.

If any part of the material to be used (for example, figures) has appeared in our publication with credit or acknowledgement to another source it is the responsibility of the user to ensure their reuse complies with the terms and conditions determined by the rights holder.

Additional Terms & Conditions applicable to each Creative Commons user license:

CC BY: The CC-BY license allows users to copy, to create extracts, abstracts and new works from the Article, to alter and revise the Article and to make commercial use of the Article (including reuse and/or resale of the Article by commercial entities), provided the user gives appropriate credit (with a link to the formal publication through the relevant DOI), provides a link to the license, indicates if changes were made and the licensor is not represented as endorsing the use made of the work. The full details of the license are available at http://creativecommons.org/licenses/by/4.0.

CC BY NC SA: The CC BY-NC-SA license allows users to copy, to create extracts, abstracts and new works from the Article, to alter and revise the Article, provided this is not done for commercial purposes, and that the user gives appropriate credit (with a link to the formal publication through the relevant DOI), provides a link to the license, indicates if changes were made and the licensor is not represented as endorsing the use made of the work. Further, any new works must be made available on the same conditions. The full details of the license are available at http://creativecommons.org/licenses/by-nc-sa/4.0.

CC BY NC ND: The CC BY-NC-ND license allows users to copy and distribute the Article, provided this is not done for commercial purposes and further does not permit distribution of the Article if it is changed or edited in any way, and provided the user gives appropriate credit (with a link to the formal publication through the relevant DOI), provides a link to the license, and that the licensor is not represented as endorsing the use made of the work. The full details of the license are available at http://creativecommons.org/licenses/by-nc-nd/4.0. Any commercial reuse of Open Access articles published with a CC BY NC SA or CC BY NC ND license requires permission from Elsevier and will be subject to a fee.

Commercial reuse includes:

- – Associating advertising with the full text of the Article
- – Charging fees for document delivery or access
- – Article aggregation
- – Systematic distribution via e-mail lists or share buttons

Posting or linking by commercial companies for use by customers of those companies.

20. **Other Conditions**:

v1.7

Questions? customercare@copyright.com or +1-855-239-3415 (toll free in the US) or +1-978-646-2777.

NATURE PUBLISHING GROUP LICENSE TERMS AND CONDITIONS

Aug 27, 2015

This is a License Agreement between Johnathan Almey ("You") and Nature Publishing Group ("Nature Publishing Group") provided by Copyright Clearance Center ("CCC"). The license consists of your order details, the terms and conditions provided by Nature Publishing Group, and the payment terms and conditions.

All payments must be made in full to CCC. For payment instructions, please see information listed at the bottom of this form.

License Number	3695530884442
License date	Aug 24, 2015
Licensed content publisher	Nature Publishing Group
Licensed content publication	Nature Structural and Molecular Biology
Licensed content title	Converging concepts of protein folding : in vitro: and : in vivo
Licensed content author	F Ulrich Hartl and Manajit Hayer-Hartl
Licensed content date	Jun 3, 2009
Volume number	16
Issue number	6
Type of Use	reuse in a dissertation / thesis
Requestor type	academic/educational
Format	print and electronic
Portion	figures/tables/illustrations
Number of figures/tables/illustrations	1
High-res required	no
Figures	Figure 1: Energy landscape scheme of protein folding and aggregation.
Author of this NPG article	no
Your reference number	None
Title of your thesis / dissertation	Inclusion body formation of familial amyotrophic lateral sclerosis associated Cu Zn superoxide dismutase mutants in Escherichia coli
Expected completion date	Sep 2015
Estimated size (number of pages)	90
Total	0.00 CAD

Terms and Conditions

Terms and Conditions for Permissions

Nature Publishing Group hereby grants you a non-exclusive license to reproduce this material for this purpose, and for no other use,subject to the conditions below:

1. NPG warrants that it has, to the best of its knowledge, the rights to license reuse of this material. However, you should ensure that the material you are requesting is original to Nature Publishing Group and does not carry the copyright of another entity (as credited in the published version). If the credit line on any part of the material you have requested indicates that it was reprinted or adapted by NPG with permission from another source, then you should also seek permission from that source to reuse the material.

2. Permission granted free of charge for material in print is also usually granted for any electronic version of that work, provided that the material is incidental to the work as a whole and that the electronic version is essentially equivalent to, or substitutes for, the print version.Where print permission has been granted for a fee, separate permission must be obtained for any additional, electronic re-use (unless, as in the case of a full paper, this has already been accounted for during your initial request in the calculation of a print run).NB: In all cases, web-based use of full-text articles must be authorized separately through the 'Use on a Web Site' option when requesting permission.

3. Permission granted for a first edition does not apply to second and subsequent editions and for editions in other languages (except for signatories to the STM Permissions Guidelines, or where the first edition permission was granted for free).

4. Nature Publishing Group's permission must be acknowledged next to the figure, table or abstract in print. In electronic form, this acknowledgement must be visible at the same time as the figure/table/abstract, and must be hyperlinked to the journal's homepage.

5. The credit line should read:
   Reprinted by permission from Macmillan Publishers Ltd: [JOURNAL NAME] (reference citation), copyright (year of publication)
   For AOP papers, the credit line should read:
   Reprinted by permission from Macmillan Publishers Ltd: [JOURNAL NAME], advance online publication, day month year (doi: 10.1038/sj.[JOURNAL ACRONYM].XXXXX)

   Note: For republication from the *British Journal of Cancer,* the following credit lines apply.
   Reprinted by permission from Macmillan Publishers Ltd on behalf of Cancer Research UK: [JOURNAL NAME] (reference citation), copyright (year of publication)For AOP papers, the credit line should read:
   Reprinted by permission from Macmillan Publishers Ltd on behalf of Cancer Research UK: [JOURNAL NAME], advance online publication, day month year (doi: 10.1038/sj.[JOURNAL ACRONYM].XXXXX)

6. Adaptations of single figures do not require NPG approval. However, the adaptation should be credited as follows:

   Adapted by permission from Macmillan Publishers Ltd: [JOURNAL NAME] (reference citation), copyright (year of publication)

Note: For adaptation from the *British Journal of Cancer,* the following credit line applies.
Adapted by permission from Macmillan Publishers Ltd on behalf of Cancer Research UK: [JOURNAL NAME] (reference citation), copyright (year of publication)

7. Translations of 401 words up to a whole article require NPG approval. Please visithttp://www.macmillanmedicalcommunications.com for more information.Translations of up to a 400 words do not require NPG approval. The translation should be credited as follows:

   Translated by permission from Macmillan Publishers Ltd: [JOURNAL NAME] (reference citation), copyright (year of publication).

   Note: For translation from the *British Journal of Cancer,* the following credit line applies.
   Translated by permission from Macmillan Publishers Ltd on behalf of Cancer Research UK: [JOURNAL NAME] (reference citation), copyright (year of publication)

We are certain that all parties will benefit from this agreement and wish you the best in the use of this material. Thank you.

Special Terms:

v1.1

Questions? customercare@copyright.com or +1-855-239-3415 (toll free in the US) or +1-978-646-2777.

References

(1) Voet, D. Voet, J. G. *Biochemistry*, 4th ed.; John Willey & Sons: Hoboken, 2011.

(2) Atkins, P.; De Paula, J. *Physical Chemistry for the life sciences*, 2nd ed.; W.H Freeman and Company: New York, 2011.

(3) Berg, J. T.; Stryer, L. *Biochemistry*, 6th ed.; W.H. Freeman: New York, 2006.

(4) Doyle, C. M.; Rumfeldt, J. a.; Broom, H. R.; Broom, A.; Stathopulos, P. B.; Vassall, K. a.; Almey, J. J.; Meiering, E. M. Energetics of oligomeric protein folding and association. *Arch. Biochem. Biophys.* **2013**, *531* (1-2), 44–64 DOI: 10.1016/j.abb.2012.12.005.

(5) Goodsell, D. S.; Olson, A. J. S s p f. **2000**.

(6) Valentine, J. S.; Doucette, P. a; Zittin Potter, S. Copper-zinc superoxide dismutase and amyotrophic lateral sclerosis. *Annu. Rev. Biochem.* **2005**, *74*, 563–593 DOI: 10.1146/annurev.biochem.72.121801.161647.

(7) Vabulas, R. M.; Raychaudhuri, S.; Hayer-hartl, M.; Hartl, F. U. Heat Shock Response. **2010**, 1–18 DOI: 10.1101/cshperspect.a004390.

(8) Kim, Y. E.; Hipp, M. S.; Bracher, A.; Hayer-Hartl, M.; Hartl, F. U. *Molecular chaperone functions in protein folding and proteostasis.*; 2013; Vol. 82.

(9) Castillo, V.; Espargaró, A.; Gordo, V.; Vendrell, J.; Ventura, S. Deciphering the role of the thermodynamic and kinetic stabilities of SH3 domains on their aggregation inside bacteria. *Proteomics* **2010**, *10* (23), 4172–4185 DOI: 10.1002/pmic.201000260.

(10) Gething, M.; Sambrook, J. Protein Folding in the Cell. *Nature* **1992**, *355* (6355), 33–45.

(11) Dill, K. A.; Maccallum, J. L.; Folding, P. The Protein-Folding Problem , 50 Years On. **2012**, No. NOVEMBER, 1042–1047.

(12) Benkovic, S. J.; Hammes-Schiffer, S. A perspective on enzyme catalysis. *Science* **2003**, *301* (5637), 1196–1202 DOI: 10.1126/science.1085515.

(13) Fink, A. L. Protein aggregation: Folding aggregates, inclusion bodies and amyloid. *Fold. Des.* **1998**, *3* (1), 9–23 DOI: 10.1016/S1359-0278(98)00002-9.

(14) Hartl, F. U.; Hayer-Hartl, M. Converging concepts of protein folding in vitro and in vivo. *Nat. Struct. Mol. Biol.* **2009**, *16* (6), 574–581 DOI: 10.1038/nsmb.1591.

(15) Eisenberg, D.; Jucker, M. The amyloid state of proteins in human diseases. *Cell* **2012**, *148* (6), 1188–1203 DOI: 10.1016/j.cell.2012.02.022.

(16) Morimoto, R. I. Stress, aging, and neurodegenerative disease. *N. Engl. J. Med.* **2006**, *355* (21), 2254–2255 DOI: 10.1056/NEJMcibr065573.

(17) Wang, Q.; Johnson, J. L.; Agar, N. Y. R.; Agar, J. N. Protein aggregation and protein instability govern familial amyotrophic lateral sclerosis patient survival. *PLoS Biol.* **2008**, *6* (7), 1508–1526 DOI: 10.1371/journal.pbio.0060170.

(18) Ross, C. a; Poirier, M. a. Protein aggregation and neurodegenerative disease. *Nat. Med.* **2004**, *10 Suppl* (July), S10–S17 DOI: 10.1038/nm1066.

(19) Furukawa, Y.; Fu, R.; Deng, H.-X.; Siddique, T.; O'Halloran, T. V. Disulfide cross-linked protein represents a significant fraction of ALS-associated Cu, Zn-superoxide dismutase aggregates in spinal cords of model mice. *Proc. Natl. Acad. Sci. U. S. A.* **2006**, *103* (18), 7148–7153 DOI: 10.1073/pnas.0602048103.

(20) Furukawa, Y. Pathological roles of wild-type Cu, Zn-superoxide dismutase in amyotrophic lateral sclerosis. *Neurol. Res. Int.* **2012**, *2012* DOI: 10.1155/2012/323261.

(21) Ventura, S.; Villaverde, A. Protein quality in bacterial inclusion bodies. *Trends Biotechnol.* **2006**, *24* (4), 179–185 DOI: 10.1016/j.tibtech.2006.02.007.

(22) Belli, M.; Ramazzotti, M.; Chiti, F. Prediction of amyloid aggregation in vivo. *EMBO Rep.* **2011**, *12* (7), 657–663 DOI: 10.1038/embor.2011.116.

(23) Chiti, F.; Stefani, M.; Taddei, N.; Ramponi, G.; Dobson, C. M. Rationalization of the effects of mutations on peptide and protein aggregation rates. *Nature* **2003**, *424* (6950), 805–808 DOI: 10.1038/nature01891.

(24) Fernandez-Escamilla, A.-M.; Rousseau, F.; Schymkowitz, J.; Serrano, L. Prediction of sequence-dependent and mutational effects on the aggregation of peptides and proteins. *Nat. Biotechnol.* **2004**, *22* (10), 1302–1306 DOI: 10.1038/nbt1012.

(25) Tartaglia, G. G.; Vendruscolo, M. The Zyggregator method for predicting protein aggregation propensities. *Chem. Soc. Rev.* **2008**, *37* (7), 1395–1401 DOI: 10.1039/b706784b.

(26) Kato, S.; Hayashi, H.; Nakashima, K.; Nanba, E.; Kato, M.; Hirano, a; Nakano, I.; Asayama, K.; Ohama, E. Pathological characterization of astrocytic hyaline inclusions in familial amyotrophic lateral sclerosis. *Am. J. Pathol.* **1997**, *151* (2), 611–620.

(27) Yamagishi, S.; Koyama, Y.; Katayama, T.; Taniguchi, M.; Hitomi, J.; Kato, M.; Aoki, M.; Itoyama, Y.; Kato, S.; Tohyama, M. An in vitro model for lewy body-like hyaline inclusion/astrocytic hyaline inclusion: Induction by ER stress with an ALS-linked SOD1 mutation. *PLoS One* **2007**, *2* (10) DOI: 10.1371/journal.pone.0001030.

(28) Johnston, J. a; Dalton, M. J.; Gurney, M. E.; Kopito, R. R. Formation of high molecular weight complexes of mutant Cu, Zn-superoxide dismutase in a mouse model for familial amyotrophic lateral sclerosis. *Proc. Natl. Acad. Sci. U. S. A.* **2000**, *97* (23), 12571–12576 DOI: 10.1073/pnas.220417997.

(29) Peternel, S.; Komel, R. Isolation of biologically active nanomaterial (inclusion bodies) from bacterial cells. *Microb. Cell Fact.* **2010**, *9*, 66 DOI: 10.1186/1475-2859-9-66.

(30) Matsumoto, G.; Stojanovic, A.; Holmberg, C. I.; Kim, S.; Morimoto, R. I. Structural properties and neuronal toxicity of amyotrophic lateral sclerosis-associated Cu/Zn superoxide dismutase 1 aggregates. *J. Cell Biol.* **2005**, *171* (1), 75–85 DOI: 10.1083/jcb.200504050.

(31) García-Fruitós, E.; Vázquez, E.; Díez-Gil, C.; Corchero, J. L.; Seras-Franzoso, J.; Ratera, I.; Veciana, J.; Villaverde, A. Bacterial inclusion bodies: Making gold from waste. *Trends Biotechnol.* **2012**, *30* (2), 65–70 DOI: 10.1016/j.tibtech.2011.09.003.

(32) García-Fruitós, E.; Villaverde, A. Friendly production of bacterial inclusion bodies. *Korean J. Chem. Eng.* **2010**, *27* (2), 385–389 DOI: 10.1007/s11814-010-0161-3.

(33) De Groot, N. S.; Sabate, R.; Ventura, S. Amyloids in bacterial inclusion bodies. *Trends Biochem. Sci.* **2009**, *34* (8), 408–416 DOI: 10.1016/j.tibs.2009.03.009.

(34) Wang, L.; Maji, S. K.; Sawaya, M. R.; Eisenberg, D.; Riek, R. Bacterial inclusion bodies contain amyloid-like structure. *PLoS Biol.* **2008**, *6* (8), 1791–1801 DOI: 10.1371/journal.pbio.0060195.

(35) Upadhyay, A. K.; Murmu, A.; Singh, A.; Panda, A. K. Kinetics of inclusion body formation and its correlation with the characteristics of protein aggregates in escherichia coli. *PLoS One* **2012**, *7* (3) DOI: 10.1371/journal.pone.0033951.

(36) Rinas, U.; Bailey, J. E. Protein compositional analysis of inclusion bodies produced in recombinant Escherichia coil. **1992**, 609–614.

(37) Mizusawa, H.; Ph, D. Hyaline and Skein-like Inclusions in Amyotrophic Lateral Sclerosis. **1993**, 201–208.

(38) Bergh, J.; Zetterström, P.; Andersen, P. M.; Brännström, T.; Graffmo, K. S.; Jonsson, P. A.; Lang, L.; Danielsson, J.; Oliveberg, M.; Marklund, S. L. Structural and kinetic analysis of protein-aggregate strains in vivo using binary epitope mapping. *Proc. Natl. Acad. Sci.* **2015**, 201419228 DOI: 10.1073/pnas.1419228112.

(39) Leinweber, B.; Barofsky, E.; Barofsky, D. F.; Ermilov, V.; Nylin, K.; Beckman, J. S. Aggregation of als mutant superoxide dismutase expressed in Escherichia coli. *Free Radic. Biol. Med.* **2004**, *36* (7), 911–918 DOI: 10.1016/j.freeradbiomed.2003.12.021.

(40) Stathopulos, P. B.; Rumfeldt, J. a O.; Scholz, G. a; Irani, R. a; Frey, H. E.; Hallewell, R. a; Lepock, J. R.; Meiering, E. M. Cu/Zn superoxide dismutase mutants associated with amyotrophic lateral sclerosis show enhanced formation of aggregates in vitro. *Proc. Natl. Acad. Sci. U. S. A.* **2003**, *100* (12), 7021–7026 DOI: 10.1073/pnas.1237797100.

(41) Banci, L.; Bertini, I.; Durazo, A.; Girotto, S.; Gralla, E. B.; Martinelli, M.; Valentine, J. S.; Vieru, M.; Whitelegge, J. P. Metal-free superoxide dismutase forms soluble oligomers under physiological conditions: a possible general mechanism for familial ALS. *Proc. Natl. Acad. Sci. U. S. A.* **2007**, *104* (27), 11263–11267 DOI: 10.1073/pnas.0704307104.

(42) Gross-Selbeck, S.; Margreiter, G.; Obinger, C.; Bayer, K. Fast quantification of recombinant protein inclusion bodies within intact cells by FT-IR spectroscopy. *Biotechnol. Prog.* **2007**, *23* (3), 762–766 DOI: 10.1021/bp070022q.

(43) García-Fruitós, E.; Carrió, M. M.; Arís, A.; Villaverde, A. Folding of a misfolding-prone β-galactosidase in absence of DnaK. *Biotechnol. Bioeng.* **2005**, *90* (7), 869–875 DOI: 10.1002/bit.20496.

(44) Wu, W.; Xing, L.; Zhou, B.; Lin, Z. Active protein aggregates induced by terminally attached self-assembling peptide ELK16 in Escherichia coli. *Microb. Cell Fact.* **2011**, *10* (1), 9 DOI: 10.1186/1475-2859-10-9.

(45) Nahalka, J.; Nidetzky, B. Fusion to a Pull-Down Domain: A Novel Approach of Producing Trigonopsis variabilis D-Amino Acid Oxidase as Insoluble Enzyme Aggregates. *Biotechnol. Bioeng.* **2007**, *97* (3), 454–461 DOI: 10.1002/bit.

(46) Bruijn, L. I.; Miller, T. M.; Cleveland, D. W. Unraveling the mechanisms involved in motor neuron degeneration in ALS. *Annu. Rev. Neurosci.* **2004**, *27*, 723–749 DOI: 10.1146/annurev.neuro.27.070203.144244.

(47) Kiernan, M. C.; Vucic, S.; Cheah, B. C.; Turner, M. R.; Eisen, A.; Hardiman, O.; Burrell, J. R.; Zoing, M. C. Amyotrophic lateral sclerosis. *Lancet* **2011**, *377* (9769), 942–955 DOI: 10.1016/S0140-6736(10)61156-7.

(48) Mitchell, J. D.; Borasio, G. D. Amyotrophic lateral sclerosis. *Lancet* **2007**, *369* (9578), 2031–2041 DOI: 10.1016/S0140-6736(07)60944-1.

(49) Robberecht, W.; Philips, T. The changing scene of amyotrophic lateral sclerosis. *Nat. Rev. Neurosci.* **2013**, *14* (4), 248–264 DOI: 10.1038/nrn3430.

(50) Marangi, G.; Traynor, B. J. Genetic causes of amyotrophic lateral sclerosis: New genetic analysis methodologies entailing new opportunities and challenges. *Brain Res.* **2014** DOI: 10.1016/j.brainres.2014.10.009.

(51) Wood, J. D.; Beaujeux, T. P.; Shaw, P. J. Protein aggregation in motor neurone disorders. *Neuropathol. Appl. Neurobiol.* **2003**, *29* (6), 529–545 DOI: 10.1046/j.0305-1846.2003.00518.x.

(52) Brotherton, T. E.; Li, Y.; Glass, J. D. Cellular toxicity of mutant SOD1 protein is linked to an easily soluble, non-aggregated form in vitro. *Neurobiol. Dis.* **2013**, *49* (1), 49–56 DOI: 10.1016/j.nbd.2012.08.010.

(53) Jonsson, P. A.; Ernhill, K.; Andersen, P. M.; Bergemalm, D.; Brännström, T.; Gredal, O.; Nilsson, P.; Marklund, S. L. Minute quantities of misfolded mutant superoxide dismutase-1 cause amyotrophic lateral sclerosis. *Brain* **2004**, *127* (1), 73–88 DOI: 10.1093/brain/awh005.

(54) Beghi, E.; Chiò, A.; Couratier, P.; Esteban, J.; Hardiman, O.; Logroscino, G.; Millul, A.; Mitchell, D.; Preux, P.-M.; Pupillo, E.; et al. The epidemiology and treatment of ALS: focus on the heterogeneity of the disease and critical appraisal of therapeutic trials. *Amyotroph. Lateral Scler.* **2011**, *12* (1), 1–10 DOI: 10.3109/17482968.2010.502940.

(55) Macchi, Z.; Wang, Y.; Moore, D.; Katz, J.; Saperstein, D.; Walk, D.; Simpson, E.; Genge, A.; Bertorini, T.; Fernandes, J. A.; et al. A multi-center screening trial of rasagiline in patients with amyotrophic lateral sclerosis: Possible mitochondrial biomarker target engagement. *Amyotroph. Lateral Scler. Front. Degener.* **2015**, No. November 2014, 1–8 DOI: 10.3109/21678421.2015.1026826.

(56) Ray, S. S.; Nowak, R. J.; Brown, R. H.; Lansbury, P. T. Small-molecule-mediated stabilization of familial amyotrophic lateral sclerosis-linked superoxide dismutase mutants against unfolding and aggregation. *Proc. Natl. Acad. Sci. U. S. A.* **2005**, *102* (10), 3639–3644 DOI: 10.1073/pnas.0408277102.

(57) Glicksman, M. a. The preclinical discovery of amyotrophic lateral sclerosis drugs. *Expert Opin. Drug Discov.* **2011**, *6* (11), 1127–1138 DOI: 10.1517/17460441.2011.628654.

(58) Hsu, J. L.; Hsieh, Y.; Tu, C.; O'Connor, D.; Nick, H. S.; Silverman, D. N. Catalytic properties of human manganese superoxide dismutase. *J. Biol. Chem.* **1996**, *271* (30), 17687–17691.

(59) Borgstahl, G. E.; Parge, H. E.; Hickey, M. J.; Beyer, W. F.; Hallewell, R. a; Tainer, J. a. The structure of human mitochondrial manganese superoxide dismutase reveals a novel tetrameric interface of two 4-helix bundles. *Cell* **1992**, *71* (1), 107–118 DOI: 10.1016/0092-8674(92)90270-M.

(60) Adachi, T.; Marklund, S. L. Interactions between human extracellular superoxide dismutase C and sulfated polysaccharides. *J. Biol. Chem.* **1989**, *264* (15), 8537–8541.

(61) Broom, H. R.; Rumfeldt, J.; Meiering, E. M. Many roads lead to rome? Multiple modes of Cu,Zn superoxide dismutase destabilization, misfolding and aggregation in amyotrophic lateral sclerosis. *Essays Biochem.* **2014**, *56*, 149–165.

(62) Strange, R. W.; Antonyuk, S.; Hough, M. a.; Doucette, P. a.; Rodriguez, J. a.; Hart, P. J.; Hayward, L. J.; Valentine, J. S.; Hasnain, S. S. The structure of holo and metal-deficient wild-type human Cu, Zn superoxide dismutase and its relevance to familial amyotrophic lateral sclerosis. *J. Mol. Biol.* **2003**, *328* (4), 877–891 DOI: 10.1016/S0022-2836(03)00355-3.

(63) Benov, L. How superoxide radical damages the cell. *Protoplasma* **2001**, *217* (1-3), 33–36 DOI: 10.1007/BF01289410.

(64) Borchelt, D. R.; Leeo, M. K.; Sluntt, H. S.; Guarnierit, M.; Xu, Z.; Wong, P. C.; Brown, R. H.; Price, D. L.; Sisodia, S. S.; Clevelandt, D. O. N. W. Superoxide dismutase 1 with mutations linked to familial amyotrophic lateral sclerosis psesses significant activity. *Neurobiology* **1994**, *91* (August), 8292–8296.

(65) Saccon, R. a.; Bunton-Stasyshyn, R. K. a; Fisher, E. M. C.; Fratta, P. Is SOD1 loss of function involved in amyotrophic lateral sclerosis? *Brain* **2013**, *136* (8), 2342–2358 DOI: 10.1093/brain/awt097.

(66) Hunter, G. .; Hunter, T. GroESL protects superoxide dismutase (SOD)-deficient cells against oxidative stress and is a chaperone for SOD. *Health (Irvine. Calif).* **2013**, *5* (10), 1719–1729.

(67) Alves-Rodrigues, A.; Gregori, L.; Figueiredo-Pereira, M. E. Ubiquitin, cellular inclusions and their role in neurodegeneration. *Trends Neurosci.* **1998**, *21* (12), 516–520 DOI: 10.1016/S0166-2236(98)01276-4.

(68) Trumbull, K. a; Beckman, J. S. A role for copper in the toxicity of zinc-deficient superoxide dismutase to motor neurons in amyotrophic lateral sclerosis. *Antioxid. Redox Signal.* **2009**, *11* (7), 1627–1639 DOI: 10.1089/ars.2009.2574.

(69) Legname, G.; Giachin, G.; Benetti, F. *Non-fibrillar Amyloidogenic Protein Assemblies - Common Cytotoxins Underlying Degenerative Diseases*; 2012.

(70) Andersen, J. K. Oxidative stress in neurodegeneration: cause or consequence? *Nat. Med.* **2004**, *10 Suppl* (July), S18–S25 DOI: 10.1038/nrn1434.

(71) Al-Chalabi, A.; Institute of Psychiatry, Psychology & Neuroscience (IoPPN) DeCrespigny Park, Denmark Hill, L. S. 8AF. Gene Overview of Key Published Studies for ALS http://alsod.iop.kcl.ac.uk/Overview/gene.aspx?gene_id=SOD1 (accessed Jul 20, 2015).

(72) Broom, H. R.; Primmer, H. A.; Rumfeldt, J. a O.; Stathopulos, P. B.; Vassall, K. a.; Hwang, Y.; Meiering, E. M. Folding and aggregation of Cu, Zn-Superoxide Dismutase. In *Amyotrophic Lateral Sclerosis*; Maurer, M., Ed.; 2012; pp 265–300.

(73) Rumfeldt, J. a O.; Stathopulos, P. B.; Chakrabarrty, A.; Lepock, J. R.; Meiering, E. M. Mechanism and thermodynamics of guanidinium chloride-induced denaturation of ALS-associated mutant Cu,Zn superoxide dismutases. *J. Mol. Biol.* **2006**, *355* (1), 106–123 DOI: 10.1016/j.jmb.2005.10.042.

(74) Prudencio, M.; Hart, P. J.; Borchelt, D. R.; Andersen, P. M. Variation in aggregation propensities among ALS-associated variants of SOD1: Correlation to human disease. *Hum. Mol. Genet.* **2009**, *18* (17), 3217–3226 DOI: 10.1093/hmg/ddp260.

(75) Vassall, K. a; Stubbs, H. R.; Primmer, H. a; Tong, M. S.; Sullivan, S. M.; Sobering, R.; Srinivasan, S.; Briere, L.-A. K.; Dunn, S. D.; Colón, W.; et al. Decreased stability and increased formation of soluble aggregates by immature superoxide dismutase do not account for disease severity in ALS. *Proc. Natl. Acad. Sci. U. S. A.* **2011**, *108* (6), 2210–2215 DOI: 10.1073/pnas.0913021108.

(76) Stathopulos, P. B.; Scholz, G. a; Hwang, Y.-M.; Rumfeldt, J. a O.; Lepock, J. R.; Meiering, E. M. Sonication of proteins causes formation of aggregates that resemble amyloid. *Protein Sci.* **2004**, *13* (11), 3017–3027 DOI: 10.1110/ps.04831804.

(77) Noor, R.; Mittal, S.; Iqbal, J. Superoxide dismutase--applications and relevance to human diseases. *Med. Sci. Monit.* **2002**, *8* (9), RA210–A215 DOI: 2653 [pii].

(78) Auclair, J. R.; Boggio, K. J.; Petsko, G. a; Ringe, D.; Agar, J. N. Strategies for stabilizing superoxide dismutase (SOD1), the protein destabilized in the most common form of familial amyotrophic lateral sclerosis. *Proc. Natl. Acad. Sci. U. S. A.* **2010**, *107* (50), 21394–21399 DOI: 10.1073/pnas.1015463107.

(79) Lelie, H. L.; Liba, A.; Bourassa, M. W.; Chattopadhyay, M.; Chan, P. K.; Gralla, E. B.; Miller, L. M.; Borchelt, D. R.; Valentine, J. S.; Whitelegge, J. P. Copper and zinc metallation status of copper-zinc superoxide dismutase from amyotrophic lateral sclerosis transgenic mice. *J. Biol. Chem.* **2011**, *286* (4), 2795–2806 DOI: 10.1074/jbc.M110.186999.

(80) Baneyx, F. Recombinant protein expression in Escherichia coli. *Curr. Opin. Biotechnol.* **1999**, *10*, 411–420 DOI: 10.1016/S0958-1669(99)00003-8.

(81) Furukawa, Y.; Kaneko, K.; Watanabe, S.; Yamanaka, K.; Nukina, N. Intracellular seeded aggregation of mutant Cu,Zn-superoxide dismutase associated with amyotrophic lateral sclerosis. *FEBS Lett.* **2013**, *587* (16), 2500–2505 DOI: 10.1016/j.febslet.2013.06.046.

(82) Furukawa, Y.; Torres, A. S.; O'Halloran, T. V. Oxygen-induced maturation of SOD1: a key role for disulfide formation by the copper chaperone CCS. *EMBO J.* **2004**, *23* (14), 2872–2881 DOI: 10.1038/sj.emboj.7600276.

(83) Ahl, I. M.; Lindberg, M. J.; Tibell, L. a E. Coexpression of yeast copper chaperone (yCCS) and CuZn-superoxide dismutases in Escherichia coli yields protein with high copper contents. *Protein Expr. Purif.* **2004**, *37* (2), 311–319 DOI: 10.1016/j.pep.2004.06.006.

(84) Schmidt, P. J.; Kunst, C.; Culotta, V. C. Copper activation of superoxide dismutase 1 (SOD1) in vivo: Role for protein-protein interactions with the copper chaperone for SOD1. *J. Biol. Chem.* **2000**, *275* (43), 33771–33776 DOI: 10.1074/jbc.M006254200.

(85) Carroll, M. C.; Girouard, J. B.; Ulloa, J. L.; Subramaniam, J. R.; Wong, P. C.; Valentine, J. S.; Culotta, V. C. Mechanisms for activating Cu- and Zn-containing superoxide dismutase in the absence of the CCS Cu chaperone. *Proc. Natl. Acad. Sci. U. S. A.* **2004**, *101* (16), 5964–5969 DOI: 10.1073/pnas.0308298101.

(86) Hayward, L. J.; Rodriguez, J. a.; Kim, J. W.; Tiwari, A.; Goto, J. J.; Cabelli, D. E.; Valentine, J. S.; Brown, R. H. Decreased metallation and activity in subsets of mutant superoxide dismutases associated with familial amyotrophic lateral sclerosis. *J. Biol. Chem.* **2002**, *277* (18), 15923–15931 DOI: 10.1074/jbc.M112087200.

(87) Stathopulos, P. B.; Rumfeldt, J. a O.; Karbassi, F.; Siddall, C. a.; Lepock, J. R.; Meiering, E. M. Calorimetric analysis of thermodynamic stability and aggregation for Apo and Holo amyotrophic lateral sclerosis-associated Gly-93 mutants of superoxide dismutase. *J. Biol. Chem.* **2006**, *281* (10), 6184–6193 DOI: 10.1074/jbc.M509496200.

(88) Vassall, K. a.; Stathopulos, P. B.; Rumfeldt, J. a O.; Lepock, J. R.; Meiering, E. M. Equilibrium thermodynamic analysis of amyotrophic lateral sclerosis-associated mutant Apo Cu,Zn superoxide dismutases. *Biochemistry* **2006**, *45* (23), 7366–7379 DOI: 10.1021/bi0600953.

(89) Crow, J. P.; Sampson, J. B.; Zhuang, Y.; Thompson, J. a; Beckman, J. S. Decreased zinc affinity of amyotrophic lateral sclerosis-associated superoxide dismutase mutants leads to enhanced catalysis of tyrosine nitration by peroxynitrite. *J. Neurochem.* **1997**, *69* (5), 1936–1944 DOI: 10.1046/j.1471-4159.1997.69051936.x.

(90) J. Ghasemi,*,† H. Peyman, and M. M. is the element of the absorbance matrix A of size n,m being measured for n solutions with known total concentrations of three basic components, c. *J. Chem. Eng. Data* **2007**, *52*, 1171–1178.

(91) Säbel, C. E.; Shepherd, J. L.; Siemann, S. A direct spectrophotometric method for the simultaneous determination of zinc and cobalt in metalloproteins using 4-(2-pyridylazo)resorcinol. *Anal. Biochem.* **2009**, *391* (1), 74–76 DOI: 10.1016/j.ab.2009.05.007.

(92) Strange, R. W.; Antonyuk, S. V.; Hough, M. a.; Doucette, P. a.; Valentine, J. S.; Hasnain, S. S. Variable metallation of human superoxide dismutase: Atomic resolution crystal structures of Cu-Zn, Zn-Zn and as-isolated wild-type enzymes. *J. Mol. Biol.* **2006**, *356* (5), 1152–1162 DOI: 10.1016/j.jmb.2005.11.081.

(93) Natvig, D. O.; Imlay, K.; Touati, D.; Hallewell, R. a. Human copper-zinc superoxide dismutase complements superoxide dismutase-deficient Escherichia coli mutants. *J. Biol. Chem.* **1987**, *262* (30), 14697–14701.

(94) Miller, J. F. Bacterial Transformation by Electroporation. *Methods Enzymol.* **1994**, *235*, 375–385.

(95) Liochev, S. I.; Chen, L. L.; Hallewell, R. a; Fridovich, I. The familial amyotrophic lateral sclerosis-associated amino acid substitutions E100G, G93A, and G93R do not influence the rate of inactivation of copper- and zinc-containing superoxide dismutase by H2O2. *Arch. Biochem. Biophys.* **1998**, *352* (2), 237–239 DOI: DOI 10.1006/abbi.1998.0616.

(96) Rodriguez, J. a.; Valentine, J. S.; Eggers, D. K.; Roe, J. a.; Tiwari, A.; Brown, R. H.; Hayward, L. J. Familial amyotrophic lateral sclerosis-associated mutations decrease the thermal stability of distinctly metallated species of human copper/zinc superoxide dismutase. *J. Biol. Chem.* **2002**, *277* (18), 15932–15937 DOI: 10.1074/jbc.M112088200.

(97) Marklund, S.; Marklund, G. Involvement of the superoxide anion radical in the autoxidation of pyrogallol and a convenient assay for superoxide dismutase. *Eur. J. Biochem.* **1974**, *47* (3), 469–474 DOI: 10.1111/j.1432-1033.1974.tb03714.x.

(98) De Beus, M. D.; Chung, J.; Colón, W. Modification of cysteine 111 in Cu/Zn superoxide dismutase results in altered spectroscopic and biophysical properties. *Protein Sci.* **2004**, *13* (5), 1347–1355 DOI: 10.1110/ps.03576904.

(99) Rasband, W. S. ImageJ. National Institutes of Health: Bethesda Maryland.

(100) Doyle, C. A Refined Method for Quantitation of Divalent Metal Ions in Metalloproteins and Local Stability and Conformational Heterogeneity of Amyotrophic Lateral Sclerosis-Associated Cu , Zn Superoxide Dismutase, University of Waterloo, 2014.

(101) Davydov, D. R.; Deprez, E.; Hoa, G. H.; Knyushko, T. V; Kuznetsova, G. P.; Koen, Y. M.; Archakov, a I. High-pressure-induced transitions in microsomal cytochrome P450 2B4 in solution: evidence for conformational inhomogeneity in the oligomers. *Arch. Biochem. Biophys.* **1995**, *320* (2), 330–344 DOI: 10.1016/0003-9861(95)90017-9.

(102) Martínez-Alonso, M.; García-Fruitós, E.; Villaverde, A. Yield, solubility and conformational quality of soluble proteins are not simultaneously favored in recombinant Escherichia coli. *Biotechnol. Bioeng.* **2008**, *101* (6), 1353–1358 DOI: 10.1002/bit.21996.

(103) Lindberg, M. J.; Byström, R.; Boknäs, N.; Andersen, P. M.; Oliveberg, M. Systematically perturbed folding patterns of amyotrophic lateral sclerosis (ALS)-associated SOD1 mutants. *Proc. Natl. Acad. Sci. U. S. A.* **2005**, *102* (28), 9754–9759 DOI: 10.1073/pnas.0501957102.

(104) Jezorek, J. R.; Freiser, H. 4-(Pyridylazo)resorcinol-based continuous detection system for trace levels of metal ions. *Anal. Chem.* **1979**, *51* (3), 373–376 DOI: 10.1021/ac50039a012.

(105) Atanassova, A.; Lam, R.; Zamble, D. B. A high-performance liquid chromatography method for determining transition metal content in proteins. *Anal. Biochem.* **2004**, *335* (1), 103–111 DOI: 10.1016/j.ab.2004.08.013.

(106) Rae, T. D.; Schmidt, P. J.; Pufahl, R. a; Culotta, V. C.; O'Halloran, T. V. Undetectable intracellular free copper: the requirement of a copper chaperone for superoxide dismutase. *Science* **1999**, *284* (5415), 805–808 DOI: 10.1126/science.284.5415.805.

(107) Gonzalez, M. H.; Souza, G. B.; Oliveira, R. V.; Forato, L. a.; Nóbrega, J. a.; Nogueira, a. R. a. Microwave-assisted digestion procedures for biological samples with diluted nitric acid: Identification of reaction products. *Talanta* **2009**, *79* (2), 396–401 DOI: 10.1016/j.talanta.2009.04.001.

(108) Rodriguez, J. a; Shaw, B. F.; Durazo, A.; Sohn, S. H.; Doucette, P. a; Nersissian, A. M.; Faull, K. F.; Eggers, D. K.; Tiwari, A.; Hayward, L. J.; et al. Destabilization of apoprotein is insufficient to explain Cu,Zn-superoxide dismutase-linked ALS pathogenesis. *Proc. Natl. Acad. Sci. U. S. A.* **2005**, *102* (30), 10516–10521 DOI: 10.1073/pnas.0502515102.

(109) Soshanna Zittin Potter, J. S. V. The perplexing role of copper-zinc superoxide dismutase in amyotrophic lateral sclerosis (Lou Gehrig's disease). *J. Biol. Inorg. Chem.* **2003**, *8* (4), 373–380.

(110) Leslie A. Pratt, Weihong Hsing, K. E. G.; Silhavy, and T. J. From acids to osmZ multiple factors influence synthesis of the OmpF and OmpC porins in Escherichia COD. *Mol. Microbiol.* **1996**, *20* (5), 911–917.

(111) Bednarska, N. G.; Schymkowitz, J.; Rousseau, F.; Van Eldere, J. Protein aggregation in bacteria: The thin boundary between functionality and toxicity. *Microbiol. (United Kingdom)* **2013**, *159* (PART 9), 1795–1806 DOI: 10.1099/mic.0.069575-0.

(112) Villa, R.; Lotti, M.; Gatti-Lafranconi, P. Components of the E. coli envelope are affected by and can react to protein over-production in the cytoplasm. *Microb. Cell Fact.* **2009**, *8*, 32 DOI: 10.1186/1475-2859-8-32.

(113) Calloni, G.; Zoffoli, S.; Stefani, M.; Dobson, C. M.; Chiti, F. Investigating the effects of mutations on protein aggregation in the cell. *J. Biol. Chem.* **2005**, *280* (11), 10607–10613 DOI: 10.1074/jbc.M412951200.

(114) Mayer, S.; Rüdiger, S.; Ang, H. C.; Joerger, A. C.; Fersht, A. R. Correlation of Levels of Folded Recombinant p53 in Escherichia coli with Thermodynamic Stability in Vitro. *J. Mol. Biol.* **2007**, *372* (1), 268–276 DOI: 10.1016/j.jmb.2007.06.044.

(115) Chrunyk, B. a; Evans, J.; Lillquist, J.; Young, P.; Wetzel, R. Inclusion Body Formation and Protein Stability in Sequence Variants of Interleukin-lfl*. *J. Biol. Chem.* **1993**, *268* (24), 18053–18061.

(116) Rumfeldt, J. a O.; Lepock, J. R.; Meiering, E. M. Unfolding and Folding Kinetics of Amyotrophic Lateral Sclerosis-Associated Mutant Cu,Zn Superoxide Dismutases. *J. Mol. Biol.* **2009**, *385* (1), 278–298 DOI: 10.1016/j.jmb.2008.10.003.

(117) Andersen, P. M.; Nilsson, P.; Keränen, M. L.; Forsgren, L.; Hägglund, J.; Karlsborg, M.; Ronnevi, L. O.; Gredal, O.; Marklund, S. L. Phenotypic heterogeneity in motor neuron disease patients with CuZn-superoxide dismutase mutations in Scandinavia. *Brain* **1997**, *120 (Pt 1*, 1723–1737 DOI: 10.1093/brain/120.10.1723.

(118) Amen, T.; Kaganovich, D. Dynamic droplets: the role of cytoplasmic inclusions in stress, function, and disease. *Cell. Mol. Life Sci.* **2015**, *72* (3), 401–415 DOI: 10.1007/s00018-014-1740-y.

(119) Keller, B. a.; Volkening, K.; Droppelmann, C. a.; Ang, L. C.; Rademakers, R.; Strong, M. J. Co-aggregation of RNA binding proteins in ALS spinal motor neurons: Evidence of a common pathogenic mechanism. *Acta Neuropathol.* **2012**, *124* (5), 733–747 DOI: 10.1007/s00401-012-1035-z.

(120) Karch, C. M.; Prudencio, M.; Winkler, D. D.; Hart, P. J.; Borchelt, D. R. Role of mutant SOD1 disulfide oxidation and aggregation in the pathogenesis of familial ALS. *Proc. Natl. Acad. Sci. U. S. A.* **2009**, *106* (19), 7774–7779 DOI: 10.1073/pnas.0902505106.

(121) Redler, R. L.; Fee, L.; Fay, J. M.; Caplow, M.; Dokholyan, N. V. Non-native soluble oligomers of Cu/Zn superoxide dismutase (SOD1) contain a conformational epitope linked to cytotoxicity in amyotrophic lateral sclerosis (ALS). *Biochemistry* **2014**, *53* (14), 2423–2432 DOI: 10.1021/bi500158w.

(122) Grad, L. I.; Yerbury, J. J.; Turner, B. J.; Guest, W. C.; Pokrishevsky, E.; O'Neill, M. a; Yanai, A.; Silverman, J. M.; Zeineddine, R.; Corcoran, L.; et al. Intercellular propagated misfolding of wild-type Cu/Zn superoxide dismutase occurs via exosome-dependent and -independent mechanisms. *Proc. Natl. Acad. Sci. U. S. A.* **2014**, *111* (9), 3620–3625 DOI: 10.1073/pnas.1312245111.

(123) Garbuzynskiy, S. O.; Lobanov, M. Y.; Galzitskaya, O. V. FoldAmyloid: A method of prediction of amyloidogenic regions from protein sequence. *Bioinformatics* **2009**, *26* (3), 326–332 DOI: 10.1093/bioinformatics/btp691.

(124) Trovato, A.; Chiti, F.; Maritan, A.; Seno, F. Insight into the structure of amyloid fibrils from the analysis of globular proteins. *PLoS Comput. Biol.* **2006**, *2* (12), 1608–1618 DOI: 10.1371/journal.pcbi.0020170.

(125) Maurer-Stroh, S.; Debulpaep, M.; Kuemmerer, N.; Lopez de la Paz, M.; Martins, I. C.; Reumers, J.; Morris, K. L.; Copland, A.; Serpell, L.; Serrano, L.; et al. Exploring the sequence determinants of amyloid structure using position-specific scoring matrices. *Nat. Methods* **2010**, *7* (3), 237–242 DOI: 10.1038/NMETH.1432.

(126) Goldschmidt, L.; Teng, P. K.; Riek, R.; Eisenberg, D. Identifying the amylome, proteins capable of forming amyloid-like fibrils. *Proc. Natl. Acad. Sci. U. S. A.* **2010**, *107* (8), 3487–3492 DOI: 10.1073/pnas.0915166107.

(127) Primmer, H. Predicting and Measuring Molecular Mechanisms of Protein Aggregation. M.Sc. Thesis, University of Waterloo, 2011.

(128) De Groot, N. S.; Ventura, S. Effect of temperature on protein quality in bacterial inclusion bodies. *FEBS Lett.* **2006**, *580* (27), 6471–6476 DOI: 10.1016/j.febslet.2006.10.071.

(129) Villaverde, A.; Carrió, M. M. Protein aggregation in recombinant bacteria: Biological role of inclusion bodies. *Biotechnol. Lett.* **2003**, *25* (17), 1385–1395 DOI: 10.1023/A:1025024104862.

(130) Pratt, a. J.; Shin, D. S.; Merz, G. E.; Rambo, R. P.; Lancaster, W. a.; Dyer, K. N.; Borbat, P. P.; Poole, F. L.; Adams, M. W. W.; Freed, J. H.; et al. Aggregation propensities of superoxide dismutase G93 hotspot mutants mirror ALS clinical phenotypes. *Proc. Natl. Acad. Sci.* **2014**, *111* (43), E4568–E4576 DOI: 10.1073/pnas.1308531111.

(131) Lindberg, M. J.; Tibell, L.; Oliveberg, M. Common denominator of Cu/Zn superoxide dismutase mutants associated with amyotrophic lateral sclerosis: decreased stability of the apo state. *Proc. Natl. Acad. Sci. U. S. A.* **2002**, *99* (26), 16607–16612 DOI: 10.1073/pnas.262527099.

(132) Furukawa, Y. Redox environment is an intracellular factor to operate distinct pathways for aggregation of Cu,Zn-superoxide dismutase in amyotrophic lateral sclerosis. *Front. Cell. Neurosci.* **2013**, *7* (November), 240 DOI: 10.3389/fncel.2013.00240.

(133) Deng, H.-X.; Shi, Y.; Furukawa, Y.; Zhai, H.; Fu, R.; Liu, E.; Gorrie, G. H.; Khan, M. S.; Hung, W.-Y.; Bigio, E. H.; et al. Conversion to the amyotrophic lateral sclerosis phenotype is associated with intermolecular linked insoluble aggregates of SOD1 in mitochondria. *Proc. Natl. Acad. Sci. U. S. A.* **2006**, *103* (18), 7142–7147 DOI: 10.1073/pnas.0602046103.

(134) Roberts, B. L. T.; Patel, K.; Brown, H. H.; Borchelt, D. R. Role of Disulfide Cross-Linking of Mutant SOD1 in the Formation of Inclusion-Body-Like Structures. *PLoS One* **2012**, *7* (10), 1–7 DOI: 10.1371/journal.pone.0047838.

(135) Karch, C. M.; Borchelt, D. R. A limited role for disulfide cross-linking in the aggregation of mutant SOD1 linked to familial amyotrophic lateral sclerosis. *J. Biol. Chem.* **2008**, *283* (20), 13528–13537 DOI: 10.1074/jbc.M800564200.

(136) Culotta, V. C.; Yang, M.; O'Halloran, T. V. Activation of superoxide dismutases: Putting the metal to the pedal. *Biochim. Biophys. Acta - Mol. Cell Res.* **2006**, *1763* (7), 747–758 DOI: 10.1016/j.bbamcr.2006.05.003.

(137) Fee, J. a; Briggs, R. G. STUDIES ON THE RECONSTITUTION OF BOVINE ERYTHROCYTE SUPEROXIDE DISMUTASE. *Biochim. Biophys. Acta* **1975**, *400*, 439–450.

(138) Brenner, I. B.; Zander, a.; Cole, M.; Wiseman, a. Comparison of Axially and Radially Viewed Inductively Coupled Plasmas for Multi-element Analysis: Effect of Sodium and Calcium. *J. Anal. At. Spectrom.* **1997**, *12* (9), 897–906 DOI: 10.1039/a700465f.

(139) José Luis Todolí *, Luis Gras, V. H. and J. M. Elemental matrix effects in ICP-AES. *J. Anal. At. Spectrom.* **2002**, *17*, 142–169.

(140) Carrió, M.; González-Montalbán, N.; Vera, A.; Villaverde, A.; Ventura, S. Amyloid-like properties of bacterial inclusion bodies. *J. Mol. Biol.* **2005**, *347* (5), 1025–1037 DOI: 10.1016/j.jmb.2005.02.030.

(141) Wang, L.; Schubert, D.; Sawaya, M. R.; Eisenberg, D.; Riek, R. Multidimensional structure-activity relationship of a protein in its aggregated states. *Angew. Chemie - Int. Ed.* **2010**, *49* (23), 3904–3908 DOI: 10.1002/anie.201000068.

(142) Ihara;, Y.; Nobukuni;, K.; Takata;, H.; Hayabara, T. Oxidative stress and metal content in blood and cerebrospinal fluid of amyotrophic lateral sclerosis patients with and without a Cu, Zn-superoxide dismutase mutation. *Neurol. Res.* **2005**, *27* (1), 105–108.

Appendix

Appendix 1: Normalized aggregation prediction algorithm results for various aggregation prediction algorithms used to analyze SOD1 mutants, from Heather Primmer[127].

	Zyggregator	Chiti-dobson	Wang agar	Ztox	fold amyloid	Pasta	Tango	Waltz	Profile 3D
WT	0.7	0.56	0.47	0.65	0.51	0.59	0.45	0.83	0.39
A4V	0.94	0.69	0.61	0.96	0.77	0.61	1	0.83	0.41
G37R	0.41	0.39	0.24	1	0.67	0.59	0.45	0.61	0.19
G41D	0.45	0.2	0.02	0	0.54	0.59	0.45	0	0.59
G41S	0.65	0.58	0.45	0.19	0.55	0.59	0.45	0.45	1
H43R	0.5	0.26	0.15	0.09	0.51	0.59	0.45	0.35	0.39
H46R	0.6	0.41	0.27	0.29	0.52	0.59	0.45	0.41	0.2
L84V	0.8		0	0.73	0.51	0.59	0.45	0.92	0.39
G85R	0.56	0.39	0.24	0.68	0.62	0.59	0.45	0.71	0
D90A	0.91	1	1	0.85	0.53	0.59	0.45	0.88	0.41
G93A	0.68	0.55	0.48	0.78	0.6	0.6	0.45	0.83	0.2
E100G	0.98	0.75	0.76	0.64	0.51	0.61	0.45	0.95	0.59
I113T	0.78	0.39	0.24	0.72	0.21	0	0.45	0.79	0.2
L144F	0.91	0.58	0.5	0.97	0.5	0.59	0.73	1	0.6
V148G	0.58	0.35	0.26	0.62	0.62	0.59	0	0.85	0.15
V148I	0.68	0.5	0.39	0.82	0	0.59	0.43	0.9	0.6